

**Structural and functional characterisation of a novel
signalling molecule in *Arabidopsis thaliana***

by

Takalani Mulaudzi

**Submitted in fulfilment of the requirements for the degree of Doctor of
Philosophy (PhD) in Biotechnology in the Department of Biotechnology,
University of the Western Cape, South Africa**

**Supervisor: Professor Christoph A. Gehring
Co-Supervisor Professor Emmanuel I. Iwuoha**

May 2011

Declaration

I, Takalani Mulaudzi, declare that the thesis entitled "Structural and functional characterisation of a novel signalling molecule in *Arabidopsis thaliana*" is my work and has not been submitted for any degree or examination at any other university and that all sources of my information have been quoted as indicated in the text and/or list of references.

Name: Takalani Mulaudzi

Date: May 2011

Signature:

Date:

Dedication

*To My Family: Khethokwakhe, Akhonamahle, Mesuli, Matlakala, Naledzani,
Mulalo, Batlile, Sepati, Lebogang, Lerato and Gape*

Acknowledgements

First and foremost I would like to show and express my appreciation to my supervisor **Professor Christoph A. Gehring** and my co-supervisor **Professor Emmanuel I. Iwuoha** for giving me the opportunity to do this project in their laboratories. My special thanks go to both my supervisors for their guidance during the entire project and without them all this work would have not been possible.

I am also grateful to my colleagues in the sensor lab “Chemistry Department” special thanks go to **Dr. N. Hendricks, Dr. A. Arotiba, Dr. T. Waryo, Miss F. Ngece and Miss S. Botha** for their technical and scientific inputs concerning electrochemical experiments.

I thank **Professor L. Ludidi and Dr. M. Morse** for the identification and cloning of the novel *AtNOGCI* protein. I would also like to give special thanks to my colleagues in the plant laboratory ‘Department of Biotechnology’ **Dr. O. Ruzvidzo, Dr. R. Bastian, Dr. L. Kwezi, Mr. L. Mungur, Mr. A. Ojekale** for their moral support, friendship and encouragement during the period of this project. For the assistance during the proteomics works I would like to thank **Professor B. Ndimba and Dr. R. Ngara**.

For their friendship and technical assistance with the work, my thanks go to **Mr. A. Faro, and Mr. V. Muleya**. I would also like to thank my friends for their moral support during this journey, **Miss N. Sibuyi, Miss K. Molapo, Mr D. Modibane, Mr T. Mamphogoro and Mrs N. Clarence and the Clarence family**.

I thank the **North West University** “Mafikeng Campus: Department of Biology” for affording me with an opportunity to be part of their research visiting student and for being such a wonderful host, special thanks goes to **Dr. O. Ruzvidzo** for organising the visit.

I would like to thank my husband **Mr W.K. Masuku** for encouraging me to do this PHD, my daughter **Akhonamahle Nhlalohle Felicity Masuku**, my son **Siboniso Nungo Mesuli Masuku**, my mother **Mrs M.J. Ngwenya**, for their patience and support when this project kept me away from them in their hour of need. Also to my brother **Mulalo Mulaudzi**, my Uncle **Dr B.P. Maseko** and my cousin **Dr. L. Maseko** for their family support.

I wish to thank the **National Research Foundation** for its financial support for my entire studies.

Thanks to all Almighty “**GOD**” for the strength and courage that he gave me to finish up this project under certain circumstances “*Nothing is impossible with God*”.

Abbreviations

1D:	One dimension
2D:	Two dimension
3D:	Three dimension
ABA:	Abscisic acid
APS:	Ammonium persulfate
AtBRI1:	<i>Arabidopsis thaliana</i> Brassinosteroid receptor 1
AtCNG2:	<i>Arabidopsis thaliana</i> cyclic nucleotide-gated 2
AtGC1:	<i>Arabidopsis thaliana</i> guanylyl cyclase 1
AtNOGCI:	<i>Arabidopsis thaliana</i> a Nitric Oxide binding with a guanylyl cyclase activity 1
AtNOS1:	<i>Arabidopsis thaliana</i> nitric oxide synthase 1
ATP:	Adenosine 5`-triphosphate
AtPSK1:	<i>Arabidopsis thaliana</i> Phytosulfokine
AtWAKL10:	<i>Arabidopsis thaliana</i> wall associated kinase-like 10
bp:	base pair
BSA:	Bovine serum albumin
cADPR:	Cyclic adenosine diphosphate ribose
cAMP:	Cyclic 3`, 5`-adenosine monophosphate
cGMP:	Cyclic 3`, 5`-guanosine monophosphate
CO:	Carbon monoxide
CV:	Cyclic voltammetry
DEA/NO:	2-(N,N-diethylamino)-diazene-2-oxide
DDAB:	Didodecyldimethylammonium bromide
DTT:	Dithiothreitol

EGTA:	Ethylene glycol-bis (β -aminoethyl ether)-N,N,N',N'-tetraacetic acid
EIA:	Enzyme immunoassay
FAD:	Flavin adenine dinucleotide
FMO:	Flavin-containing monooxygenase
GC:	Guanylyl cyclase
GCE:	Glassy carbon electrode
GTP:	Guanosine 5`-triphosphate
HNOX:	Heme Nitric Oxide and/or Oxygen
IEC:	Ion exchange chromatography
IEF:	Isoelectric focusing
iNOS:	inducible nitric oxide synthase
IMAC:	Immobilized metal affinity chromatography
IPG:	Immobilised pH gradient
IPTG:	Isopropyl-1-thio-D-galactopyranoside
kDa:	Kilo dalton
LB:	Luria broth
N ₂ :	Nitrogen gas
NADP:	Nicotinamide adenine dinucleotide phosphate
NH ₃ ⁺ :	Ammonia
NH ₃ OH ⁺ :	Hydroxylamine
Ni-NTA:	Nickel-nitrilotriacetic acid
NMR:	Nuclear magnetic resonance
NO ₃ ⁻ :	Nitrate
NiR:	Nitrite reductase
NO ₂ ⁻ :	Nitrite

N ₂ O:	Nitrous oxide
NR:	Nitrate reductase
NO:	Nitric Oxide
NOS:	Nitric oxide synthase
ONOO ⁻ :	Perocynitrite ion
O ₂ :	Oxygen
PAL:	Phenylalanine lyase
PCD:	Programmed cell death
PCR:	Polymerase chain reaction
PMSF:	Phenylmethanesulfonylfluoride
PNP:	Plant natriuretic peptide
PR-1:	Pathogenesis-related 1
PSB:	Phosphate buffered saline
ROS:	Reactive oxygen species
SWV:	Square wave voltammetry
SDS:	Sodium dodecyl sulphate
SDS-PAGE:	Sodium dodecyl sulphate polyacrylamide gel electrophoresis
SNP :	Sodium nitropruside
TEMED:	1,2-Bis(dimethylamino)ethane

Keywords

Recombinant protein

H-NOX domain

Signalling molecule

Flavin-containing monooxygenase

Nitric oxide

Oxygen

Electrochemistry

Guanylyl cyclase

cGMP assays

Homology modelling

List of figures and tables

Figure 1.1: Chemical nature of NO and its reactions.....	6
Figure 1.2: Chemical reactions showing the synthesis of NO from L-arginine catalysed by NOS.....	9
Figure 1.3: Structural conformations of the second messengers (cyclic nucleotides).....	16
Figure 1.4: Structure model of the heme-binding pocket from rat soluble GC.....	21
Figure 1.5: Domain organisation and the alignment of different motifs of the FMOs found in <i>Arabidopsis thaliana</i>	23

Chapter 2

Table 2.1: The concentration and absorbance of the standard (BSA) protein and the dilutions factors of <i>AtNOGCI</i>	131
Figure 2.1: Circular map of the Champion™ pET SUMO expression vector.....	28
Figure 2.2: Sequence of the <i>Arabidopsis thaliana</i> NO-binding protein <i>AtNOGCI</i>	42
Figure 2.3: Determination of the <i>AtNOGCI</i> protein parameters from the expasy server.....	43
Figure 2.4: A 1 % agarose gel electrophoresis analysis of the <i>AtNOGCI</i> clone.....	44
Figure 2.5: A 12 % SDS-PAGE gel analysis of expression and affinity purification of <i>AtNOGCI</i> fusion protein.....	46

Figure 2.6: Separation of <i>AtNOGCI</i> fusion protein from the residual crude proteins.....	47
Figure 2.7: 2D SDS-PAGE gels showing the recombinant <i>AtNOGCI</i> before and after purification by anion exchange chromatography.....	48
Figure 2.8: A 12 % SDS-PAGE gel stained with coomasie Brilliant blue showing the final concentrated <i>AtNOGCI</i> fusion protein.....	49
Figure 2.9: Standard curve of the BSA for the Bradford assay to determine the concentration of recombinant <i>AtNOGCI</i>	132
Figure 2.10: UV absorption spectrum of <i>AtNOGCI</i> protein determined using NanoDrop spectrometer.....	132

Chapter 3

Figure 3.1: Apparatus representing the Production of NO from Cu turnings and HNO ₃	59
Figure 3.2: Characterisation of the <i>AtNOGCI</i> bioelectrode at different scan rates.....	62
Figure 3.3: Cyclic voltammogram showing the response of <i>AtNOGCI</i> in phosphate buffer in the presence or absence of O ₂	63
Figure 3.4: Electrochemical characterisation of <i>AtNOGCI</i> in phosphate buffer.....	65
Figure 3.5: Electrochemical characterisation of <i>AtNOGCI</i> , bare GCE and GCE modified with DDAB-BSA film in phosphate buffer.....	67
Figure 3.6: Cyclic voltammograms of <i>AtNOGCI</i> responding to O ₂ and NO.....	69

Chapter 4

Figure 4.1: Expression of <i>AtNOGCI</i> fusion protein and determination of its <i>in vitro</i> GC activity.....	81
Figure 4.2: Competitive <i>in vitro</i> GC activity assays of <i>AtNOGCI</i> using both GTP and ATP as substrates.....	82
Figure 4.3: <i>in vitro</i> GC activity assays of <i>AtNOGCI</i> and its activation by NO.....	83
Figure 4.4: Effect of calcium on the GC activity of the purified recombinant <i>AtNOGCI</i>	85

Chapter 5

Figure 5.1: Alignment of <i>AtNOGCI</i> with structures of the FMO from <i>Methylophaga Sp.</i> Strain SK1 and a Phenylacetone monoxygenase a Baeyer-Villager monooxygenase.....	95
Figure 5.2: Three-dimensional model of <i>AtNOGCI</i>	96
Figure 5.3: Evaluation of <i>AtNOGCI</i> model by procheck.....	96
Figure 5.4: Fold recognition to determine secondary structure of <i>AtNOGCI</i>	97
Figure 5.5: Alignment of At5g57690 with template structures <i>Salmonella typhimurium</i> Yegs (pdb code: 2p1r) and <i>E. coli</i> lipid kinase (pdb code: 2bon).....	99
Figure 5.6: Evaluation of the model structure obtained for At5g57690.....	100
Figure 5.7: Fold recognition to determine secondary structure of At5g57690.....	101

Table of contents

Declaration	ii
Dedication.....	iii
Acknowledgements.....	iv
Abbreviations.....	vi
Keywords.....	ix
List of figures and tables.....	x
Summary	1
CHAPTER 1: Literature Review.....	4
<i>1.1 Introduction.....</i>	<i>4</i>
<i>1.2 Nitric oxide signalling.....</i>	<i>5</i>
1.2.1 Chemistry of NO	5
1.2.2 NO synthesis in plants	7
1.2.3 NO signalling mediated by second messengers.....	9
1.2.4 Functions of NO in plant systems	11
<i>1.3 Guanylyl cyclases</i>	<i>15</i>
<i>1.4 Cyclic nucleotides as second messengers</i>	<i>15</i>
<i>1.5 Heme sensor family of proteins</i>	<i>17</i>
1.5.1 The heme environment	20
<i>1.6 Flavin-containing monooxygenase family of proteins.....</i>	<i>21</i>
1.6.1 Structure of FMOs.....	22
1.6.2 Functions of FMOs.....	24
<i>1.7 Objectives of the study</i>	<i>24</i>
1.7.1 Specific objectives.....	24
CHAPTER 2: Identification of <i>AtNOGC1</i> and the Production of a Recombinant Protein for Functional Studies.....	26
Abstract	26
<i>2.1 Introduction.....</i>	<i>27</i>
<i>2.2 Materials and Methods</i>	<i>31</i>
2.2.1 Identification of <i>AtNOGC1</i>	31

2.2.2 Verification of the correct <i>AtNOGCI</i> gene	31
2.2.2.1 Re-amplification by polymerase chain reaction (PCR)	31
2.2.2.2 Restriction digestion	32
2.2.2.3 DNA sequencing.....	33
2.2.3 Plasmid DNA isolation.....	33
2.2.4 Production of the recombinant protein.....	34
2.2.4.1 Transformation of plasmid DNA into competent cells.....	34
2.2.4.2 Expression of recombinant <i>AtNOGCI</i>	34
2.2.4.3 Affinity purification of His-tagged proteins using a Ni-NTA column	35
2.2.4.3.1 Preparation of the cleared lysate	35
2.2.4.3.2 Purification	35
2.2.4.4 Anion exchange chromatography	36
2.2.5 SDS-PAGE gel electrophoresis of proteins.....	37
2.2.5.1 1D electrophoresis of proteins.....	37
2.2.5.2 2D electrophoresis of proteins.....	38
2.2.5.2.1 Rehydration of the strips	38
2.2.5.2.2 First dimensional IEF of IPG Strips	38
2.2.5.2.3 Equilibration of IPG strips	39
2.2.5.2.4 Second dimension SDS-PAGE for mini format gels	39
2.2.6 Determination of protein concentration using the Bradford assay.....	40
2.3 Results.....	41
2.3.1 Identification of <i>AtNOGCI</i> and prediction of its parameters	41
2.3.2 Verification of the <i>AtNOGCI</i> clone	44
2.3.3 Recombinant expression and purification of <i>AtNOGCI</i>	45
2.3.4 Purification of <i>AtNOGCI</i> by anion exchange chromatography	46
2.3.5 Determination of protein concentration.....	48
2.4 Discussion	51

CHAPTER 3: Electrochemical Characterization of a Novel Nitric Oxide Binding Protein from *Arabidopsis thaliana* 53

Abstract 53

3.1 Introduction.....	54
3.2 Materials and methods.....	57
3.2.1 Electrochemical apparatus and procedures.....	57
3.2.2 Preparation of <i>AtNOGCI</i> protein electrode.....	57
3.2.3 Generation of nitric oxide.....	58
3.2.4 Cyclic and square wave voltammetric experiments.....	59
3.2.5 Binding affinities of the heme site	60
3.3 Results.....	61

3.3.1 Initial electrochemical characterization of <i>AtNOGCI</i>	61
3.3.2 Electrochemical characterization of <i>AtNOGCI</i> in O ₂	62
3.3.3 Electro-catalytic characterisation of <i>AtNOGCI</i> for binding to NO.....	63
3.3.4 Electrochemical characterization of the <i>AtNOGCI</i> bioelectrode, bare GCE and bare GCE modified with DDAB-BSA in the presence or absence of NO.	66
3.3.5 Investigation of NO and O ₂ affinity to the <i>AtNOGCI</i> heme binding site.....	67
3.4 Discussion.....	70
CHAPTER 4: <i>AtNOGCI</i> is a Novel <i>Arabidopsis thaliana</i> Nitric Oxide Binding Protein that Functions as a Guanylyl Cyclase <i>in vitro</i> in an NO-dependent Manner.....	74
Abstract.....	74
4.1 Introduction.....	75
4.2 Materials and methods.....	78
4.2.1 Guanylyl cyclase activity assays.....	78
4.2.2 Activation of <i>AtNOGCI</i> GC activity by NO and Ca ²⁺	78
4.3 Results.....	80
4.3.1 Effects of cofactor and time dependence on the activity of the <i>AtNOGCI</i>	80
4.3.2 Activation of the GC activity of the <i>AtNOGCI</i> by NO.....	82
4.3.3 Effect of calcium on GC activity assays of <i>AtNOGCI</i>	84
4.4 Discussion.....	86
CHAPTER 5: Modelling <i>AtNOGCI</i>, a Flavin-containing Monooxygenase and At5g57690, a Diacylglycerol Kinase from <i>Arabidopsis thaliana</i>.....	90
Abstract.....	90
5.1 Introduction.....	91
5.2 Materials and methods.....	93
5.2.1 Modelling of <i>AtNOGCI</i> and At5g57690.....	93
5.3 Results.....	94
5.3.1 <i>AtNOGCI</i> model.....	94
5.3.1 At5g57690 model.....	98
4.4 Discussion.....	102
6. Final conclusion and future perspective.....	105
7. References.....	109
8. Appendix.....	124
Appendix I: Chemicals, stock solutions, buffers and bacterial strains.....	124

<i>Appendix II: Prediction of protein parameters for the AtNOGCI protein.....</i>	<i>126</i>
<i>Appendix III: DNA sequencing results: Sequence analysis of AtNOGG1 cloned into pET SUMO vector sequenced at INQABA Biotechnical industries (Pty) Ltd.....</i>	<i>128</i>
<i>Appendix IV: Data for the determination of protein concentration using Bradford assay</i>	<i>131</i>
<i>Appendix V: Results for AtNOGCI and At5g57690 obtained from the Fugue server</i>	<i>133</i>
Keys	<i>136</i>
<i>Appendix VI: Microarray data showing the expression profiles for AtNOGCI obtained from Genevestigator</i>	<i>137</i>

Summary

Nitric Oxide (NO) influences a wide range of physiological processes in plants including growth and development, responses to abiotic and biotic stress and pathogen responses. NO binds to the heme group of the mammalian soluble guanylyl cyclase, which activates the enzyme to convert guanosine 5' triphosphate (GTP) to a second messenger guanosine 3', 5' cyclic monophosphate (cGMP). Cyclic GMP further activates other signalling cascades including the regulation of protein kinases, ion gated channels and phosphodiesterases. In plants, a few GCs have been identified and these include AtGC1, AtBRI1, AtWAKL10, and AtPSKR1, however, a GC that contains a heme binding motif that senses NO has yet to be identified. In order to identify such molecules, a search motif based on conserved HNOX domains and the conserved and functionally assigned amino acid residues in the catalytic centres of annotated GCs was designed and used to search the *Arabidopsis thaliana* proteome. Several candidate molecules were identified including a flavin-containing monooxygenase (FMO)-like protein and the At5g57690 which is currently annotated as a diacylglycerol kinase. FMOs found in bacteria, yeast, and animals are the most important monooxygenases since they are involved in xenobiotic metabolism and variability in drug response. FMOs in plants are implicated in catalysing specific steps in auxin biosynthesis, metabolism of glucosinolates and pathogen defense mechanisms. The human diacylglycerol kinase acts as a lipid kinase that mediates a wide range of biological processes which include cell proliferation, differentiation and tumorigenesis. In prokaryotes, the structure of *Escherichia coli* lipid kinase has been solved however, its function has not yet been demonstrated. So far, the occurrence of the diacylglycerol kinases in plants has not yet been reported, and their structure and function also remain elusive. The domain architecture of the

molecules (*AtNOGCI* and At5g57690) identified by the HNOX-based search strategy revealed that these molecules contain a GC and a heme-binding motif that is conserved among all known heme-binding proteins.

In this study, the role of *AtNOGCI*, a novel NO binding protein in higher plants was investigated and the results showed that this molecule contains an NO-dependant active GC domain. The sequence was first analysed and the location of the HNOX and the GC motifs highlighted. The protein was then recombinantly expressed as a His-SUMO fusion protein and the purification optimised by a second step of ion exchange chromatography. Electrochemical techniques such as cyclic voltammetry and square wave voltammetry were used to demonstrate the binding of NO and O₂ to the *AtNOGCI*. Electrochemical data revealed that *AtNOGCI* has a lower affinity for O₂ and a higher affinity for NO, an important signalling molecule in plants.

The presence of the GC activity in *AtNOGCI* was investigated by conducting GC activity assays *in vitro* in the presence or absence of NO. The GC activity assays demonstrated that *AtNOGCI* can synthesize cGMP from GTP *in vitro*. It was also noted that NO was required for the maximum activation of *AtNOGCI* catalytic activity. NO-activated catalysis resulted in a >2 fold excess of cGMP production compared to an NO-independent GC activity assay. The effect of calcium in regulating the GC activity was also investigated and an increase in cGMP levels was observed however, this was just a preliminary finding that requires further experimentation.

Homology models for both the FMO-like (*AtNOGCI*) and the diacylglycerol kinase (At5g57690) were built using Modeller program, and important amino acid residues underlying the heme-binding and GC motifs were identified. Residues corresponding to the motifs, which give signature to *AtNOGCI* as an FMO, were also noted. In addition, computational functional prediction also suggested the role of *AtNOGCI* in a number of processes which include ion binding and functioning as an FMO.

Taken together, these findings suggest that *AtNOGCI* is a novel *Arabidopsis thaliana* heme-binding protein that senses NO with higher affinity than for O₂. Though *AtNOGCI* is currently annotated as a FMO-like protein, it contains a NO-sensitive GC activity and shares limited sequence similarities with mammalian sGC and the recently identified HNOX domains. Homology modelling strongly suggests that *AtNOGCI* and At5g57690 belong to the families of FMOs and diacylglycerol kinases respectively. The domain organisation of *AtNOGCI* suggests that more of its functions still remain to be identified. The cloning and characterisation of the At5g57690 gene will provide possible means for further experimentation as well as affording more insights into the exact functions of lipid kinases in plants.

CHAPTER 1: Literature Review

1.1 Introduction

Molecular genetic manipulation and biochemical studies have created a means of characterising and elucidating physiological functions of novel signalling molecules in several living organisms. This aids in understanding signalling pathways that regulate growth, development (Gouvêa et al., 1997; Leshem et al., 1998) and defense mechanism in both plants and animals. Key molecules such as nitric oxide (NO) and cyclic nucleotides are important effectors of animal redox-regulated signalling and have also been shown to mediate diverse physiological processes in plants (Newton and Smith, 2004; Kaplan et al., 2007).

This thesis examines the functional and structural properties of a novel signalling molecule in *Arabidopsis thaliana*, *AtNOGCI*. This chapter entails the role of NO as a signalling molecule in plants, especially looking into its sources, its role as a signalling molecule via its second messengers and a brief description of its functions. A short description on the different kinds of heme-binding proteins and their structures will also be discussed. An outline of signalling pathways of guanylyl cyclases and their associated cyclic nucleotides will also be discussed. Finally, flavin-containing monooxygenases (FMOs) will also be elaborated highlighting their structural features and functional characteristics.

1.2 Nitric oxide signalling

Nitric oxide (NO) was first identified as an endothelium-derived relaxation factor and has been implicated to be an important mediator of several animal cell functions. The interaction of NO and redox proteins is now recognised as an important component of signal transduction pathways which regulates processes such as gene expression and control a number of biological processes including gene transcription and translation (Fan et al., 2004), neurotransmission, immunological and inflammation response, relaxation and vascular smooth muscle (Besson-Bard et al., 2008b). NO also has a major role in protecting the immune system against tumour cells and intracellular parasites (Casero et al., 2000; Durner et al., 1999). Although NO plays an important role in the immune system of animals, it has been implicated in the generation of weak levels of antioxidant and an excess accumulation of reactive oxygen species (ROS) that then lead to its toxicity. In animals, the interaction of NO with ROS induces apoptosis of tumour cells and the killing of bacteria by macrophages. A similar mechanism in plants has been reported where the interaction prevents tissue invasion by pathogens (De Stefano et al., 2005). Due to its size and the lack of charge, NO is able to diffuse rapidly and freely between cells, which makes it an important biomolecule (Casero et al., 2000). In addition, NO has the ability to react with oxygen (O₂), metal ions, and thiols (Boon and Marletta, 2005a, b).

1.2.1 Chemistry of NO

NO is a relatively small free radical gas with a long half life ranging from minutes to hours at low concentrations (less than 1 μmol L⁻¹) and a short half life of about seconds at high concentrations (Manjunatha et al., 2010). Because of its high diffusivity rate (4.8 x 10⁻⁵ cm²

s¹ in water) (Hakim et al., 1996) NO can diffuse over several cell layers and longer distances in intracellular spaces exhibiting its hydrophobic properties. Its half life is also dependent on the presence of its targets such as proteins, O₂, heme proteins, bound iron, copper, cysteine, tyrosine and ascorbic acid (Procházková and Wilhelmová, 2011). NO is a highly reactive molecule that reacts with O₂ to form compounds such as NO₂[•], N₂O₃ and N₂O₄, which further react with amines and thiols or being hydrolysed to NO₂⁻ and NO₃⁻. NO[•] can also form an unstable peroxynitrite ion (ONOO⁻) from its reaction with superoxide anion-radical (O₂^{-•}), under physiological pH ONOO⁻ protonates to form peroxo-dioxonitric acid and a hydroxyl radical (HO[•]). The radical form of NO can either be oxidised to produce a nitrosonium cation (NO⁺) or reduced to form a nitroxyl anion (NO⁻) (Figure 1.1) (Arasimowicz and Floryszak-Wieczorek, 2007).

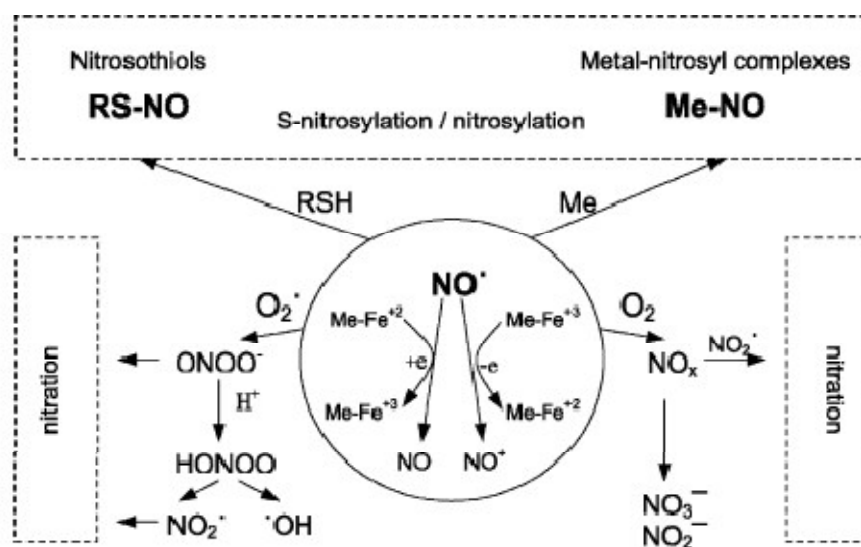


Figure 1.1: Chemical nature of NO and its reactions. NO[•], nitric oxide radical; NO⁺, nitrosonium cation; NO⁻ nitroxyl anion; Me, transition metal; O₂, oxygen; nitric oxides (NO₂[•], N₂O₃, N₂O₄); NO₂⁻, nitrite; NO₃⁻, nitrate; RSH, thiols, O₂^{-•} superoxide anion; ONOO⁻ peroxynitrite; HONOO, pernitrous acid; OH[•], hydroxyl radical (adapted from, (Arasimowicz and Floryszak-Wieczorek, 2007)).

1.2.2 NO synthesis in plants

In plants, different sources of NO are reported however, its physiological roles dependent on plant species, cell type, external conditions and the potential activation of the signal pathway in the plant. In animals, NO is produced by a NO synthase (NOS) that catalyses the conversion of L-arginine to L-citrulline and NO, in the presence of O₂ involving an NADPH-dependent reaction (Figure 1.2). In plants, NO is produced from both L-arginine and nitrite-dependent pathways.

Plants use different systems to produce NO both involving enzymatic and non-enzymatic reactions. Enzymatic synthesis of NO involves three different kinds of enzymes including a nitrite reductase (NiR), a nitrate reductase (NR) and a NO synthase (NOS). Like in the animal system, NO is also produced from L-arginine by the action of NOS-like enzymes. The presence of NOS activity in plants was first reported in roots and nodules (Leshem and Haramaty, 1996; Ninnemann and Maier, 1996). Although NOS-like activity has been detected in plants and NOS-like enzymes identified, they share no sequence similarity with the animal NOS. However inhibitors of the animal NOS abolished NO generation in plants supporting the presence of NOS activity. NOS-like enzymes reported in plants include the pathogen-inducible NOS from *Arabidopsis thaliana* and tobacco (iNOS) and an *Arabidopsis thaliana* hormone activated NOS (AtNOS1) (Guo et al., 2003). Production of NO by iNOS was demonstrated in plants that were resisting infection by turnip crinkle virus and in tobacco plants treated with tobacco mosaic virus or were unaffected by the fungal elicitor cryptogein. Though AtNOS1 does not share any sequence identity with iNOS and the mammalian NOS, it displays a flavin, heme and tetrahydrobiopterin-independent NOS activity. A gene encoding AtNOS1 protein was reported to be involved in growth and hormonal signalling

(Guo et al., 2003), and that NO production by AtNOS1 is stimulated by responses to abscisic acid (ABA), hormones and other signals. Since AtNOS1 shares no similarities to animal NOS, it suggests that NO activity in plants may have evolved from different types of enzymes (Wendehenne et al., 2004).

NO is also synthesized from nitrite in a one step reaction catalysed by NiR, and from the reduction of nitrate to nitrite by NR then to NO in a reaction that requires NADPH (Delledonne et al., 1998). NO production catalysed by NR has been demonstrated both *in vivo* and *in vitro* occurring in different plant species including cucumber, sunflower, maize, *Arabidopsis*, wheat, orchid, aloe, spinach, tobacco and in a small plant *Chlamydomonas reinhardtii* (Arasimowicz and Floryszak-Wieczorek, 2007). A plasma membrane nitrite: NO-reductase (Ni-NOR), an enzyme identified in tobacco roots, is also responsible for the synthesis of NO from nitrite using cytochrome *c* as an electron donor *in vitro* (Misra et al., 2010).

A non-enzymatic reaction involves the conversion of nitrite to NO by carotenoids in an acidic pH medium, and the same reaction can also happen due to hormonal response such as gibberellin and ABA. NO synthesis can also occur through nitrification, denitrification, N₂ fixation and respiration. Other sources of NO may include horseradish peroxidase, cytochrome P450, catalase and haemoglobin (Arasimowicz and Floryszak-Wieczorek, 2007).

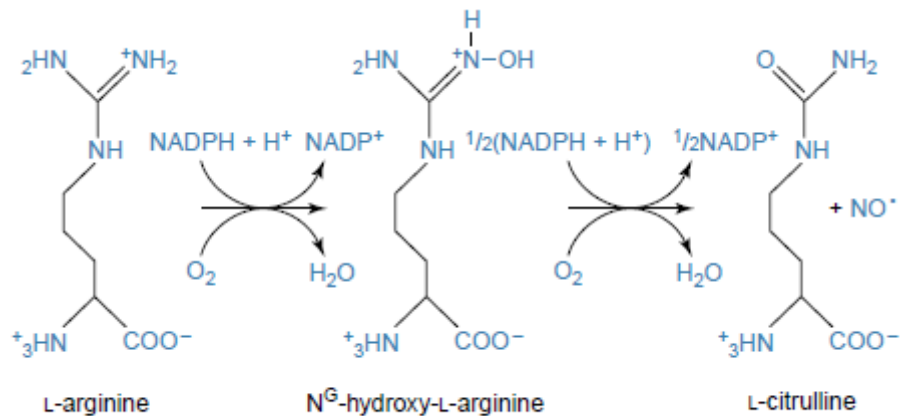


Figure 1.2: Chemical reactions showing the synthesis of NO from L-arginine catalysed by NOS. L-arginine is converted to L-citrulline and NO, in a two-step reaction catalysed by NOS. In the first step, L-arginine is converted to N^{G} -hydroxy-L-arginine in the presence of oxygen, followed by the second step where N^{G} -hydroxy-L-arginine is oxygenated to L-citrulline and NO. The reaction requires NADPH as an electron donor (adapted from (Wendehenne et al., 2001)).

1.2.3 NO signalling mediated by second messengers

Due to its simple structure, small size and high diffusivity rate, NO fits the characteristic of a signalling molecule. NO signalling in mammals can either be cGMP dependent or independent such as is in the *S*-nitrosylation/denitrosylation of proteins. Guanylyl cyclase (GC), the enzyme which catalyses the synthesis of cGMP, is an important target for NO signalling. NO binds to the heme of soluble GC (sGC) and increases its activity significantly, resulting in the synthesis of cGMP. Cyclic GMP in turn activates various cGMP targets including the regulation of protein kinases, ion gated channels and phosphodiesterases. In plants, the same signalling pathway is also thought to occur in the same manner although this pathway is poorly understood. The presence of cGMP in plants has long been reported (Durner et al., 1999) however it is only until recently that a few GCs have been identified and characterised, and these include the AtGC1 (Ludidi and Gehring, 2003), the AtBRI1 (Kwezi

et al., 2007), the AtWAKL10 (Meier et al., 2010). Though these GCs have been identified, none of them requires NO-activation, suggesting that an NO-sensitive GC is yet still to be identified.

Cyclic GMP plays major roles as a second messenger in a NO-dependent manner. An increase in endogenous cGMP was reported in several aspects including tobacco plants treated with NO inducers (Durner et al., 1999), response to stimuli such as the gibberellic acid treatment of barely aleurone, light stimulation of bean cells and the treatment of spruce needles with NO (Durner et al., 1999). Tobacco plants and suspension cultures treated with NO activated the expression of defence genes encoding the pathogenesis-related (PR-1) protein and the phenylalanine lyase (PAL) however, this induction was blocked by sGC inhibitors, suggesting the presence of a NO-activated sGC in plants (Durner et al., 1999).

NO was also proposed to regulate signalling pathways through cyclic adenosine diphosphoribose (cADPR) and Ca^{2+} mobilisation. Cyclic ADPR was first identified as a cyclic derivative of NAD^+ that is formed by ADP-ribosyl cyclase and metabolised to adenosine diphosphate by cADPR hydrolase (Guse, 1999). Cyclic ADPR plays a role in the ABA signalling pathway in tomato and Arabidopsis plants and acts synergistically with cGMP to induce the expression of PAL and PR-1 genes in tobacco (Durner et al., 1999; Durner et al., 1998; Wendehenne et al., 2004). Furthermore it acts as a second messenger in cGMP-dependent signalling pathways (Denninger and Marletta, 1999) and in Ca^{2+} mobilisation in *Vicia faba* guard cells, through modulation of vacuolar Ca^{2+} channels. NO acts through its second messengers cGMP and cADPR to modulate Ca^{2+} permeable channels (Durner et al., 1999; Wendehenne et al., 2004) which increases free cytosolic Ca^{2+} levels in cells. NO also regulates an increase of cytosolic Ca^{2+} in plants in response to a number of

stimuli including applied osmotic stress, treatment with fungal elicitor, a *Borrytis cinerea* endopolygalacturonase 1 elicitor in grapes and in ABA-induced stomatal guard cell movements (Arasimowicz and Floryszak-Wieczorek, 2007).

NO has also been shown to cause activation of the mitogen-activated protein (MAP) kinase in *Arabidopsis* (Clarke et al., 2000) and in tobacco cells (Kumar and Klessig, 2000; Pagnussat et al., 2004), and its presence induces the biosynthesis of jasmonic acid (Jih et al., 2003; Orozco-Cardenas and Ryan, 2002; Polverari et al., 2003), salicylic acid and ethylene. Apart from its interaction with GCs, NO can also interact and positively or negatively regulate other iron containing proteins, such as the iron-sulphur enzyme (aconitase), catalase, peroxidase and haemoglobin. NO can also interact with cysteines and tyrosines found in proteins and thiol groups containing molecules (Wendehenne et al., 2001).

1.2.4 Functions of NO in plant systems

NO influences a wide range of physiological processes in plants. It is known to be involved in the developmental role of plants by promoting seed germination (Beligni and Lamattina, 2000), roots growth (Correa-Aragunde et al., 2004), leaf extension and flowering (He et al., 2004; Leshem et al., 1998), fruit ripening (Leshem, 2000; Manjunatha et al., 2010), reproduction and causes pollen tube re-orientation (Prado et al., 2004). NO also modulates disease resistance in plants by triggering cell death and inducing the expression of disease resistance genes (Neill et al., 2003; Romero-Puertas et al., 2004) and triggering responses to biotic stresses caused by pathogens (Delledonne et al., 1998; Durner et al., 1998; Manjunatha et al., 2008), and abiotic stresses involved in drought resistance (Desikan et al., 2002), wounding (Huang et al., 2004), and programmed cell death (Beligni et al., 2002; Murgia et

al., 2004). NO has also been implicated in the modulation of plant hormones such as cytokinin (Wilhelmova et al., 2006), auxin (Otvos et al., 2005) and ethylene (Leshem and Haramaty, 1996).

Furthermore, NO has been shown to induce cell death in plant systems such as the programmed cell death (PCD) which is also observed in animal systems. Evidence of NO-related cell death has been observed in a number of plant systems and these include, *Citrus sinensis* suspension cultured cells, *Arabidopsis thaliana* plants that were challenged with avirulent *Pseudomonas syringae* (Delledonne et al., 1998; Saviani et al., 2002), tobacco plants and root cultures of alfalfa that over-produced haemoglobin after they were treated with avirulent pathogens or under hypoxic conditions. Other plant systems such as soybean cells increase NO in relation to ROS, which then increases the hypersensitive responses and programmed cell death (Delledonne et al., 1998; Delledonne et al., 2001).

In addition to regulating plant cell death, NO is also implicated to have some anti-apoptotic properties including the protection of barley aleurone layers against gibberellin-induced cell death (Beligni et al., 2002; Garcia-Mata and Lamattina, 2001). NO prevented cell death in potato leaves which were treated with a pathogen *Phytophthora infestans* or treated with ROS-producing herbicides, thus acting as an anti-oxidant (Beligni and Lamattina, 1999). NO also has a role in protecting cells from ROS-mediated cellular damage and cytotoxicity by increasing the levels of cryo-protective enzymes such as catalase, superoxide dismutase, glutathione S-transferase and alternative oxidases (Beligni et al., 2002). It has also been suggested that NO might have a protective effect against oxidative stress by abrogating the superoxide anion-radical-mediated cytotoxic effects through the conversion of O₂ into the perocynitrite ion (Delledonne et al., 2001).

NO has been demonstrated to have a regulatory effect in the process of seed germination, root growth and it also protects plant seedlings against the effects of heavy metals. In an elegant experiment, Kopyra and Gwózdź (2003) showed that NO increased seed germination in seeds treated with the NO-donor sodium nitropruside (SNP) under both normal and stressed conditions (Kopyra and Gwózdź, 2003). However, at high NO concentrations, there was a decreased rate of seed germination, shorter root length and other morphological changes such as browning and curling of root tips. The effect of sodium chloride stress in germination was reversed due to the action of NO. Lupin roots treated with heavy metals cadmium and lead were protected, suggesting a role of NO in seed germination, and protection against the toxicity of heavy metals (Kopyra and Gwózdź, 2003). In another study, the effect of NO in increasing the root hair surface on the root was investigated in lettuce and Arabidopsis plants, in the presence of an NO-donor. NO caused a significant increase in root hairs on the surface of the root compared to plants grown in water only for both plant systems (Lombardo et al., 2006). NO is also required in auxin-mediated root hair formation in roots, suggesting that both NO and auxin are key factors in increasing the root hair growth in plants (Lombardo et al., 2006).

Plant response to abiotic and biotic stresses such as drought, high and low temperatures, salinity, heavy metals, oxidative stress and pathogen attack is important in many aspects of plant growth and development, and NO has been implicated in the regulation of these different stress elicitors (Delledonne, 2005; Lamattina et al., 2003; Neill et al., 2003).

The importance of NO in drought stress was demonstrated in wheat seedlings by inducing stomatal closure, which enhanced drought tolerance in cut leaves (Lamattina et al., 2003). At

high temperatures, it was observed that NO synthesis was highly elevated and at low temperatures, NO increased the stress tolerance of tomato, wheat, and maize (Neill et al., 2003). Since abiotic stress increases polyamine biosynthesis, which in turn induces the production of NO, it suggests that NO acts as an intermediate between polyamine mediated stress responses and other mediators (Zhao et al., 2001; Kopyra and Gwózdź, 2003; Lamattina et al., 2003; Zhao et al., 2004).

Salinity is one of the major factors affecting several physiological processes in plants including growth and crop yield. It was shown that the growth of cucumber seedlings grown in sodium chloride was inhibited, but the addition of an NO-donor alleviated the salt stress to a larger degree (Fan et al., 2010). In high salt, NO increases the activity of antioxidant enzymes and the expression of salinity defence genes as was observed in rice seedlings (Arasimowicz and Floryszak-Wieczorek, 2007). Furthermore, NO can protect cucumber roots from the oxidative stress resulting from sodium chloride treatment, however, the sodium chloride stress alleviation was blocked by the addition of haemoglobin, a NO scavenger and sodium ferrocyanide (Shi et al., 2007), suggesting an important role of NO in enhancing stress tolerance in plants.

Plant cells tend to accumulate NO in response to infection by pathogens and NO is also an important signal in protecting plant cells against attack by pathogens. NO stimulates signal transduction pathways for the production of defence-related genes such as PAL in tobacco leaves and the biosynthesis of antimicrobial flavonoids in soybean cotyledons (Delledonne et al., 1998; Romero-Puertas and Delledonne, 2003). Though NO mediated physiological roles are well-documented in plants, an understanding of its signalling pathways will still remain elusive until an NO-dependent GC is identified and characterised.

1.3 Guanylyl cyclases

Guanylyl cyclases are enzymes which catalyse the synthesis of cGMP from GTP. There are two major families of GCs in animals, the particulate GCs, located in the transmembrane and the soluble GCs. Particulate GCs consist of highly conserved domain architecture which includes an N-terminal extracellular binding domain, hydrophobic domain, a regulatory domain that shows homology to protein kinases, a hinge region and an intracellular domain at the C-terminal of the protein (Durner et al., 1999; Lucas et al., 2000). Soluble GCs are heterodimers consisting of the α - and β - subunits in which the heme-binding domain is located in the β - subunit, which requires NO activation (Gerzer et al., 1981; Lucas et al., 2000; Namiki et al., 2001).

1.4 Cyclic nucleotides as second messengers

Cyclic nucleotides are small molecules that are synthesized by the adenylyl/guanylyl cyclase family of proteins and undergo degradation by phosphodiesterases. Cyclic nucleotides that act as second messengers include the adenosine 3', 5'-cyclic monophosphate, cytidine 3', 5'-cyclic monophosphate and the guanosine 3', 5' monophosphate (Figure 1.3). These molecules play major roles in both plants and animals. The biological roles of cyclic nucleotides in animals are well-characterised, however, it is only recently that their roles in plants are now being demonstrated. In general, cyclic nucleotides are involved in plant responses to abiotic and biotic stresses and responses to pathogens (Newton and Smith, 2004; Kaplan et al., 2007).

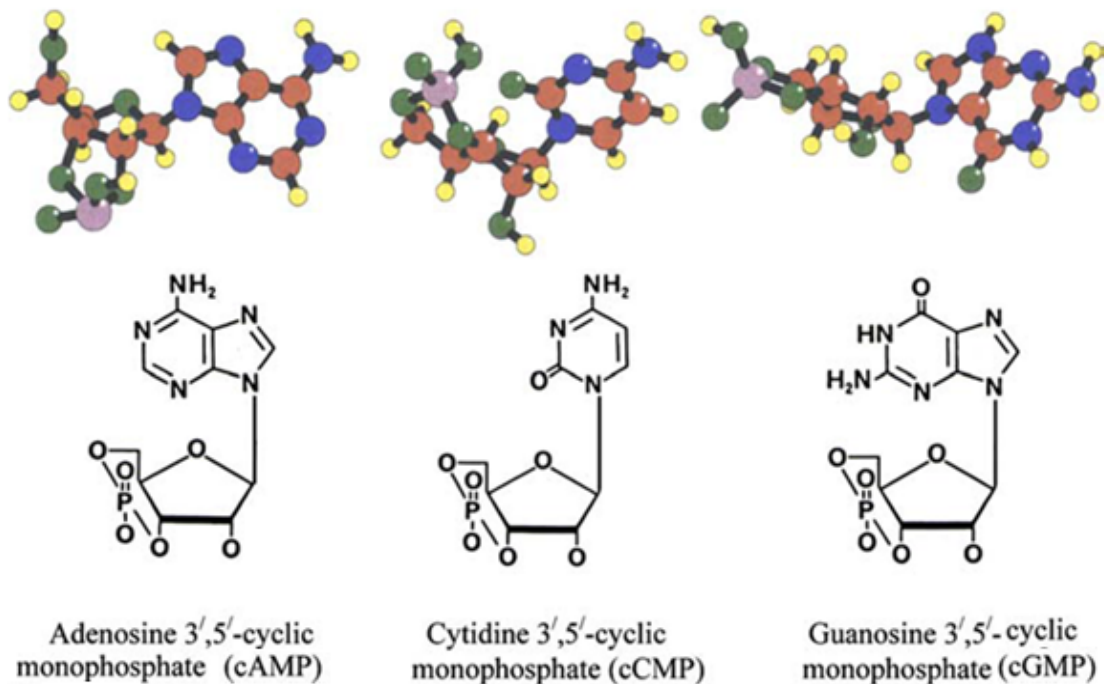


Figure 1.3: Structural conformations of the second messengers (cyclic nucleotides). The top diagram represents the physical structures of the cyclic nucleotides in a ball and stick format and at the bottom is their chemical representation (adapted from (Newton and Smith, 2004)).

Cyclic GMP has been reported to function as a second messenger in diverse physiological processes in plants (Meier et al., 2009) including NO-dependent signalling (Prado et al., 2004) and in mediating responses to abiotic and biotic stresses such as the response to pathogens (Delledonne et al., 1998) and increasing salt stress tolerance in plants (Maathuis and Sanders, 2001). Cyclic AMP is implicated in similar roles and this is in line with the cyclic nucleotide monophosphate-dependent decreases of channel open-probabilities and reduced influx of Na^+ . Cyclic nucleotides are involved in many growth and developmental processes in plants such as (1) cGMP acting as a second messenger in hormone dependent signalling such as auxin-induced root growth (Penson et al., 1996), and (2) cAMP as a second messenger in pollen tube growth and re-orientation (Moitinho et al., 2001).

In summary, cyclic nucleotide monophosphates play a crucial role in controlling ion homeostasis, and it has been shown that both cAMP and cGMP increase Ca^{2+} influx in carrots and in tobacco protoplast respectively (Kurosaki and Nishi, 1993; Volotovski et al., 1998). Although there is evidence of cGMP/NO mediated signalling, a cGMP synthesising GC that is NO-dependent has not yet been reported in plants.

1.5 Heme sensor family of proteins

Heme-containing enzymes are a diverse group of molecules which bind to gases such as O_2 , NO and carbon monoxide (Chan, 2001; Pellicena et al., 2004). They are made up of two distinctive domains; the heme sensor domain (for binding gases) and the effector domain (for generating an output signal) (Pellicena et al., 2004). Heme sensors family of proteins are divided into four groups, including the bacterial oxygen sensor (FixL), HemAT, the CO sensor, CoxA from *Rhizospirillum rubrum*, and the soluble GC. These proteins are characterised by the same heme group consisting of a protophophyrin IX ring ligated to a histidine residue (Figure 1.4) however, they contain different heme-binding properties (Pellicena et al., 2004).

The FixL family of heme proteins are multi-domain proteins located in the cytoplasm and characterised by a PAS (domains containing two direct sequence repeats {S1 and S2 boxes} of ~50 residues each) domain fold. They consist of the heme sensor and the histidine kinase domain which is required for O_2 responsive transcriptional regulation. FixLs bind to either NO and/or CO, however the heme/NO recombination reaction occurs before NO diffuses out

of the heme pocket (Rodgers and Lukat-Rodgers, 2005). In turn, the HemAT family contains a globin fold, which usually consists of eight α -helices at the end of the chain that are anti-parallel, forming a helix-turn motif. Examples of protein which form the globin fold are haemoglobin and myoglobin (Gong et al., 1998; Miyatake, 2000).

The CO sensors, CooA include the bacterium *Rhodospirillum rubrum* and belong to the cAMP receptor protein family of transcriptional regulators and its fold is different from the PAS and globin domains. CooA is a 24.6 kDa protein that is made up of a sensor at the N-terminus and a DNA-binding domain. CooA is a member of the family of single-component regulators, including the fumarate nitrated reduction and the cAMP receptor proteins, which recognise specific DNA sequences upon uptake of effector molecules such as CO or sensing O₂ to form a six- and a five-coordinate with both gases respectively. CooA is important for CO-dependent expression of the two operons that encode the enzyme system for CO oxidation (Gong et al., 1998; Rodgers, 1999; Lanzilotta et al., 2000; Miyatake, 2000).

Soluble GCs are a group of signal transduction proteins that sense NO. A common structure of soluble GCs from the vertebrates is a heterodimer consisting of α - (~73-88 kDa) and β - (~70 kDa) subunits, with their protoporphyrin IX ring located at the N-terminus of the β -subunit. Soluble GCs are different in sequence to the bacterial oxygen sensor, HemAT, and the CooA heme domains (Wedel et al., 1994; Shelver et al., 1997; Zhao et al., 1998). Upon binding to NO, soluble GCs are activated significantly by small concentrations, which activate them to synthesise cGMP from GTP (Boon et al., 2005). Homologs of soluble GC have recently been identified in prokaryotes using the HNOX approach (Boon and Marletta, 2005b), these heme domains are characterized by a conserved **Y-x-S/Tx-R** motif in the

histidine heme binding ligand (Boon and Marletta, 2005b). The consensus sequence for the motif is: Hx{12}Px{14,16} YxS/TxR, where x is any amino acid and the numbers in the curly brackets represents the length of the gap. Members of the HNOX domains are found in mammalian cyclases, *Drosophila* and facultative aerobes. The heme domains from the facultative aerobes form part of the histidine kinase operon, and predicted to bind NO but not O₂ a case which is similar to the mammalian sGCs. In contrast to that, a homolog from the prokaryotic obligate anaerobe predicted as a methyl-accepting chemotaxis, showed affinity to both NO and O₂. Examples of the NO and O₂ binding domains include the *Thermoanaerobacter tengcongensis* an obligate anaerobe and the *Caenorhabditis elegans* sGC (GCY-35). The NO and O₂ binding domain were collectively referred to as the heme-nitric oxide and/or oxygen (HNOX) binding domain. These HNOX domains are characterised by a conserved tyrosine, which is not found in other heme proteins that shows no affinity to oxygen. Structural characterization using x-ray crystallization and spectroscopy showed that the conserved tyrosine forms a stable hydrogen bonding with oxygen, and this was confirmed by mutational studies which showed that tyrosine 140 in *Thermoanaerobacter tengcongensis* plays an important role in ligand discrimination against NO (Pellicena et al., 2004).

1.5.1 The heme environment

The heme group from the heme domain of *Thermoanaerobacter tengcongensis* is coordinated to β -subunit via the proximal ligand His 105 together with the heme binding residues Tyr 135, Ser 137 and Arg 139 forming the Y-x-S-x-R motif. In the HNOX domain, the propionate groups of the heme are normally buried and tightly bound by amino acid side chains including the most important Y-x-S-x-R motif (Pellicena et al., 2004). His 105 was recognised as the only proximal ligand to the heme, until recently when Rothkegel and co-workers showed that Tyr, Ser and Arg are required as propionic acid groups in the heme moiety. This was confirmed by a homology model from rat soluble GC. This model together with mutational studies added that Arg 139 forms hydrophobic interaction with Asp 44 and other hydrophobic residues (Asp 45 and Phe 74) lining the heme pocket (Figure 1.4). It was also noted that these residues are important in signal transduction upon binding of NO to the heme (Rothkegel et al., 2006).

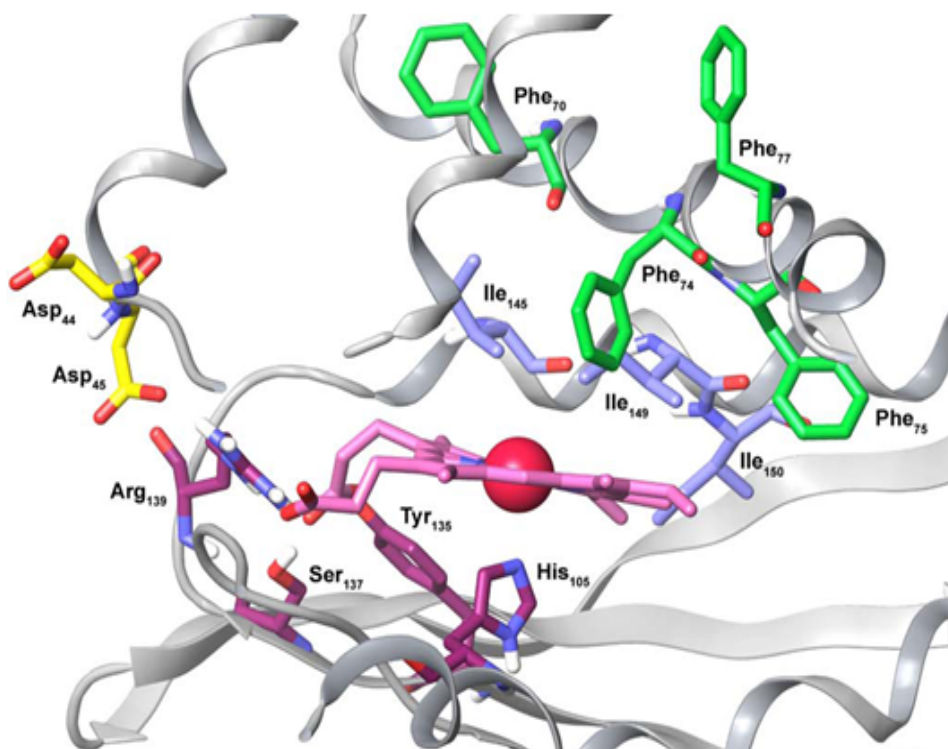


Figure 1.4: Structure model of the heme-binding pocket from rat soluble GC. The heme-binding motif Y-x-S-x-R (Tyr 135, Ser 137 and Arg 139) and the proximal ligand (His 105) are shown in magenta. The residues which form hydrophobic interactions with Arg 139 are shown in yellow (Asp 44 and Asp 45). Residues in close proximity to the heme pocket are also indicated (adapted from (Rothkegel et al., 2006)).

1.6 Flavin-containing monooxygenase family of proteins

Flavin-containing monooxygenases (FMO) are a family of enzymes that catalyse the transfer of one molecule of oxygen to low molecular weight substrates, in the presence of NADPH as the co-factor and the reduction of another molecule to water (Schlaich, 2007). FMOs have been identified in animals, bacteria, yeast and plants. There are five genes encoding FMOs in animals (FMO1-5), one gene in yeast, several in bacteria, and plants are reported to contain the largest number of genes encoding the FMO proteins as compared to other species. To date, the Arabidopsis plant encodes 29 FMO-related genes, suggesting that plants might conduct a wide variety of functions using FMOs (Schlaich, 2007).

1.6.1 Structure of FMOs

FMO genes generally encode proteins of ~50 kDa, which bind flavin adenine dinucleotide (FAD) with a conserved 'GxGxxG' motif known as the Rossmann fold (Eswaramoorthy et al., 2006). The FAD binding motif is located at the N-terminus, followed by the nicotinamide adenine dinucleotide phosphate-binding (NADP) motif (GxGxxG) located at the centre of the protein (Stehr et al., 1998). The NADP-binding motif is similar to the FAD motif however, less conserved among the FMOs. Another motif is, the 'FATGY' located towards the C-terminus of the protein and this motif occurs in enzymes which oxidise nitrogen-containing substrates. The 'FATGY' motif is well-conserved amongst the bacterial, yeast and animal kingdoms. Arabidopsis exhibits two different kinds of motifs with the 'LATGY' motif found in 11 FMOs (also known as YUCCA FMOs) and the 'HCTGYK' motif which occurs in the other 16 Arabidopsis genes. The 'HCTGYK' motif shares three similar amino acids with the 'LATGY' motif, however, they differ in their location with the 'HCTGYK' and 'LATGY' motifs, where the amino acids occur before and after the FMO-identifying sequence ('FxGxxxHxxxY/F') respectively. The FMO identifying sequence is present in all known FMOs in plants and is found at different locations (Figure 1.3) (Stehr et al., 1998; Fraaije et al., 2002).

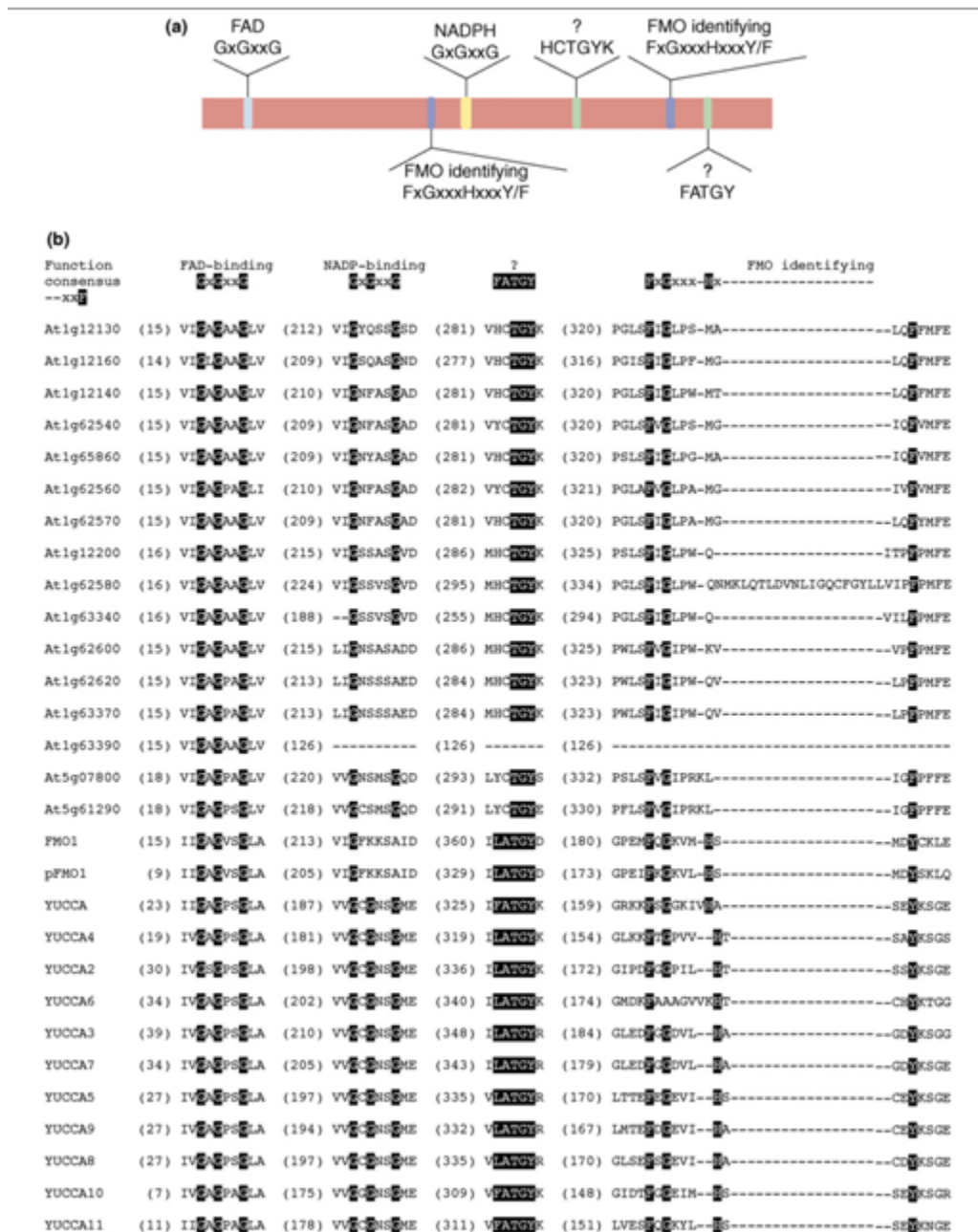


Figure 1.5: Domain organisation and the alignment of different motifs of the FMOs found in *Arabidopsis thaliana*. (A) The FAD-binding (GxGxxG), the NADPH-binding (GxGxxG), the ‘FATGY/LATGY/HCTGYK’ and the FMO identifying motifs and their locations are indicated. The locations of the ‘FATGY/LATGY/HCTGYK’ and the FMO identifying motifs are different for every FMO gene. (B) Alignment of the *Arabidopsis thaliana* FMO genes showing the locations of the different motifs (adapted from (Schlauch, 2007)).

1.6.2 Functions of FMOs

FMOs appear in the 4 α -hydroperoxy flavin (FAD) form which gives them a large range to interact with a number of substrates. In animals, FMOs are thought to produce ROS, like monooxygenases, and they are implicated in the metabolism of xenobiotic compounds and variability of drug responses. Yeast FMOs have a key role in oxidizing biological molecules which in turn facilitate the processes of protein folding and cellular responses to reductive stress. Unlike mammalian FMOs, yeast FMOs do not oxidize nitrogen-containing substrates, rather use O₂ and NADPH to oxidize thiol compounds such as cysteamine, glutathione and cysteine (Suh et al., 1999). Yeast FMO is also implicated in redox regulation (Suh et al., 2000). Functional roles in plants indicate that FMOs play crucial roles such as catalysing auxin-biosynthesis (Zhao et al., 2001) and a role in pathogen defence (Bartsch et al., 2006). Since a number of genes have been annotated as FMOs in plants, this also suggests that a number of physiological roles are yet to be discovered.

1.7 Objectives of the study

The main aim of this research was to characterise the functions and structure of the novel signalling molecule from *Arabidopsis thaliana*, the *AtNOGCI*.

1.7.1 Specific objectives

1. To recombinantly express the *AtNOGCI* as 6x His-SUMO fusion protein and purify under native conditions using the Ni-NTA affinity system together with the application of the anion exchange chromatography system

2. To investigate the mechanism by which AtNOGC1 binds to NO and/or O₂ using cyclic voltammetry and square wave voltammetry.
3. To demonstrate that *AtNOGCI* catalyse the synthesis of cGMP from GTP *in vitro* using GC activity assays.
4. To build homology models of *AtNOGCI* a flavin containing monooxygenase and At5g57690 a diacylglycerol kinase using homology modelling, and also predict their secondary structure using PSI-PRED server.

CHAPTER 2: Identification of *AtNOGCI* and the Production of a Recombinant Protein for Functional Studies

Abstract

Various molecular and physiological processes influenced by NO and cGMP signalling in plants have been reviewed. These include regulation of intracellular Ca²⁺ concentrations and protein kinases, modulation of plant responses to pathogens, promotion of stomatal closure and regulation of plant responses to abiotic stress. Several guanylyl cyclases have been identified in plants, which include the AtGC1, the AtBRI1, and the AtWAKL10. However, none of these molecules require NO for GC activation. In an attempt to bring insight and understanding of the NO/cGMP mediated processes, a novel plant signalling molecule was identified from *Arabidopsis thaliana*, *AtNOGCI*, which contain a heme-binding motif and a GC motif. Molecular characterization of its NO binding properties together with its GC activity would contribute greatly to the understanding of these processes. In order to investigate and demonstrate these functional properties the *AtNOGCI* protein was expressed as a 6xHis-SUMO fusion protein and purified under native conditions using the Ni-NTA affinity system. The purification was completed using an anion exchange chromatography system.

2.1 Introduction

Recombinant protein expression is an important means to discover how protein structures and functions are related. Proteins are usually engineered to be expressed in a suitable expression host such as *E. coli* and as fusion proteins, usually tagged with glutathione-S-transferase (GST) (Smith and Johnson., 1988), a 6xHis tag, a small ubiquitin like modifier (Marblestone et al., 2006), thioredoxin (LaVallie et al., 1993) and sometimes, a maltose binding protein (Kapust and Waugh, 1999). The above mentioned systems increase the solubility and purity of the expressed target protein and also associated with a single purification step however, the 6xHis tag expression system usually requires additional steps. The 6xHis tag is one of the most extensively used system for the expression and purification of recombinant proteins and provides an integrated system for the expression, purification and detection of 6xHis fusion proteins (QIAexpressionist., 2003).

Though the production of recombinant proteins in *E. coli* is well established, successful preparation of pure soluble fusion proteins tends to be difficult (Smith and Johnson., 1988). However, the presence of strong promoters, which are induced by high concentration of inducers such as isopropyl-1-thio-D-galactopyranoside (IPTG), amino acids and L-arabinose, causes proteins to accumulate in inclusion bodies, making the purification of a stable native protein difficult. For this reason, one of the pET vectors was modified to include a small tag, the ubiquitin-like modifier (ChampionTM pET SUMO). The ChampionTM pET SUMO expression vector system was used for high level protein expression and purification. This expression system utilizes an 11 kDa protein known as the small ubiquitin-like modifier (SUMO). The SUMO-based expression system increases the solubility of recombinant

proteins and also decreases proteolytic degradation that is often associated with recombinant protein expression. The SUMO moiety is easily separated from the target protein using a SUMO protease (ULP-1) which cleaves at the carbonyl terminal of SUMO (Invitrogen, Life technologies; Catalogue#: K300-01). In addition to the SUMO fusion, the Champion™ pET SUMO vector also contains a T7 *lac* promoter which yields high levels of expression of the target protein. Figure 2.1 shows the features of the Champion™ pET SUMO expression vector system.

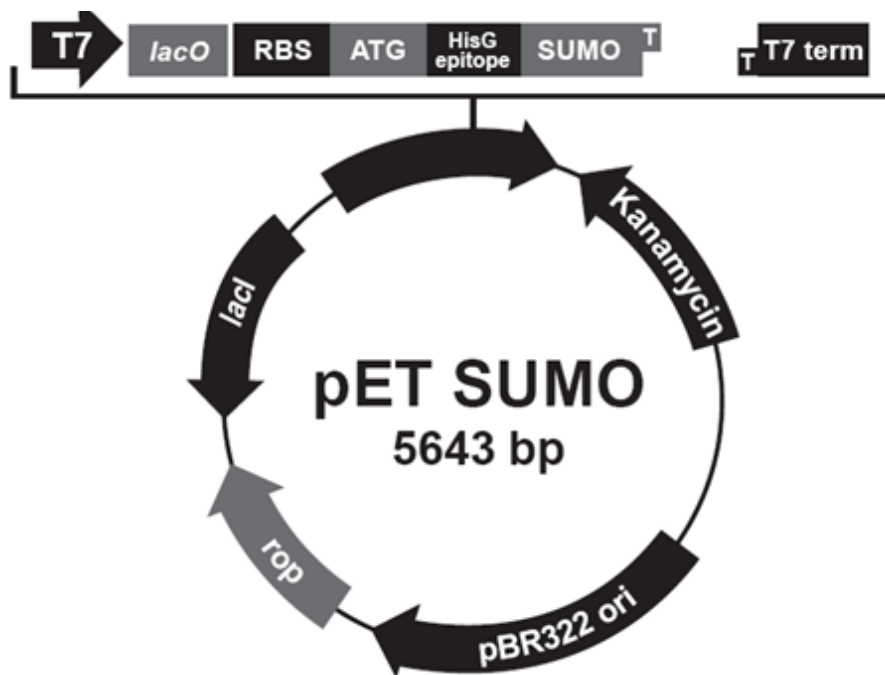


Figure 2.1: Circular map of the Champion™ pET SUMO expression vector. The map shows the T7 *lac* promoter which increases expression of high levels of proteins under induction by IPTG, and the 6xHis-tag, which facilitate purification using the Ni-NTA purification system. The 11-kDa SUMO fusion tag enhances the solubility of expressed proteins (Invitrogen, Life technologies).

Functional studies may require large amounts of soluble recombinant protein that has been purified to electrophoretic homogeneity. Therefore, optimization and determination of a

purification system that is efficient is a critical step in the process of preparation of the recombinant proteins. Affinity chromatography is a powerful tool for purifying these recombinant proteins from crude extracts to a nearly homogenous preparation in a single step. It takes advantage of the biological properties of the sample to be purified, and utilizes specific reversible interactions between biomolecules. However, most naturally occurring proteins lack tags which would allow purification by affinity purification, so they require modification through addition of either N- or C- terminal tags such as those mentioned above. Because of its small size and the simplicity that goes with its incorporation, the 6xHis tag is widely used for the purification of recombinant proteins and is less likely to interfere with protein structure and function (Niiranen et al., 2007).

Immobilized metal affinity chromatography (IMAC) utilizes the coordination of transitional metals ions and amino acids such as histidine, cysteine and tryptophan (Deutscher, 1990). Some bacterial proteins contain a high number of histidine residues in their sequences which bind to Ni-NTA columns, leading to poor purification of the target protein. Since a single step purification of a 6xHis-tagged protein is not sufficient to yield a pure sample ready for further characterization, a second or a third step of purification is often required to obtain a pure sample of the target protein. Ion exchange chromatography (IEC) is one of the methods that are employed as a second or final step of purification to obtain pure protein samples. IEC uses an insoluble matrix that carries ionic charges that retard the movement of molecules of opposite charge, thus proteins are separated depending on their electrostatic properties. Binding of the target protein to the column is ensured by choosing a buffer that will confer an opposite net charge to the target protein to that of the column matrix (Deutscher, 1990).

This chapter describes the verification of the cloned *AtNOGCI* in the pET SUMO expression vector using PCR, restriction double digestion and DNA sequencing. Recombinant expression and purification of the recombinant *AtNOGCI* will also be discussed.

2.2 Materials and Methods

2.2.1 Identification of AtNOGC1

In order to discover candidate GCs with NO-binding domains, an extended consensus motif (Hx₁₂Px_{14,16}YxSxR) motif was deduced and then applied to search for conserved HNOX domains and identified a novel plant signalling protein in *Arabidopsis thaliana*, which was termed *AtNOGC1* for *Arabidopsis thaliana* a Nitric Oxide binding with a guanylyl cyclase activity (TAIR protein locus At1g62580, GenPept accession number, NP_176446).

2.2.2 Verification of the correct *AtNOGC1* gene

The *AtNOGC1* expression construct, pET SUMO-*AtNOGC1*, was a generous gift from Dr. M. Morse (Department of Molecular Cell Biology, University of Cape Town). Verification of the correct *AtNOGC1* insert was done by a combination of PCR amplification using *AtNOGC1*-specific oligonucleotide primers, restriction endonuclease double digestion and DNA sequencing.

2.2.2.1 Re-amplification by polymerase chain reaction (PCR)

Primers for PCR amplification were designed based on the *Arabidopsis thaliana*, At1g62580 gene mRNA isoform sequence (TAIR protein locus At1g62580, GenPept accession number, NP_176446). The forward primer incorporated a *Bam* HI restriction site: *AtNOGC1* fwd (5'-gat gga tcc atg gta cca gca gta aat cct-3'), while the reverse primer incorporated an *EcoR* I restriction site: *AtNOGC1* rev (5'-gct aga att ctc agc ttg tat att ctc ttt cga-3'). PCR

amplifications were carried out in reactions containing 12.5 μL of DreamTaq master mix (Fermentas, Life Sciences), 1 μL each of 10 μM primers and 1 μL of the template pET SUMO-*AtNOGCI* plasmid DNA. The final volume was made up to 25 μL with sterile, nuclease-free water. The PCR tubes were briefly centrifuged and the amplification was carried out under the following conditions: 96 °C for 2 min to denature the double stranded DNA, followed by 25 cycles each consisting of the following steps: 94 °C for 1 min to denature the double stranded DNA, 60 °C for 1 min to anneal the double strands, 72 °C for 1 min to extend the DNA. The final step consisted of holding the tubes at 72 °C for 10 min. The products were analysed on 0.8 % agarose gels.

2.2.2.2 Restriction digestion

A double restriction digest was conducted to release the insert and check the correct size of the *AtNOGCI* gene. The restriction digest reaction was conducted in a reaction containing 5 μg vector (pET SUMO-*AtNOGCI*), 4 μL 10x FastDigest® Green Buffer, 1 μL each of the FastDigest® *Bam* HI and *EcoR* I enzymes (Fermentas, Life Sciences) and the volume was made to 20 μL using nuclease-free water. The reagents were mixed gently in a 1.5 mL microfuge-centrifuge tube, centrifuged for 1 min and incubated at 37 °C for 30 min. After incubation, the enzymes were inactivated by heating for 5 min at 80 °C. The samples were then analyzed by electrophoresis on a 0.8 % agarose gel.

2.2.2.3 DNA sequencing

The plasmid pET SUMO-*AtNOGCI* was transformed into MC1061 cells, and plated on Luria Bertani (LB) agar plates containing 50 µg/mL kanamycin. Plates containing single colonies were sent for sequencing at Inqaba Biotechnical Industries (Pty) Ltd. Validation of the base calling was performed by inspection of the raw sequencing trace, using the Finch TV software suite (<http://www.geospiza.com/finchtv>). Sequences were compared with the expected sequences using the Blast 2 sequence alignment tool (<http://www.ncbi.nlm.nih.gov/BLAST/bl2seq/wblast2.cgi> (Tatusova and Madden, 1999)). Translations into protein sequences were carried out using the EXPASY Translate Tool (<http://au.expasy.org/tools/dna.html>).

2.2.3 Plasmid DNA isolation

Small scale plasmid DNA isolation was performed using the alkaline lysis method (Birnboim and Doly, 1979). A single colony was used to inoculate 5 mL LB broth containing 50 µg/mL kanamycin and incubated overnight at 37 °C with shaking at 200 rpm. From the overnight culture, 900 µL was added to 100 µL of sterile glycerol for storage at -70 °C. The remaining cell suspension was centrifuged at 5000 *g* for 10 min and the supernatant discarded. Extraction and purification of the plasmid DNA was done using the peqGOLD Plasmid Miniprep Kit I (peqLab, Biotechnologie GmbH).

2.2.4 Production of the recombinant protein

2.2.4.1 Transformation of plasmid DNA into competent cells

Competent cells were thawed on ice for 5 min and 2 μL of the pET SUMO-*AtNOGCI* plasmid was added into 50 μL of *E. coli* BL21 pLysS competent cells followed by an incubation on ice for 30 min. The cells were heat-shocked at 42 °C for 45 sec and incubated on ice for a further 2 min. Then 900 μL of pre-warmed LB was added and the tubes incubated at 37 °C for 1 h with shaking. Hundred μL of the culture was plated on LB agar plates containing 50 $\mu\text{g}/\text{mL}$ kanamycin and incubated at 37 °C overnight. For the controls, untransformed cells were also plated on LB plates with or without the antibiotic.

2.2.4.2 Expression of recombinant *AtNOGCI*

The plasmid pET SUMO-*AtNOGCI* was transformed into *E. coli* BL21 cells, and single colonies containing the pET SUMO-*AtNOGCI* expression plasmid were then inoculated into 100 mL of LB broth containing 50 $\mu\text{g}/\text{mL}$ kanamycin and 34 $\mu\text{g}/\text{mL}$ chloramphenicol. The culture was incubated at 37 °C overnight with shaking. The following morning, the overnight culture was then scaled-up to 1000 mL by addition of 900 mL media containing the same concentrations of antibiotics and again, incubated at 37 °C with shaking until an optical density of 0.5 at 600 nm was reached. Induction of protein expression was then done at this optical cell density at an induction temperature of 30 °C and by adding isopropyl-1-thio-D-galactopyranoside at a final concentration of 2 mM for 2.5 h. Following induction, the

bacterial cells were recovered by centrifugation at 5000 *g* for 10 min at 4 °C and the pellet stored at -20 °C until needed.

2.2.4.3 Affinity purification of His-tagged proteins using a Ni-NTA column

2.2.4.3 1 Preparation of the cleared lysate

The frozen cell pellet was thawed on ice and re-suspended in 10 mL lysis buffer (50 mM sodium phosphate, pH 8.0; 300 mM NaCl; 20 mM β -mercaptoethanol; 0.1 % Triton x100; 50 μ g/mL lysozyme; 1x protease inhibitors cocktail). The suspension was incubated at 4 °C for 1 h while shaking. The mixture was sonicated for a total of 4 min (30 sec power on-off cycles) followed by centrifugation for 30 min at 5 000 *g*. The supernatant was then transferred to a fresh tube and stored at -80 °C until further purification.

2.2.4.3 2 Purification

Purification of *AtNOGCI* was undertaken on a Ni-NTA affinity system (Lindwall et al., 2000; Stempfer et al., 1996) under native conditions (QIAexpressionist., 2003). The His-select nickel affinity gel is an immobilized metal ion affinity chromatography (IMAC) product. The affinity gel is supplied as a 50 % suspension in 30 % ethanol. In this study, the affinity gel was re-suspended thoroughly and an appropriate aliquot removed and poured gently into a 20 mL disposable plastic column to make up a 5 mL gel column volume. The gel was washed with 2 column volumes of distilled H₂O to remove the ethanol. The affinity gel was equilibrated with 3 column volumes of equilibration buffer (50 mM NaH₂PO₄, 300 mM NaCl, 30 mM Imidazole, and pH adjusted to 8.0 with NaOH). Ten mL of the protein

sample was added to the column and the flow through collected. The column was then washed with 5 column volumes of wash buffer and the flow through collected. To elute the retained fusion protein, 1 column volume of elution buffer (50 mM NaH₂PO₄, 300 mM NaCl, 250 mM Imidazole and pH adjusted to 8.0 with NaOH) was added to the column and the flow through collected in 5 mL fractions. Finally the column was washed with 5 column volumes of 2 M NaCl and stored in 20 % ethanol at 4 °C.

2.2.4.4 Anion exchange chromatography

Anion exchange chromatography was carried out using a MonoQ anion exchanger (GE Healthcare) in the column formats HR 5/5 and HR 10/10. The buffer used was 50 mM Tris-Cl, pH: 8.0 flowing at a rate of 1.5 mL/min. The instrument was operated using a pre-programmed sequence comprising of a 10 column volume equilibration step, a sample injection step, a 10 column volume washing step, a 15 column volume of 0-0.5 M NaCl gradient spanning step, and a final washing step consisting of 5 column volumes of 1 M NaCl. Eluted proteins were monitored at λ_{280} using an in-line UV detector and the NaCl concentration were monitored using an in-line conductivity meter. Some 2 mL fractions were collected using a GILSON® FC-203B automated fraction collector and the presence of eluted proteins was confirmed by analysing fractions on SDS-PAGE gels.

2.2.5 SDS-PAGE gel electrophoresis of proteins

Proteins were analysed by both one dimensional and two dimensional SDS-PAGE on 16 % polyacrylamide gels following the Laemmli's method (Laemmli, 1970).

2.2.5.1 1D electrophoresis of proteins

The separating gel was prepared from 8 mL 40 % 37:5:1 polyacrylamide, 0.12 mL 10 % APS, 0.21 mL 10 % SDS, 5.25 mL separating buffer, 0.021 mL TEMED and the volume was made up to 20 mL using distilled water. The stacking gel was prepared from 1.5 mL 40 % 37:5:1 polyacrylamide, 0.05 mL 10 % APS, 0.1 mL 10 % SDS, 2.5 mL stacking buffer, 0.02 mL TEMED and the volume made up to 10 mL using distilled water.

Samples were mixed with equal volumes of 2 x SDS sample buffer, incubated on a heating block at 100 °C for 10 min and centrifuged at full speed. The samples were then electrophoresed at 1-10 V/cm using a Hoefer Mighty Small II gel electrophoresis system. Once the dye front had reached the end of the gel, the gel was removed from the apparatus and incubated in Coomassie staining solution for 30 min. Thereafter, it was transferred into a destaining solution until the background was clear.

2.2.5.2 2D electrophoresis of proteins

2.2.5.2.1 Rehydration of the strips

Protein samples which were originally in Na-phosphate buffer were precipitated by adding 4 volumes of ice cold acetone. The samples were vortexed and incubated at -20 °C for 1 hr and centrifuged for 10 min at 13 000 xg. The supernatant was discarded carefully without disturbing the pellet, and the acetone was allowed to evaporate at room temperature for 30 min. Protein extracts (100-150 µg) were mixed with 2 µL of 50 % (v/v) DTT, 1.25 µL of 0.2 % (v/v) ampholytes (BIORAD), a pinch of bromophenol blue and made up to a final volume of 125 µL with urea buffer pH 8.0. The samples were mixed by vortexing and pulse-spinned using a bench top microfuge (Eppendorf-Nerthelends; Germany) and then placed in individual channels of an Immobiline™ Dry Strip Reswelling Tray (GE healthcare, Amersham, UK). Linear 7 cm Ready IPG strips of pH range 4-7 (BIO-RAD) were carefully placed on top of the sample, gel side being directly in contact with the sample and avoiding trapping any air bubbles. The strips were then covered with mineral oil (PlusOne DryStrip Cover Fluid; GE Healthcare) to prevent sample evaporation during the rehydration process and left to passively re-swell to their original gel thickness of 0.5 mm for at least 15 h at room temperature.

2.2.5.2.2 First dimensional IEF of IPG Strips

After rehydration, the IPG strips were briefly rinsed with distilled water to remove unabsorbed protein sample and carefully blotted with moist filter paper. The strips were then placed gel side up on the focusing platform of an Etan™ IPGphor II™ (GE Healthcare, Amersham, UK) system. Moist wicks were placed at the extreme ends of both the anodic and

cathodic ends of the IPG strips to collect excess salts and impurities from the sample during focusing. The IPG strips were then covered with mineral oil to avoid sample evaporation and carbon dioxide adsorption during focusing. Isoelectric focussing was then performed in a three phase step-wise programme at 20 °C and according to the following conditions: Step 1 at 250 volts for 0.15 h; step 2 at 4000 volts for 1 h and finally, step 3 at 4000 volts for 12000 volt h.

2.2.5.2.3 Equilibration of IPG strips

After IEF, IPG strips were equilibrated in SDS containing buffer in order to solubilise focussed proteins and allow SDS binding prior to second dimension SDS-PAGE. The focused IPG strips were then incubated gel side up in re-swelling tray channels containing 2.5 mL equilibration buffer (6 M urea; 2 % (w/v) SDS; 50 mM Tris/HCL, pH; 8.8 and 20 % (v/v) glycerol) and 2 % DTT for 15 min. The focused IPG strips were again equilibrated for another 15 min in the same buffer contents containing 2.5 % (w/v) iodoacetamide instead of DTT with gentle agitation at room temperature. After equilibration of the isoelectric focused samples, the proteins were ready for second dimension analysis on a mini format SDS-PAGE gels.

2.2.5.2.4 Second dimension SDS-PAGE for mini format gels

Twelve % SDS-PAGE gels were prepared as described in Section 2.2.4.1. The equilibrated IPG strips were then gently rinsed with 1 X SDS-PAGE running buffer and placed on top of the 12 % SDS-PAGE resolving gels with the plastic backing against the spacer plates. Five µL of Pre-stained Page Ruler ladder (Fermentas, Life sciences) were spotted on small pieces of filter paper, air dried and placed at the anodic side of each IPG strip. The IPG strips were

then overlaid with 1 mL of 0.5 % molten agarose prepared in 1 X SDS-PAGE running buffer containing a pinch of bromophenol blue, which was used as a migration tracking dye during electrophoresis. Electrophoresis was then carried out using a Hoefer Mighty Small II gel electrophoresis system, at 100 V for the first 30 min and then at 150 V until the bromophenol dye had reached the bottom of the glass plates. After electrophoresis, the gels were stained with Coomassie Brilliant Blue as described in Section 2.2.5.1

2.2.6 Determination of protein concentration using the Bradford assay

Protein concentrations were determined using the Bradford Assay with BSA as a standard as shown in Appendix III:Table 2.1. From a stock solution of 1 mg/mL BSA, a serial dilution was made in the range of 20 µg/mL to 125 µg/mL, using the same buffer as the one used for the sample. The protein sample was diluted to a 1:10 dilution; 200 µL each of the sample and the standard were then added in duplicate to a cuvette. 800 µL of the Bradford reagent was then added to each cuvette and the samples allowed to stand for 5 min at room temperature. The absorbance was measured at 595 nm using a spectrophotometer (Thermo Spectronic, Germany). The average of each pairs of duplicates was calculated and the standard curve plotted using Microsoft Office Excel 2007. The concentration of the *AtNOGCI* protein was also determine by measuring its absorbance at 280 nm (A_{280}) using a NanoDrop® ND 1000 spectrophotometer (Nano Drop technologies, Inc). In this case, a 2 µL sample was used for each measurement and the spectrophotometer calibrated using the same buffer as was in the assayed sample.

2.3 Results

In order to study the novel signalling protein (*AtNOGCI*) at a molecular level, the gene encoding the *AtNOGCI* protein was amplified and cloned into the Champion™ pET SUMO expression vector system. The recombinant protein was expressed as a His-SUMO fusion protein, using the Champion™ pET SUMO expression System (Catalogue #: K300-01). The pET SUMO expression vector contains the T7 *lac* promoter which under IPTG induction, drives the expression of soluble recombinant proteins at high levels, and soluble fusion proteins are obtained due to the presence of a small ubiquitin-related modifier, SUMO. The N-terminal 6xHis tag allows for affinity purification using the Ni-NTA column.

2.3.1 Identification of *AtNOGCI* and prediction of its parameters

The search for a consensus term for use to identify candidate Arabidopsis HNOX proteins yielded a motif that occurs in four Arabidopsis proteins, one of which is annotated as FMO (Figure 2.2). Incidentally, this protein also contains the 14 amino acid core motif (Figure 2.2) found in currently annotated and experimentally tested plant GCs (Ludidi and Gehring, 2003; Kwezi et al., 2007; Meier et al., 2010).

Prediction of protein molecular weights, pI and nitrogen content were made using the online server EXPASY Ttranslate Tool (<http://au.expasy.org/cgi-bin/protparam>). Figure 2.3 shows the parameters for *AtNOGCI*. The *AtNOGCI* gene encodes a protein of 56739.2 Da, comprising of 497 amino acids. The pI of the protein is predicted to be 5.82 and the amino acid composition is also shown in Figure 2.3.

H-NOX motif: $Hx\{12\}Px\{14,16\}YxSxR$ **Relaxed GC motif:** $[RKS]x[GCTHS]x\{9,10\}[KR]$

5'
 -MVPVAVNPPTTNSHVAVIGAGAAGLVAARELRREGHSVVVFERGNHIGGV
 WAYTPNVEPDPLSIDPTRPVIHSSLYSSLRTIIPQECMGFTDFPFSTRLE
 NGSRDPRRHPPGHSEVLAYLRDFVREFKIEEMIRFETEVVRVEQAGENPKK
 WRVKSRNFGDISDEIYDAVVVCNGHYTEPRHALIPGNKINH **SFSIGLGID**
TWPGKQIHSHNYRVPEQVKDQVVVIGSSVSGVDISRDIANVTKEVHISS
 RSTKPETYEKLPGYDNLWLHSNIETVREDGSVVFKNKGTVYADTIMHCTG
 YKYYFPFLDTKGEVTVEDNRVGPLYKHVFPPALSPGLSFIGLPWQNMKLO
 TLDVNELIGQCFGYLLVIPPMPFELQSKWVAAVLAGRVSLPSQEEMEDTK
 MFYLKLEASCIPKRYTHLMAELDSQFVYNNWLADQCDYPRIEKWREQMFY
 KVFKRIQSQASTYKDDWDDDHLIAEAYEDFVKFPSNYPSSLIEREYTS--

Figure 2.2: Sequence of the *Arabidopsis thaliana* NO-binding protein *AtNOGCI*. The HNOX (H-x{12}-P-x{14,16}-Y-x-S-x-R) motif ("x" stands for any amino acid and curly brackets indicate the gap size) is highlighted in blue and the GC catalytic centre (SFSIGLGIDTWPGK) is highlighted in red. The putative metal-binding residues that take part in GC catalysis are highlighted in aquamarine. The black arrow points to the PPI-binding residue and the green arrows indicate exon borders.

```

Number of amino acids: 497

Molecular weight: 56739.2

Theoretical pI: 5.82

Amino acid composition

Ala (A) 24 4.8% Lys (K) 25 5.0% Arg (R) 28 5.6% Met (M) 10 2.0%
Asn (N) 21 4.2% Phe (F) 23 4.6% Asp (D) 28 5.6% Pro (P) 32 6.4%
Cys (C) 6 1.2% Ser (S) 37 7.4% Gln (Q) 15 3.0% Thr (T) 24 4.8%
Glu (E) 37 7.4% Trp (W) 9 1.8% Gly (G) 30 6.0% Tyr (Y) 23 4.6%
His (H) 17 3.4% Val (V) 46 9.3% Ile (I) 29 5.8% Pyl (O) 0 0.0%
Leu (L) 33 6.6% Sec (U) 0 0.0%

(B) 0 0.0% (Z) 0 0.0% (X) 0 0.0%

Total number of negatively charged residues (Asp + Glu): 65
Total number of positively charged residues (Arg + Lys): 53

Atomic composition:

Carbon      C      2558
Hydrogen    H      3909

```

Figure 2.3: Determination of the *AtNOGCI* protein parameters from the expasy server. *AtNOGCI* is made up of 497 amino acid residues, with a molecular weight of ~56.7 kDa. The protein's pI is determined to be 5.82 and an extension coefficient of 83770 M⁻¹cm⁻¹ (predictions are made by the expasy server: <http://www.expasy.org/tools/protparam.html>, full detailed information is available in the appendix II).

2.3.2 Verification of the *AtNOGCI* clone

Before expression of the recombinant *AtNOGCI* was carried out, the clone was verified for the presence of the desired insert by re-amplification and restriction double digest of the plasmid. Figure 2.4 shows a 0.8 % agarose gel resolution of the re-amplified *AtNOGCI* and the digested pET SUMO-*AtNOGCI* clone. As shown in Figure 2.4A, lane 2, the expected 1.4 kb fragment, which encodes the 497 amino acid *AtNOGCI* sequence, is visible. Figure 2.4B lane 1 shows the uncut plasmid and lane 2 shows two bands with the top band at 5.4 kb, corresponding to the linear pET SUMO plasmid and the lower band corresponding to the 1.4 kb *AtNOGCI* DNA fragment. Both the re-amplified and the restriction double digested fragments confirm the presence of the correct *AtNOGCI* insert size.

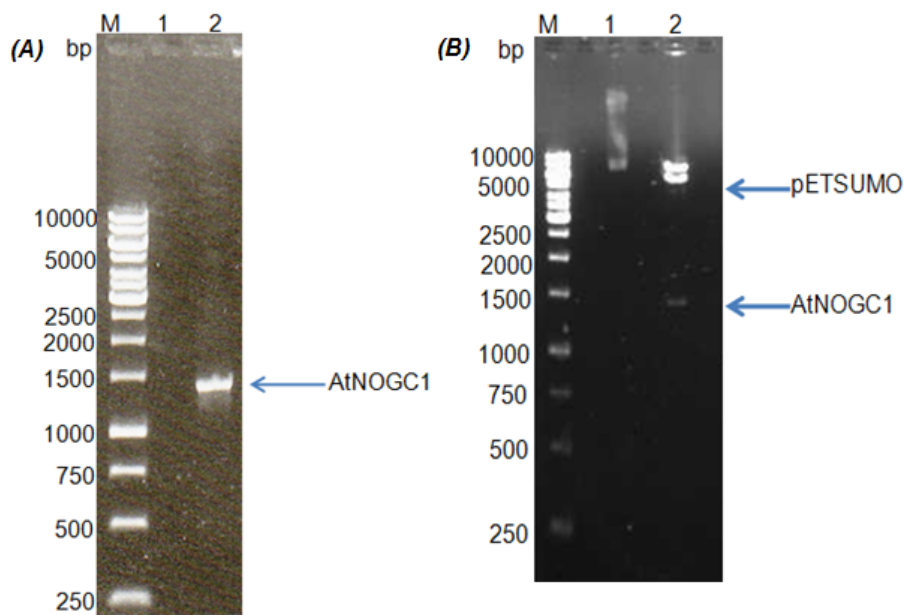


Figure 2.4: A 1 % agarose gel electrophoresis analysis of the *AtNOGCI* clone. (A) PCR amplification of *AtNOGCI* from the pET SUMO-*AtNOGCI* clone. Lane 1 and 2 correspond to the negative control and the 1.4 kb *AtNOGCI* PCR fragment respectively. (B) Restriction double digestion of pET SUMO-*AtNOGCI* construct with *Bam* HI and *EcoR* I. Lane 1 and 2 correspond to the uncut plasmid and the digested plasmid respectively. The bands corresponding to the 5.4 kb pET SUMO and the 1.4 kb *AtNOGCI* fragments are indicated by arrows. M refers to the O³GeneRuler 1 kb DNA Ladder, #SM1163, Fermentas Life Sciences.

The pET SUMO-*AtNOGCI* clones were sequenced at Inqaba Biotechnical industries [(Pty) Ltd]. Sequences were analysed as described in Section 2.2.3 (Appendix II). The results confirmed the presence of the correct clone sequence with no mutations. The translated sequence of the sequenced *AtNOGCI* still contained the important motifs required for functional characterization, including the heme-binding and the GC motifs.

2.3.3 Recombinant expression and purification of *AtNOGCI*

The recombinant plasmid pET SUMO-*AtNOGCI* was used to transform BL21 (DE) pLysS, a strain designed for gene expression regulated by the T7 *lac* promoter, and expressed as described in Section 2.2.2.2. Recombinant clones were inoculated into fresh LB medium, and incubated in a shaking incubator at 37 °C until OD₆₀₀ was 0.5. IPTG was then added to a final concentration of 2 mM for induction at 30 °C. The bacterial cells were collected by centrifugation and lysed by sonication. The expected band at ~67.7 kDa for the fusion His-SUMO-*AtNOGCI* was more pronounced in the induced fraction (Figure 2.5 lane 3) as compared to the uninduced fraction (Figure 2.5 lane 1). This band was observed in soluble fractions and no band corresponding to this size was seen in the insoluble fraction (Figure 2.5 lane 2). *AtNOGCI* was purified with the Ni-NTA purification system under native conditions using Na-phosphate buffer (50 mM NaH₂PO₄, 300 mM NaCl, 30 mM Imidazole, pH 8.0) as described in Section 2.2.2.3. The target protein was eluted in fractions of 5 mL (Figure 2.5, lanes 7). Some of the proteins were eluted in the wash fractions. The results show that the *AtNOGCI* fusion was successfully expressed in BL21 DE (pLysS) *E. coli* cells however, partially purified.

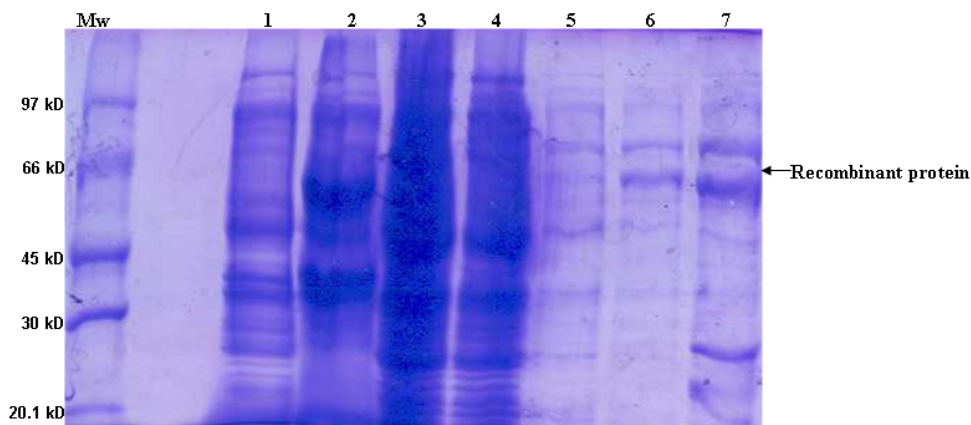


Figure 2.5: A 12 % SDS-PAGE gel analysis of the expression and affinity purification of the *AtNOGCI* fusion protein. Mw: molecular weight marker, Lane 1: uninduced fraction, lane 2: insoluble fraction, lane 3: cell lysate (soluble fraction), lane 4: flow through, lane 5-6: 1st wash (0.0 mM imidazole) and 2nd wash (30 mM imidazole), and lane: 7 elute.

2.3.4 Purification of *AtNOGCI* by anion exchange chromatography

Since the pI of *AtNOGCI* is 5.82 as determined by the Expasy server, the protein is expected to be strongly retained on an anion exchange column at pH 8.0. A partially purified sample of *AtNOGCI* was loaded onto the anion exchange column and eluted with a gradient of 0-1 M NaCl. The chromatogram in Figure 2.6A shows that *AtNOGCI* was retained by the column and that a clear separation was achieved with *AtNOGCI* eluting at the end in peak 6. From the apparent molecular weights, it is clear that *AtNOGCI* elutes in peak 6 (lane 9). These conclusions were confirmed by the SDS-PAGE gel shown in Figure 2.6B. Fractions corresponding to peak 6 were pooled and concentrated to 1.5 mL using Viva spin ultra-filtration devices (MWCO 3500 Da, Sartorius Stedim Biotech S.A).

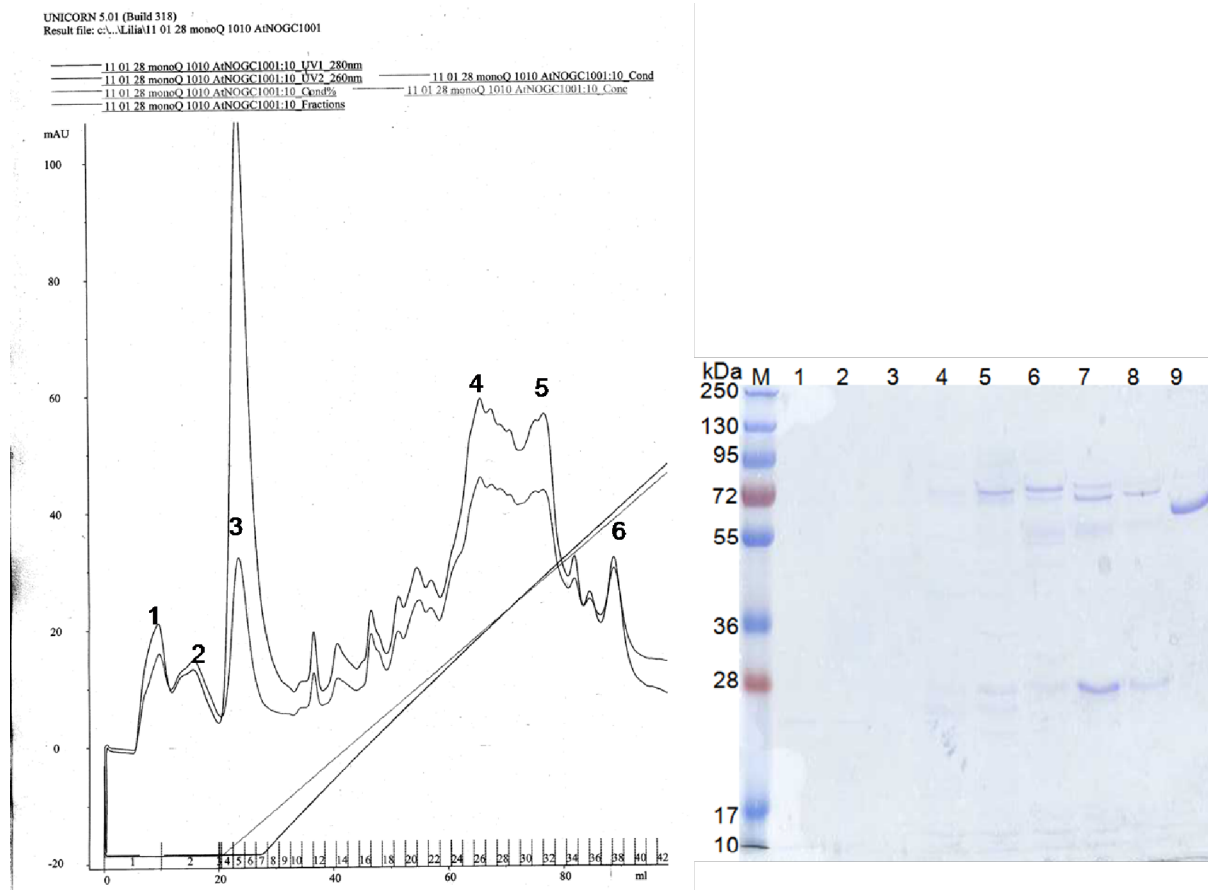


Figure 2.6: Separation of the *AtNOGC1* fusion protein from the residual crude proteins. (A) Chromatogram showing the separation of the *AtNOGC1* fusion from residual crude lysate using anion exchange chromatography. (B) A 12 % SDS-PAGE gel showing fractions that corresponds to the peaks on the chromatograms. Peaks 1, 2, and 3 correspond to fractions in lanes 1, 2, and 3 respectively on SDS-PAGE gel, peak 4 correspond to fractions in lanes 4, 5 and 6, peak 5 to fractions in lanes 7 and 8, whereas peak 6 corresponds to fraction in lane 9. A ~67.7 kDa *AtNOGC1* fusion protein was successfully separated from the rest of the residual protein.

Recombinant *AtNOGC1* was also subjected to a 2D gel electrophoresis, to further confirm its purity. In 2D gel electrophoresis, the samples were precipitated to remove any contaminants and to enable concentration. The samples were therefore re-suspended in urea buffer pH 8.0, and a 100 mg of each sample was then mixed with 0.8 % (v/v) DTT, 0.2 % (v/v) ampholytes and final volume made up to 125 μ L using urea buffer pH 8.0 following first dimension isoelectric focusing (IEF). In the second dimension, the protein was separated by

electrophoresis in the presence of SDS. Figure 2.7A shows the purification of the *AtNOGCI* fusion protein using the Ni-NTA purification system. The gel shows that a number of host protein are co-purified with the fusion protein, with a number of protein spots observed along the same expected marker band for the *AtNOGCI* fusion protein. When the protein was subjected to a second step of purification using an anion exchange chromatography, a single spot was obtained. Figure 2.7B shows the presence of a single spot corresponding to the purified *AtNOGCI* fusion protein. This gel shows that the *AtNOGCI* fusion protein was successfully purified.

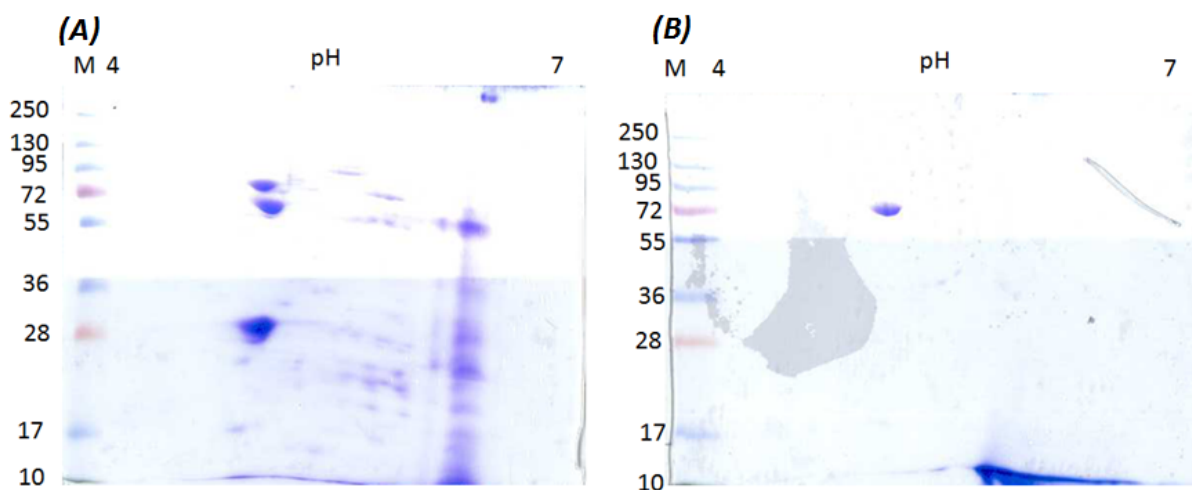


Figure 2.7: 2D SDS-PAGE gels showing the recombinant *AtNOGCI* before and after purification by anion exchange chromatography. (A) Separation of the *AtNOGCI* after its purification on a Ni-NTA column. The target recombinant *AtNOGCI* corresponds to a prominent spot at ~66 kDa of the marker. (B) Separation of the final purified recombinant *AtNOGCI* through an anion exchange column. The protein was successfully purified as is represented by a single spot on the 2D gel.

2.3.5 Determination of protein concentration

Fractions corresponding to the *AtNOGCI* fusion protein were concentrated to a final volume of 1.5 mL using Viva Spin Ultra filtration devices (MWCO 3500 Da, Sartorius Stedim,

Biotech S.A). The concentrated sample was analysed on the SDS-PAGE gel as shown in Figure 2.8. The final concentration of *AtNOGCI* fusion protein was determined using the Bradford assay as described in Section 2.2.1.5. Absorbance readings for both the protein and BSA (standard) were recorded at wavelength of 595 nm. The absorbance values for BSA recorded in Table 2.1:Appendix IV were used to construct a standard curve (Figure 2.9:Appendix IV) from which the concentration of the protein was then calculated using the formula shown in equation 1.

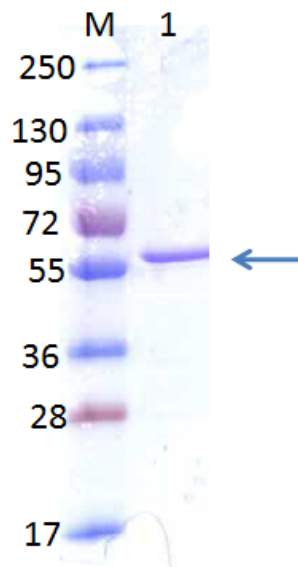


Figure 2.8: A 12 % SDS-PAGE gel stained with coomassie Brilliant blue showing the final concentrated *AtNOGCI* fusion protein. Mw: molecular weight marker, and lane 1: concentrated recombinant *AtNOGCI* protein. The sample was concentrated using Viva Spin Ultra filtration devices (MWCO 3500 Da, Satorius Stedim Biotech S.A.).

At 1:10 dilution, the absorbance of the protein was found to be 0.046 (see Table 2.2 Appendix III), which corresponds to the concentration of 57.5 $\mu\text{g}/\text{mL}$. The concentration at an absorbance of 280 nm (A_{280}) of the final *AtNOGCI* sample was determined using a

NanoDrop® ND-1000 spectrophotometer (NanoDrop technologies Inc.) and found to be 40 mg/mL (Fig 2.10; Appendix IV).

2.4 Discussion

A search for HNOX domains with a GC motif in the Arabidopsis genome identified a novel signalling molecule that is also a member of the flavin-containing monooxygenase family, which was termed *AtNOGCI*. Based on sequence identity, this study showed that *AtNOGCI* contains an HNOX-motif at its N-terminus and a GC motif located towards the C-terminus. *AtNOGCI* is composed of 497 amino acids that correspond to a 56.7 kDa protein. The aim was therefore to express *AtNOGCI* recombinantly and to optimise its purification for the production of a highly purified and functional protein.

The *AtNOGCI* expression construct, pET SUMO-*AtNOGCI*, was obtained from Dr. M. Morse (Department of Molecular Biology, University of Cape Town) and the correct identity of the insert was verified by re-amplification using PCR, restriction double digestion and DNA sequencing. Using gene specific primers, a 1.4 kb fragment was successfully amplified, and this was confirmed by the restriction double digest which released an insert of the same size as the *AtNOGCI* gene (Figure.2.4). Furthermore, DNA sequencing confirmed that the *AtNOGCI* gene was present without any mutations (results not shown).

The recombinant *AtNOGCI* was over-expressed in *E. coli* (DE) pLysS cells. The 6xHis-SUMO *AtNOGCI* fusion protein was expressed as a soluble fraction and purified using immobilised metal affinity and ion exchange chromatographic systems utilizing the Ni-NTA affinity chromatography and MonoQ anion exchange chromatography. Expression of soluble recombinant *AtNOGCI* was made possible by the fact that it was expressed using a pET

SUMO expression system (Invitrogen, Life technologies), which contains the T7 *lac* promoter to produce high levels of expression of proteins in bacteria, and has a SUMO fusion tag at the N-terminus to enhance the solubility of the target protein. Fractions corresponding to the pure *AtNOGCI* protein were collected and concentrated. The purity of the final *AtNOGCI* preparation was confirmed by 2D gel electrophoresis. Protein concentration was determined using the Bradford assay and found to be adequate for further characterisation and functional assays.

Finally, it can be said that the correct clone was supplied and was indeed verified by re-amplification, restriction double digestion and DNA sequencing to be containing the correct and desired gene, the *AtNOGCI* from *Arabidopsis thaliana*. The protein was recombinantly expressed as a soluble fraction and successfully purified by affinity and ion exchange chromatographic systems. The purified *AtNOGCI* was finally obtained in sufficient quantities for further functional and molecular characterisation of the recombinant product.

CHAPTER 3: Electrochemical Characterization of a Novel Nitric Oxide

Binding Protein from *Arabidopsis thaliana*

Abstract

Heme proteins are molecules that can interact with gases such as oxygen (O₂), nitric oxide (NO) and carbon monoxide (CO). Despite the discovery of many NO-dependent processes in plants, NO-binding proteins have remained elusive. We have searched the *Arabidopsis thaliana* proteome for the presence of the recently discovered heme-NO and oxygen-binding (HNOX) domains, making use of an extended amino acid motif diagnostic for heme-binding. One of the candidate molecules is annotated as flavin-containing monooxygenase. We have recombinantly expressed this molecule (*AtNOGCI*) and investigated its interaction with O₂ and NO using electrochemical techniques. Cyclic voltammetric (CV) and square wave voltammetric (SWV) experiments revealed that an *AtNOGCI* bioelectrode showed maximum electrocatalytic responses to NO and O₂ at -140 mV and -500 mV versus Ag/AgCl, respectively. NO binding to *AtNOGCI* is concentration dependent, as seen by a gradual increase in the electrocatalytic peak current (response) as the concentration of NO increases. Interestingly, it was also observed that NO displaces O₂ in the heme site of the protein even at high O₂ concentrations, which suggests that NO has a higher affinity for the heme site of *AtNOGCI* than O₂. In addition, this study demonstrates the use of *AtNOGCI* as a novel biosensor for the detection of both NO and O₂.

3.1 Introduction

NO has diverse signalling roles in animals; including regulation of immune responses via macrophages and neutrophils, regulation of inflammation, control of vascular tone, modulation of platelet aggregation and mediation of neurotransmission (Schmidt and Walter, 1994; Wink and Mitchell, 1998). Animal NO synthesis occurs via conversion of L-arginine to L-citrulline and NO in a reaction catalyzed by a nitric oxide synthase (Furchgott, 1995; Li and Poulos, 2005). Various molecular and physiological processes influenced by NO signalling in plants have been reviewed and include regulation of intracellular Ca^{2+} concentrations and protein kinases, modulation of plant responses to pathogens, promotion of stomatal closure, regulation of flowering, control of gene expression, growth and re-orientation of pollen tubes, pollen recognition, reduction of seed dormancy and stimulation of seed germination, regulation of plant responses to abiotic stress and regulation of fruit ripening (Besson-Bard et al., 2008a; Wilson et al., 2008; Hong et al., 2008; Qiao and Fan, 2008). With such diverse and yet crucial functions, identification and characterization of NO sensors in plants is not only interesting but also essential for our understanding of how NO mediates these functions in plants.

Considering the biochemistry of heme-binding proteins, it is quite reasonable to speculate that some of the functions of NO may be transduced via interaction of NO with heme-binding proteins. Heme-binding proteins play roles in signal transduction (Pellicena et al., 2004), electron transport or oxidation of organic compounds, and sensing gases such as O_2 , NO and CO (Capece et al., 2008). Heme proteins are characterized by a heme group with a protoporphyrin IX ring in the center that is ligated to a histidine residue (Schmidt et al., 2004; Rothkegel et al., 2007). The eukaryotic sGC is the only known ligand for NO without any

measurable affinity for O₂, however it contains the same heme protoporphyrin IX ring as that found in other members of the globins family of proteins (Boon and Marletta, 2005a) together with a conserved YxSxR motif (Pellicena et al., 2004). Based on the sequence of eukaryotic sGC, new members of the heme domains were identified in proteins from prokaryotes. Examples include gas sensing proteins in the facultative aerobe *Vibrio cholera* (which bind to NO but not O₂) and the gas sensing proteins in the obligate anaerobe from *Thermoanaerobacter tengogenesis*, which form tight hydrogen bonds with both NO and O₂ (Boon and Marletta, 2005a; Pellicena et al., 2004).

The mechanism of electrocatalytic reduction/oxidation of NO by heme proteins have been studied extensively. Electrochemical detection of NO can be seen either after oxidation to nitrite (NO₂⁻) and then to nitrate (NO₃⁻) and/or reduction to nitrous oxide (N₂O) and nitrogen gas (N₂) at positive potentials and hydroxylamine (NH₃OH) and ammonia (NH₃) at negative potentials (Kosminsky et al., 2001; de Vooy et al., 2004). NO biosensors based on myoglobin (Liu et al., 2004), hemoglobin (Fan et al., 2004) and peroxidase (Casero et al., 2000), including their immobilization techniques and detection methods, are well established. Electrochemical techniques are still the most widely used methods due to their relative simplicity and sensitivity and are amongst the most reliable methods for the determination of various gases (Ciszewski and Milczarek, 2003; Yang et al., 2009; Diaz-Gonzalez et al., 2005).

Based on the characteristic features of HNOX domains, a search for an HNOX domain in plants was set out as described in chapter 2. Electrochemical techniques were used to investigate the mechanism by which the *AtNOGCI* protein binds to either NO and/or O₂. This study present evidence to show that *AtNOGCI* is a novel NO/O₂ binding protein in

Arabidopsis thaliana, with a higher affinity for NO than for O₂ and proposes that the protein can be used as a novel gas biosensor.

3.2 Materials and methods

3.2.1 Electrochemical apparatus and procedures

All electrochemical experiments were carried out using a BAS Epsilon, integrated automated electrochemical workstation (BioAnalytical Systems, West Lafayette, IN, USA). Voltammograms were recorded with a computer interfaced to the BAS electrochemical workstation. A 20 mL custom-made three-electrode cell system was used for all electrochemical measurements at 25 °C. A 0.071 cm² glassy carbon electrode (GCE) (BioAnalytical Systems, West Lafayette, IN, USA) was used as the working electrode, Ag/AgCl with a 3 M NaCl salt bridge electrode was used as the reference electrode and a platinum wire as the auxiliary electrode. All experiments requiring anaerobic conditions were performed in solutions purged with argon for 20 min. The GCE was polished with 1.0, 0.3 and 0.05 micron alumina (Buehler, IL, USA). The electrode was then thoroughly washed with distilled water, followed by ultrasonication for 5 min in distilled water and 5 min in ethanol. The GCE was dried in a stream of N₂ for 10 sec immediately before drop coating with the protein material.

3.2.2 Preparation of *AtNOGCI* protein electrode

The bioelectrode was prepared by immobilizing an *AtNOGCI*-didodecyldimethylammonium bromide (DDAB)-BSA film on the polished GCE using an immobilization method described previously (Iwuoha et al., 1998). A 10 mM vesicle dispersion of DDAB was prepared by dissolving 4.63 mg of DDAB in 1 mL of water and the solution was sonicated for ± 8 h. A mixture of 10 µL of 10 mM DDAB and 2 mg BSA was mixed to make solution A. The

enzyme (10 μL from 3.14 mg/mL of enzyme) was diluted in 90 μL of phosphate buffer (50 mM NaH_2PO_4 ; 300 mM NaCl ; 250 mM imidazole, pH 8.0). The diluted enzyme (10 μL) was mixed with solution A to make solution B. Solution B (10 μL) was mixed with 5 μL of 2.5 % glutaraldehyde to obtain solution C. Drop coating of 5 μL of solution C was done on the previously polished GCE and allowed to dry overnight at 4 $^\circ\text{C}$ to form a thin enzyme-DDAB liquid-crystal film on the electrode surface. The final composition of the bioelectrode was *AtNOGCI* protein, DDAB and BSA. The modified electrode was rinsed with distilled water and was ready for use. When not in use the biosensor was stored at 4 $^\circ\text{C}$.

3.2.3 Generation of nitric oxide

The NO reactor was degassed with argon for ≥ 30 min prior to NO production. NO was generated by slowly adding drops of 5 M HNO_3 into a glass flask containing 10 g of copper granules while stirring gently. NO gas was purified by passing it through a 5 M NaOH solution, which traps any NO_2 that may have formed due to oxidation of NO by traces of O_2 . The NO was bubbled into 3 mL of previously degassed phosphate buffer, pH 8.0, for about 30 min as shown in figure 3.1 (Kosminsky et al., 2001; Bertotti et al., 2005). The bubbling of NO into the phosphate solution for 30 min resulted in a saturated NO solution (~ 2 mM). All experiments were carried out in a fume cupboard.

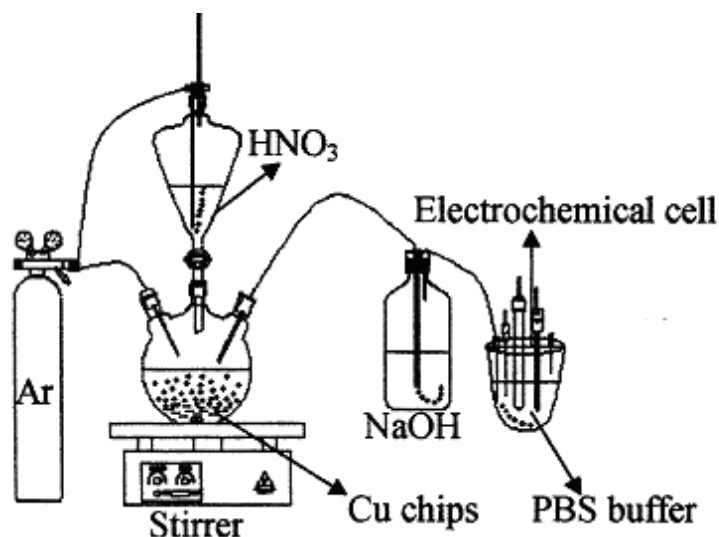


Figure 3.1: Apparatus representing the production of NO from Cu turnings and HNO₃. NO gas is produced from Cu turnings with 5 M HNO₃ slowly dropping in to the Cu turnings, and the gas is purified by passing through NaOH solution, and bubbled into phosphate buffer to obtain an NO saturated solution. (Adapted from (Mori and Bertotti, 2000)).

3.2.4 Cyclic and square wave voltammetric experiments

All electrochemical measurements were performed at 25 °C in either degassed or non-degassed phosphate buffer at pH 8.0. Anaerobic conditions were achieved by passing argon through the electrolyte for 20 min and maintaining an argon blanket on top of the solution. Voltammograms were recorded in the presence and absence of substrate at a potential scan rate of 2 mV s⁻¹ from initial potential, $E_i = +300$ mV to a switch potential, $E_\lambda = -800$ mV (for O₂-containing experiments) or -500 mV (for experiments involving only NO).

3.2.5 Binding affinities of the heme site

The experiments were conducted using two different methods. In the first method (a), the CV of the *AtNOGCI* protein bioelectrode was recorded in argon-degassed phosphate buffer pH 8.0. The buffer solution was exposed to air for 10 min while stirring gently prior to recording of the CV and then the CV of the air or O₂-saturated buffer was recorded. NO (500 μL) was added to the O₂-saturated buffer and this was followed by recording of the CV. In the second method (b), CV measurements were made before and after the addition of NO to non-degassed phosphate buffer pH 8.0. Then the cell solution containing NO was exposed to air for 10 min while stirring gently (to allow saturation of the solution with O₂) prior to recording, then the CV was recorded.

3.3 Results

3.3.1 Initial electrochemical characterization of *AtNOGCI*

AtNOGCI protein bioelectrode response was conducted in the presence of either NO or O₂ at different scan rates of 2, 5, 20, 50, and 100 mV s⁻¹. The previously modified electrode with *AtNOGCI*, the counter and the reference electrode were placed in a custom-made electrochemical cell, containing 2 mL of phosphate buffer, pH 8.0. The buffer was degassed with argon for ± 20 min and the argon was left as the blanket. CV scans were recorded in the presence of NO at scan rates of 2, 5, 20, 50, and 100 mV s⁻¹ at the potential window -150 to -800 mV. Figure 3.2A show the CV of *AtNOGCI* in the presence of NO at different scan rates, showing an increase in both the cathodic and anodic peaks. Well-defined redox peaks in the presence of NO are observed at a scan rate of 2 mV s⁻¹. For O₂ response, the buffer was equilibrated in air as described elsewhere (Section 3.2.4) and Figure 3.2B show the CV of *AtNOGCI* in the presence of O₂ at different scan rates. The cathodic peak current increased with a number of scan rates, while the anodic peak current disappeared. Well-defined cathodic peaks were observed in the presence of O₂ responses as compared to NO, whereas a more catalytic peak current was clearly observed at a scan rate of 2 mV s⁻¹ for both NO and O₂. Based on these observations, a scan rate of 2 mV s⁻¹ was selected for this study.

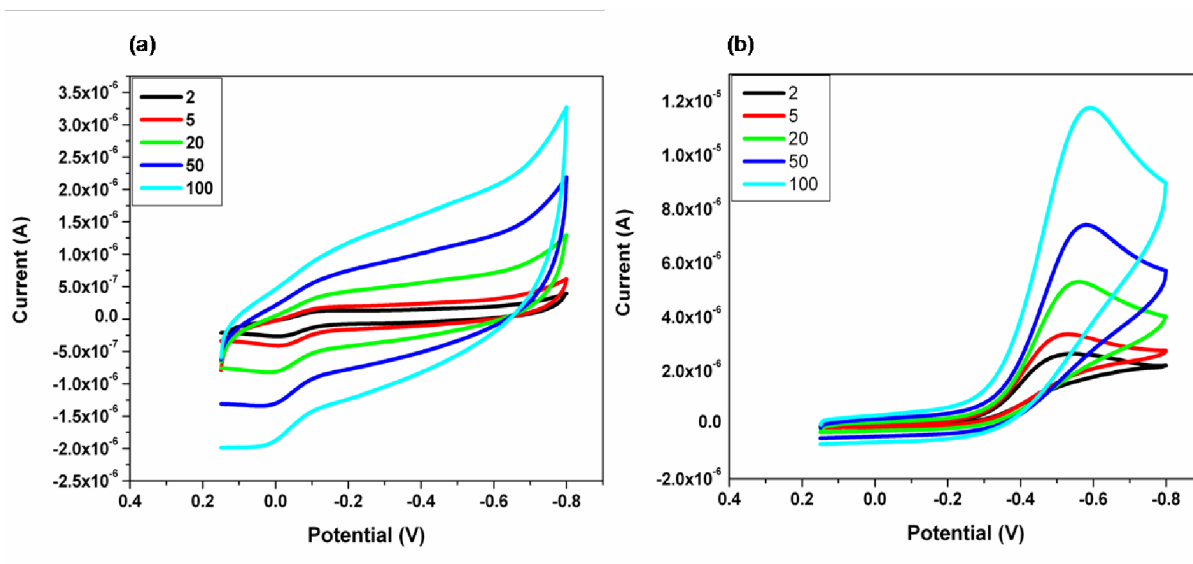


Figure 3.2: Characterisation of the *AtNOGCI* bioelectrode at different scan rates. (A) A cyclic voltammogram of the *AtNOGCI* bioelectrode in the presence of NO at scan rates of 2, 5, 20, 50 and 100 mV s⁻¹. Well-pronounced redox peaks are observed at a scan rate of 2 mV s⁻¹. (B) A cyclic voltammogram of the *AtNOGCI* bioelectrode in the presence of NO at scan rates of 2, 5, 20, 50 and 100 mV s⁻¹. The most catalytic reduction peak is well defined at a scan rate of 2 mV s⁻¹. Potential window was +0.15 to -0.8 V versus Ag/AgCl.

3.3.2 Electrochemical characterization of *AtNOGCI* in O₂

Since *AtNOGCI* is annotated as a monooxygenase, its O₂-binding capacity was also assessed. In these experiments, the buffer was purged with argon as described in ‘experimental procedures’. Figure 3.3 shows the cyclic voltammetric responses of the *AtNOGCI* electrode in the presence and absence of O₂ when the potential was scanned from +150 to -800 mV at a scan rate of 2 mV s⁻¹. Under anaerobic conditions, only the redox peaks of *AtNOGCI* protein were observed at -80 and -140 mV, and as described previously, whereas under aerobic conditions, only the cathodic response with an E_{pc} value of -500 mV was observed. This indicates the catalytic coupling of the reduction of the Fe³⁺ to the oxygenation (binding of molecular oxygen, i.e. O₂) of Fe²⁺. The cathodic peak current (2.2 μA) under aerobic conditions is by 3 orders of magnitude larger than that under anaerobic conditions (0.005

μA). This well pronounced cathodic peak is a result that depicts the coupling of a fast electron transfer reaction at the electrode surface to a fast chemical process in which the reduced electro-active species have been used up.

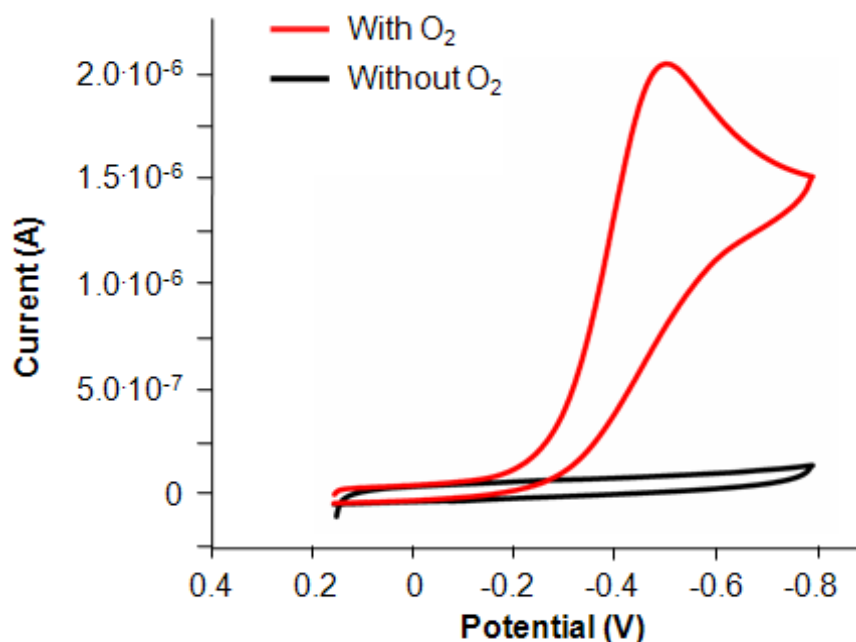


Figure 3.3: Cyclic voltammogram showing the response of *AtNOGCI* in phosphate buffer in the presence or absence of O₂. For the anaerobic conditions (black), the oxygen in the buffer was purged with argon at a flow rate of 10 L/min. Under aerobic conditions, the buffer was equilibrated with air to achieve maximum O₂ saturation (red). The scan shows a reduction peak (corresponding to the binding of oxygen) as the voltage applied to the system reaches about -0.5 V, and no species were oxidised in the reverse scan. The potential ranged from +0.15 to -0.8 V and the scan rate was 2 mV s⁻¹.

3.3.3 Electro-catalytic characterisation of *AtNOGCI* for binding to NO

Sequence characterisation showed that the *AtNOGCI* protein contains an HNOX motif, suggesting that it could bind to NO and/or O₂. To test this hypothesis and investigate these properties, a plasmid containing the *AtNOGCI* gene was expressed and the recombinant protein was investigated using cyclic and square wave voltammetric experiments. Figure 3.4A represents the voltammetric responses of the *AtNOGCI* bioelectrode in the absence

(black) and presence (red-yellow) of NO. In the absence of NO, anodic and cathodic peak currents were observed at electrode potential values of -80 and -140 mV, respectively. The peak electrode potential (E_p) values can be assigned to the oxidation ($\text{Fe}^{\text{II}}/\text{Fe}^{\text{III}}$ $E_{\text{pa}} = -80$ mV) and reduction ($\text{Fe}^{\text{II}}/\text{Fe}^{\text{III}}$ $E_{\text{pc}} = -140$ mV) of the *AtNOGCI* protein's heme group. The separation of the redox peak potential ($\Delta E_p = |E_{\text{pc}}| - |E_{\text{pa}}|$) value of 60 mV is in agreement with what would be expected for a one electron transfer process involving an immobilized electroactive system (Bard and Faulkner, 1980). After NO was added to the buffer, the cyclic voltammogram obtained showed an increase in both the cathodic and anodic peak currents (Figure 3.4A; red trace), with the cathodic (reduction) peak at -140 mV increasing as the concentration of NO in the cell solution increased. The anodic (oxidation) peak on the other hand, increased only slightly with the first two additions of NO and levelled up as the concentration of NO increases. The cyclic voltammetric responses of the bioelectrode indicate that NO binds preferentially to the reduced form of the protein immobilized on the bioelectrode (*i.e.* *AtNOGCI-Fe^{II}*). Figure 3.4A shows that E_{pa} values shift anodically as the concentration of NO increases, showing that the NO-bound heme protein (*AtNOGCI-Fe^{II}-NO*) requires higher electrode potential to oxidize it than the NO-free protein (*AtNOGCI-Fe^{II}*).

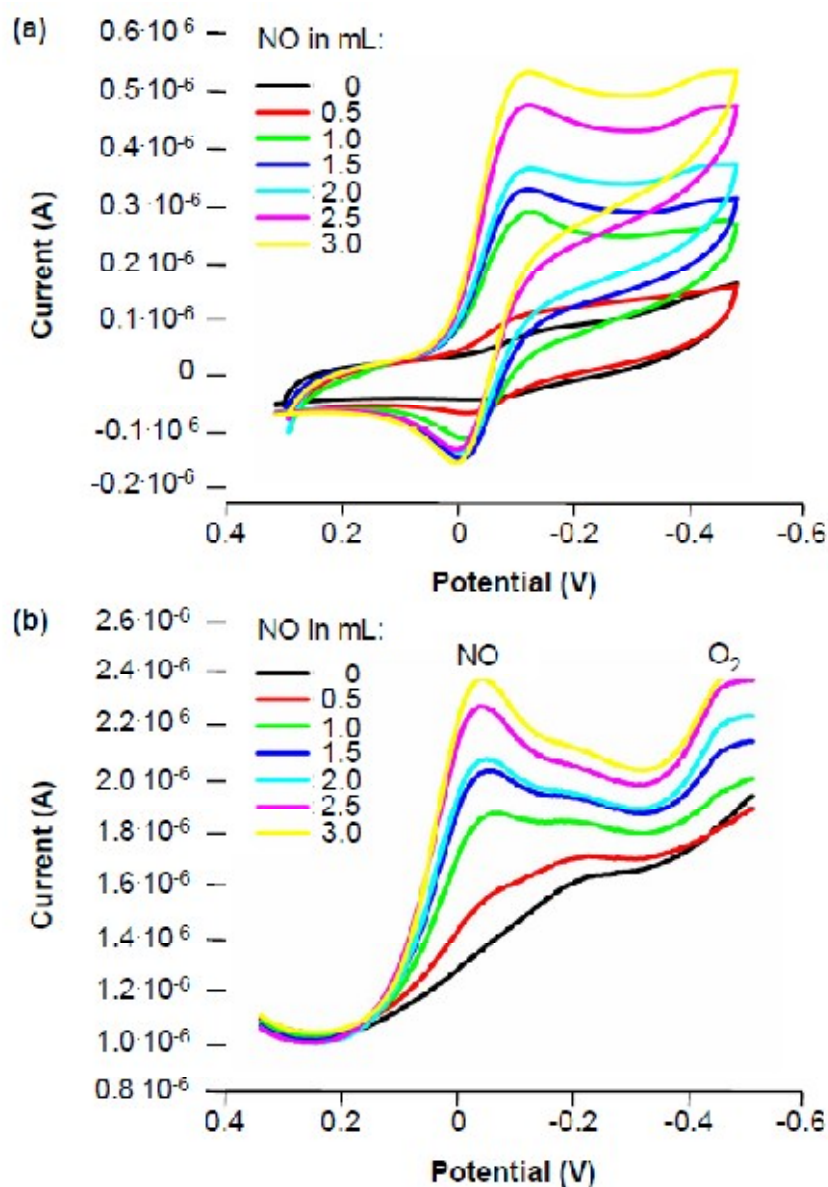


Figure 3.4: Electrochemical characterisation of *AtNOGCI* in phosphate buffer. (A) A cyclic voltammogram of *AtNOGCI* characterised in 3 mL phosphate buffer (50 mM NaH₂PO₄; 300 mM NaCl; 250 mM imidazole, pH: 8.0) in the presence of 0 mL (black), 0.5 mL (red), 1.0 mL (green), 1.5 mL (blue), 2.0 mL (cyan), 2.5 mL (magenta) and 3.0 mL NO (yellow). The potential window was +0.3 to -0.5 V and the scan rate was 2 mV s⁻¹. The scan shows an increase in the reduction peak with an increase in NO concentration as the voltage reaches -0.14 V. The oxidation peak increased slightly at a voltage of 0.08 V and ceased with an increase in NO concentration. (B) A square wave voltammogram showing the response of *AtNOGCI* in 3 mL phosphate buffer, pH: 8.0 in the presence of 0 mL (black), 0.5 mL (red), 1 mL (green), 1.5 mL (blue), 2 mL (cyan), 2.5 mL (magenta) and 3 mL NO (yellow). The potential window was +0.3 to -0.5 V and the scan rate was 2 mV s⁻¹. The scan shows two peaks at a voltage of -0.1 and 0.5 V corresponding to NO and O₂ binding respectively.

Square wave voltammetry (SWV) experiments were also performed to monitor the nature of the responses of *AtNOGCI* protein to different concentrations of NO. In SWV, the peak potential represents the redox potential relative to Ag/AgCl reference electrode (formal potential, $E^{0'}$) of the redox species. Figure 3.4B represents the SWV cathodic responses of the *AtNOGCI* bioelectrode to NO in the presence of O₂ at 25 mV amplitude and a frequency of 15 mV. The bioelectrode gave two prominent square wave voltammetric peaks at -100 mV and -500 mV, corresponding to the $E^{0'}$ values for the binding of NO and O₂, respectively, to the *AtNOGCI* protein. The occurrence of the two SWV response peaks shows that the protein binds to NO and O₂ independently of each other, which is due to small amounts of dissolved oxygen in the degassed buffer solution bound to *AtNOGCI*-Fe²⁺ species on the electrode.

3.3.4 Electrochemical characterization of the *AtNOGCI* bioelectrode, bare GCE and bare GCE modified with DDAB-BSA in the presence or absence of NO.

To confirm that the response of NO observed with the *AtNOGCI* protein bioelectrode was not due to direct reduction of NO at the bare electrode or the DDAB-BSA film, the experiment was conducted with the bare GCE and GCE modified with DDAB-BSA film. In these experiments the response for both *AtNOGCI* bioelectrode, bare GCE and GCE modified with DDAB-BSA film were determined in the presence and absence of NO in phosphate buffer pH 8.0. The buffer was purged with argon for 20 min, and CV scan was recorded at a scan rate of 2 mV s⁻¹, in the potential range of +150 to -800 mV, and NO was bubbled into the cell followed by recording a CV in the presence of NO. Figure 3.5 shows the cyclic voltammetric responses of the *AtNOGCI* bioelectrode, bare GCE, and the GCE modified with DDAB-BSA film. In this case, no redox peaks were observed in the cyclic voltammetry of NO either on bare GCE or GCE modified with DDAB-BSA films (Figure

3.5). The result indicates that DDAB acts as a surfactant that facilitates direct electron transfer between *AtNOGCI* protein and the electrode surface and does not participate in the electron transfer process at the experimental potential range.

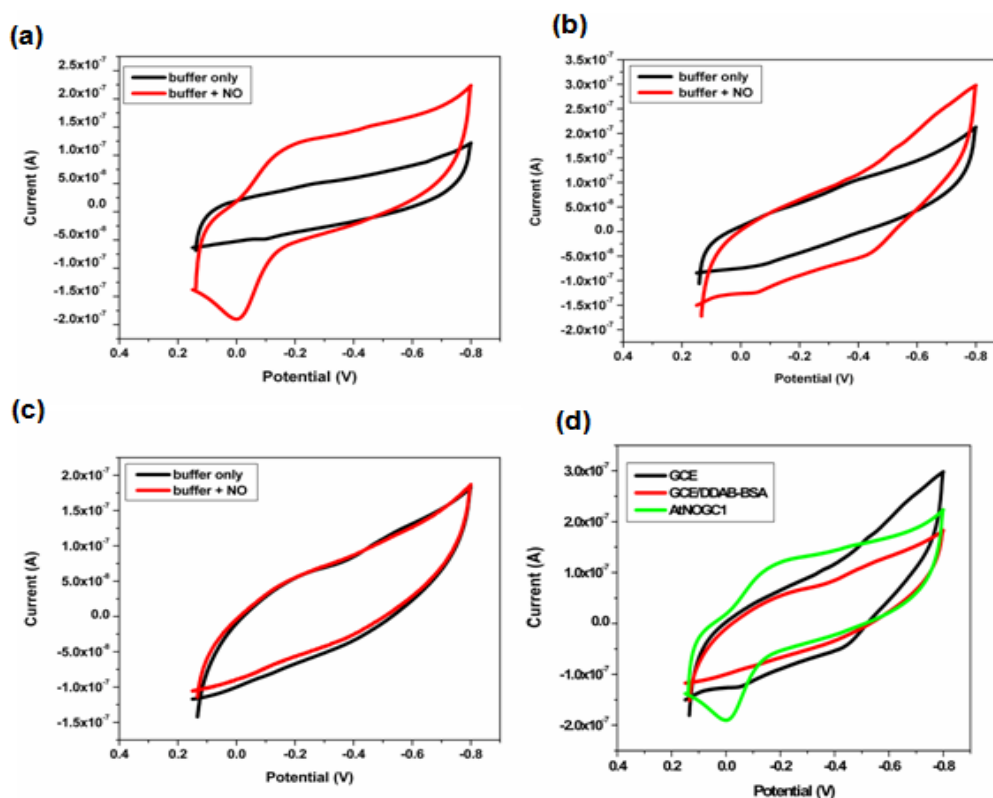


Figure 3.5: Electrochemical characterisation of *AtNOGCI*, bare GCE and GCE modified with DDAB-BSA film in phosphate buffer. (A) A cyclic voltammogram of *AtNOGCI* characterised in 3 mL phosphate buffer (50 mM NaH_2PO_4 ; 300 mM NaCl; 250 mM imidazole, pH: 8.0) in the absence and presence of NO. The scan shows an increase in the reduction peak in the presence of NO and as the voltage reaches -0.14 V. The oxidation peak increased slightly at a voltage of 0.08 V. (B) A cyclic voltammogram of the bare GCE characterised in phosphate buffer. There is no increase in either the reductive or oxidative peaks for the bare GCE at potential ~ -0.14 V in the absence or presence of NO. (C) A cyclic voltammogram of bare GCE modified with DDAB-BSA film characterised in phosphate buffer. The reductive and oxidative peaks characterised were also not observed for the GCE modified with DDA-BSA in the absence and presence of NO. (D) A cyclic voltammogram showing a plot of the bare GCE, GCE modified with DDAB-BSA film and the *AtNOGCI* bioelectrode. The potential window was $+0.15$ to -0.8 V and the scan rate was 2 mV s^{-1} .

3.3.5 Investigation of NO and O_2 affinity to the *AtNOGCI* heme binding site

The affinity of NO and O₂ to the heme active site of *AtNOGCI* was also investigated. Figure 3.6A represents the cyclic voltammogram of the *AtNOGCI* protein bioelectrode in buffer only (black trace), buffer containing O₂ (red trace), and in buffer containing O₂ after the addition of NO (green trace). In buffer only, the cyclic voltammetric redox peaks of *AtNOGCI* were observed at -80 mV and -140 mV. Under anaerobic conditions (in O₂-saturated buffer), the cyclic voltammogram shows the expected irreversible cathodic response with peak at -500 mV (red trace). The addition of NO to the O₂-saturated buffer solution resulted in a new electrocatalytic cathodic response which has peaks characteristic of both NO (at -140 mV) and O₂ (-500 mV). The peak current measured at -140 mV (i.e. 0.76 μA) was half that of the catalytic current of the O₂-saturated system (i.e. 1.51 μA).

The binding affinity of NO and O₂ to the heme of *AtNOGCI* was also investigated by adding O₂ to the *AtNOGCI*-NO bound complex. In this experiment, CVs were recorded in the buffer containing O₂ (black trace) and followed by a peak current observed at -500 mV. Figure 3.6B shows the CV of the *AtNOGCI* in NO-saturated buffer in the presence of O₂. When the buffer was degassed with argon (red trace), the cathodic peak current at E_{pc} = -500 mV disappeared, followed by two small redox peaks for the oxidation and reduction of *AtNOGCI* heme protein iron.

When 500 μL of NO was added to the argon-degassed buffer, a cathodic peak originating from E_{pc} = -140 mV was formed due to the response of *AtNOGCI* to NO. However, when the NO-containing buffer was saturated with air, the catalytic voltammetric wave that originated at -140 mV increased with no concomitant increase in the kinetic current (the difference between the peak and background currents, i.e. in this case, the actual current resulting from

the binding of O₂ to heme-Fe²⁺) for oxygenation at -500 mV. These results therefore indicate that *AtNOGCI* binds preferentially to NO for which it has higher affinity than for O₂.

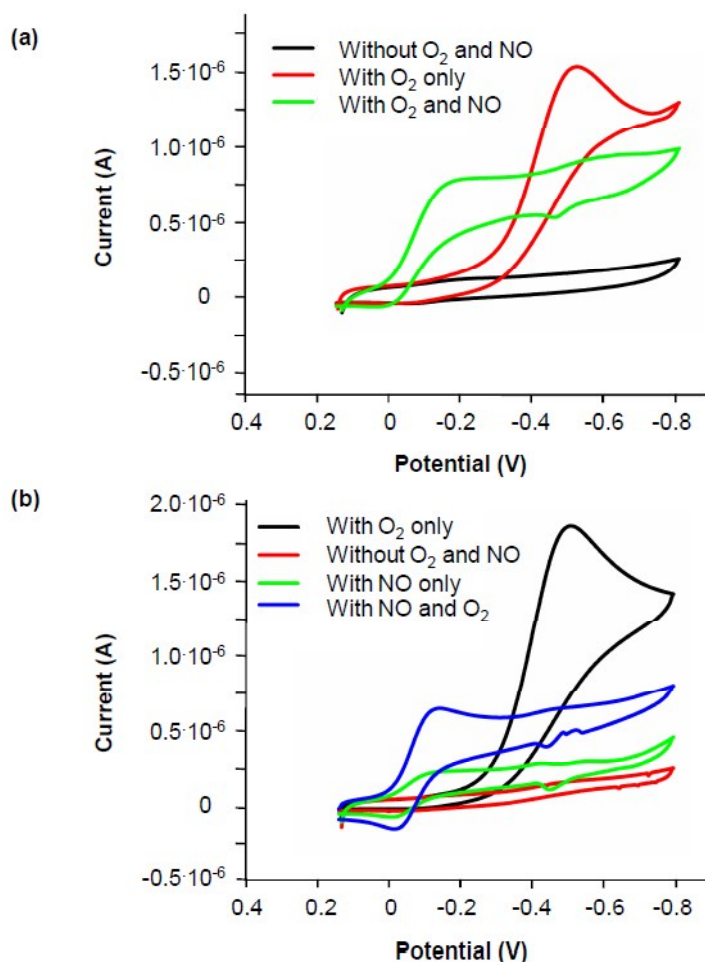


Figure 3.6: Cyclic voltammograms of *AtNOGCI* responding to O₂ and NO. (A) *AtNOGCI* was characterised in anaerobic phosphate buffer (50 mM NaH₂PO₄; 300 mM NaCl; 250 mM imidazole, pH: 8.0) purged with argon at a flow rate of 10 L/min (black) or an air equilibrated buffer (red) or buffer containing 500 μ L of NO (green). The addition of NO in an air equilibrated buffer resulted in two cathodic peaks at -0.14 and at -0.5 V, a characteristic of NO and O₂ respectively (green). (B) *AtNOGCI* was characterised in buffer with O₂ (black), buffer degassed with argon (red), buffer with NO (green), buffer with NO and air equilibrated buffer (blue). The blue scan shows the presence of two peaks at -0.14 and at -0.5 V characteristic of the response to NO and O₂ respectively. The potential window was +0.15 to -0.8 V and the scan rate was 2mV s⁻¹.

3.4 Discussion

Our principle aim here was to identify *Arabidopsis* proteins that can bind to NO. Searching for HNOX domains in *Arabidopsis thaliana*, we have identified a novel candidate protein with a conserved heme-binding motif Hx{12}Px{14,16}YxSxR. This candidate, *AtNOGCI*, is currently annotated as a flavin-containing monooxygenase based on sequence homology. The aim of the study was therefore, to recombinantly express *AtNOGCI* and investigate its interaction with NO and O₂ and in particular, its affinity for NO and O₂. Electrochemical analyses revealed that *AtNOGCI* is indeed an HNOX domain encoding a protein that can bind NO and O₂ at E_{pc} values of -140 mV and -500 mV, respectively.

Using the slow potential scan rate of 2 mV s⁻¹, we further investigated the response of *AtNOGCI* in the absence and presence of NO. In the absence of NO and O₂, the cyclic voltammogram analysis showed that *AtNOGCI* is electroactive and contains a redox couple (heme-Fe^{3+/2+}) that has anodic and cathodic peak potentials of -80 and -140 mV, respectively. This type of a response was not observed when the bare GCE or DDAB film-modified GCE were used in degassed buffer solutions, suggesting that the observed voltammetric peaks were due to the electrochemistry of *AtNOGCI*-heme-Fe^{3+/2+}.

DDAB is one of the surfactants shown to increase direct electrochemistry for a number of proteins and facilitate direct electron transport to the active site of enzymes (Hu, 2001). In this case, DDAB is facilitating electron transport between the electrode and *AtNOGCI*-heme-Fe^{3+/2+}. The two redox peaks of *AtNOGCI* were amplified by the binding of NO and no

response was observed for either bare GCE or DDAB film in the same potential window. From this, we conclude that *AtNOGCI* is responsible for the electrocatalytic reduction of NO and that an increase in peak currents is due to the specific interaction between *AtNOGCI* and NO.

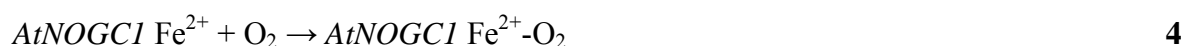
Since *AtNOGCI* is annotated as a monooxygenase, O₂-binding with the bioelectrode was assessed using cyclic voltammetry and showed (Fig. 3.3) a cathodic response with a cathodic peak potential (E_{pc}) value of -500 mV under aerobic conditions indicating catalytic coupling of the reduction of Fe³⁺ to the oxygenation of Fe²⁺. The cathodic peak current (2.2 μ A) under aerobic conditions is larger by 3 orders of magnitude than that under anaerobic conditions (0.005 μ A). During the cathodic scan, Fe²⁺ was generated and used up in a fast follow-up oxygenation reaction making it unavailable for re-oxidation during the anodic scan. The peak potential (E_p) for the binding of oxygen to the protein occurs at -500 mV while the *AtNOGCI*-Fe^{III/II} reduction process occurs at -140 mV. Large shifts to higher reduction potential under aerobic conditions mean that the monooxygenation is a catalytic redox process involving several reaction steps and the irreversible cyclic voltammograms suggest binding of O₂ to the Fe²⁺-heme redox centre.

The electro-catalytic response of *AtNOGCI* was also investigated at different concentrations of NO. When different amounts of NO were added into the buffer, the cathodic peak current increased gradually while shifting to more positive potentials. The anodic peak also increased, but diminished at high NO concentration. This behaviour of the anodic peak at low NO concentration is likely due to the oxidation of unbound heme-Fe²⁺ sites of the *AtNOGCI* protein to heme-Fe³⁺. At high NO concentrations, no unbound heme-Fe²⁺ site is available for

re-oxidation and only the catalytic cathodic current for the binding of NO to the heme-Fe²⁺ site is observed. The magnitude of the anodic peak current at low NO concentrations could be used to quantify the available heme-Fe²⁺ sites in *AtNOGCI*.

Square wave voltammetry (SWV) was also used to monitor the nature of the responses of *AtNOGCI* to different concentrations of NO. As a technique for displaying differences in voltammetric spectra, SWV is a powerful tool for detecting very small changes that are often difficult to observe with cyclic voltammetry. Importantly, the results obtained were consistent with those obtained from the CV. However, an additional cathodic peak current was observed with E_{pc} value of -500 mV, which corresponds to O₂ binding, suggesting the presence of small amounts of background (dissolved) oxygen in the ‘degassed’ buffer solution that was bound to some *AtNOGCI*-Fe²⁺ species on the electrode (Figure 3.4b).

The reaction scheme for this process can be represented as follows:



In these processes, *AtNOGCI* (Fe³⁺) is electrochemically reduced to *AtNOGCI* (Fe²⁺) on the electrode surface, and then NO is likely to diffuse into the surface of the electrode where the immobilized *AtNOGCI* reduces the NO. Affinity experiments were conducted to determine which of the ligands has more affinity to the heme site of *AtNOGCI* protein. The analyses showed that addition of NO to an O₂-bound *AtNOGCI* protein disrupted the *AtNOGCI* -Fe³⁺-

O₂ bond, as shown by a decrease in the peak current of O₂ ($E_{pc} = -500$ mV) peak and the subsequent appearance of the NO peak ($E_{pc} = -140$ mV). The experiments were also further validated by exposing the NO-bound *AtNOGCI* protein to air. However, the NO peak remained the same in the presence of O₂ and no increase in the O₂ peak was observed. This is indicative for the ability of NO to displace O₂ and proves that NO has higher affinity for *AtNOGCI* than O₂. It also points to the possibility that O₂ might be needed as an enhancer for NO binding to the heme and that NO and O₂ can be bound at the same time to the enzyme. We therefore, conclude that (i) NO and O₂ have the same binding site, namely the heme-Fe²⁺ on the *AtNOGCI* protein; (ii) NO displaces only half of the heme-bound O₂ and (iii) NO has a higher affinity for the *AtNOGCI* heme site than for O₂.

AtNOGCI is a NO sensor in plants we are currently characterising and the knowledge derived from the characterization of *AtNOGCI* can be used to discover diverse physiological and biological responses to NO. We are currently investigating the biological functions of *AtNOGCI*, and its role as a signalling molecule, particularly so since *AtNOGCI* has a potential GC catalytic centre that may function *in vivo* and be dependent on NO. Recent bioinformatics studies have shown that *AtNOGCI* levels are highly elevated during NO₃ starvation, which together with its role in NO binding may suggest a role for *AtNOGCI* in nitrogen fixation in plants. In addition to its response to both NO and O₂, the response of *AtNOGCI* is dependent on the concentration of NO. This study has therefore, demonstrated the possibility of establishing a novel biosensor suitable for the detection of both NO and O₂, based on the ability of *AtNOGCI* to bind both these gases.

CHAPTER 4: *AtNOGCI* is a Novel *Arabidopsis thaliana* Nitric Oxide Binding Protein that Functions as a Guanylyl Cyclase *in vitro* in an NO-dependent Manner.

Abstract

Soluble guanylyl cyclases are enzymes that catalyse the conversion of guanosine 5'-triphosphate (GTP) to second messenger guanosine 3', 5'-cyclic monophosphate (cGMP), which leads to downstream responses that are NO mediated. While many cGMP mediated processes have been well characterised and as it is only until recently that a few GC's have been identified in higher plant, it is also important to note that a plant GC with affinity for NO has not yet been reported. This study therefore hereby reports an *Arabidopsis thaliana*, heme-binding protein (*AtNOGCI*) that functions as a guanylyl cyclase *in vitro* in an NO-dependent manner. *AtNOGCI* catalyses the formation of cGMP using GTP as its sole substrate with higher dependence on Mn^{2+} than Mg^{2+} ions. Furthermore, *AtNOGCI* catalytic activity is enhanced by the binding of NO to synthesize cGMP, highlighting it to be the first NO-dependent plant GC. The regulatory effect of calcium on the activity of the *AtNOGCI* was also investigated and the results showed a significant increase in the synthesis of cGMP in the presence of calcium.

4.1 Introduction

Guanylyl cyclases are enzymes that catalyse the synthesis of a second messenger guanosine 3', 5'-cyclic monophosphate (cGMP) from the purine nucleotide guanosine 5'-triphosphate (GTP), and these enzymes have long been identified in many diverse prokaryotic and eukaryotic organisms (Schaap, 2005). In animals the synthesis of cGMP by GCs is influenced by signals such as NO, peptide ligands and Ca^{2+} (Lucas et al., 2000). Intracellular cGMP mediate physiological processes by activating protein kinases, gating specific ion channels and regulation of phosphodiesterases, which result in the regulation of NO-specific biological functions (Boon and Marletta, 2005b). In animals, the NO/cGMP pathways regulate diverse physiological processes including neurotransmission, vasodilation, platelet aggregation (Rothkegel et al., 2006), cellular growth, cardiovascular homeostasis and sensory transduction (Zhang et al., 2008).

While there is evidence of NO-dependent signalling via cGMP in plants, GCs have until recently remained elusive and none of the candidates identified to-date are NO-dependent. In higher plants, cGMP functions as a second messenger in diverse physiological processes (Meier et al., 2009) including NO-dependent signalling (Prado et al., 2004), abiotic and biotic stress responses, pathogen challenges (Meier et al., 2010), and seed germination (Teng et al., 2010). The role of cGMP-regulated protein kinases has also been well-studied and it has been shown that cGMP increases a number of flower buds and induces terminal buds in plants, thus showing a role in flower induction. Cyclic GMP also increased enzyme activity in the plant *Pharbitis nil*, suggesting a role of cGMP-regulated protein kinases (Szmidszt-Jaworska et al., 2009). In tobacco, cGMP is an essential downstream signalling molecule in NO-mediated pathogen defence responses and is required for the induction of defence-related genes such as

the phenylalanine ammonia lyase (PAL) and the pathogenesis-related (PR-1) encoding gene, as well as for the activation of PAL enzyme activity which generates precursors for phenylpropanoid and thus salicylic acid biosynthesis (Romero-Puertas and Delledonne, 2003 ; Meier et al., 2009).

Furthermore, it has been demonstrated that endogenous cGMP levels increase in response to plant natriuretic peptides (Pharmawati et al., 2001), ozone (Pasqualini et al., 2008), NaCl and drought stress responses (Donaldson et al., 2004). A significant increase in cGMP levels has also been reported due to pathogen challenge and that both the virulent and avirulent strains of *Pseudomonas syringae* induce an increase in cGMP generation with the avrB strain inducing a more rapid response (Meier et al., 2009).

In higher plants, the first GC was discovered using a search motif strategy based on conserved and functionally assigned amino acid residues in the catalytic centre of GCs of higher and lower eukaryotes (Ludidi and Gehring, 2003). Rational motif relaxations and site directed mutagenesis have since led to the discovery of additional GCs, including the AtBRI1 (Kwezi et al., 2007), the AtWAKL10 gene that might be involved in pathogen defense (Meier et al., 2010). However the extended consensus motif (Hx₁₂Px_{14,16}YxSxR) HNOX motif , which occurs in *AtNOGCI*, does not occur in either of these GC's neither do they require NO activation.

With such diverse functions, the identification and characterization of NO/cGMP dependent candidates in plants is not only interesting but the knowledge obtained from these sensors

may also be applied in understanding how NO does mediate various physiological processes in plants such as the induction of cGMP synthesis and the identification of novel functions in plants. In a quest to identify the first NO-dependent GC, this study searched the *Arabidopsis thaliana* genome sequence by applying a GC search motif and an extended consensus motif (Hx{12}Px{14,16}YxSxR) motif deduced from the HNOX domains as described in chapter 2 (Boon et al., 2005) and the search managed to identify a novel plant signalling protein, *AtNOGCI*. We noted that that this molecule contained both the HNOX and GC motif.

This chapter describes the GC activity assays conducted on *AtNOGCI* to demonstrate that it can catalyse the synthesis of cGMP from GTP *in vitro*. Furthermore, the NO-dependence of the GC activity of *AtNOGCI* was also demonstrated, while the investigations of the regulatory effects of Ca²⁺ on the GC activity of the *AtNOGCI* is also described.

4.2 Materials and methods

4.2.1 Guanylyl cyclase activity assays

The GC activity assays of the *AtNOGCI* were conducted in a reaction mixture containing 50 mM Tris-HCl, pH: 7.5; 1 mM GTP or ATP; 5 mM MgCl₂ and/or 5 mM MnCl₂ and 10 µg of the recombinant protein. The samples were incubated at room temperature for 20 min, and cGMP levels measured using the cGMP Enzyme Immunoassay kit (EIA cyclic GMP kit, Sigma-Aldrich, Inc.), according to the manufactures instructions for the acetylation protocol. To monitor the effect of time on the GC activity of *AtNOGCI*, the GC activity assays were conducted in reaction experiments that were subsequently terminated at time intervals of 0, 5, 10, and 20 min. At the end of each time interval the reactions were stopped by boiling at 100 °C in a water bath for 10 min. The reaction mixtures were clarified by centrifugation at 13 000 rpm for 10 min and the supernatants collected for cGMP assaying.

4.2.2 Activation of *AtNOGCI* GC activity by NO and Ca²⁺

The possibility of NO and Ca²⁺ to induce the synthesis of cGMP by *AtNOGCI* were also investigated. A NO donor, 2-(N,N-diethylamino)-diazene-2-oxide (DEA/NO) (Sigma-Aldrich, Inc.) was used as the source for NO at reaction final concentrations of 0, 5, 20, and 50 µM. A 1 mM stock solution of the DEA/NO was prepared in 10 mM NaOH solution and diluted in a working solution of Na-phosphate buffer, pH 7.2 from which different concentrations of the NO donor were then prepared. To demonstrate the effect of Ca²⁺ on *AtNOGCI*'s GC activity, a 1 mM stock solution of Ca²⁺ was prepared in distilled water by

dissolving 1.1098 mg of CaCl_2 to a final volume of 10 mL. Concentrations of 0, 0.1, 1 and 10 μM were then prepared from a 1 mM stock. All NO and Ca^{2+} reactions were carried out as detailed in section 4.2.1 over a time period of 20 min.

4.3 Results

The principle of determining GC activity assays is based on the conversion of guanosine 5'-triphosphate to second messenger guanosine 3', 5'-cyclic monophosphate and the subsequent measurement of the generated cGMP levels by either a radioactive or non radioactive immunoassay systems. In this study, a non-radioactive, competitive immunoassay system (Sigma-Aldrich, Inc.) was used for the quantitation of the cGMP, and using a purified protein sample of the recombinant *AtNOGCI*. The immunoassay system uses a polyclonal antibody to cGMP to competitively bind free cGMP or the conjugate cGMP that is covalently linked to an alkaline phosphatase molecule. The assay is performed in a 96 well plate that is coated with anti-rabbit IgG antibody. The addition of *p*-Nitrophenyl phosphatase substrate to the plate containing a cGMP-linked to the enzyme produces a coloured product, which can be measured at 405 nm. The intensity of the colour obtained is inversely proportional to the concentration of cGMP present in the wells (Sigma-Aldrich, Inc.).

4.3.1 Effects of cofactor and time dependence on the activity of the *AtNOGCI*

The *in vitro* GC activity assays of the *AtNOGCI* fusion protein was determined using the protein sample expressed and purified as described in chapter 2 of this thesis. Figure 4.1A below shows the SDS PAGE gel of the purified *AtNOGCI* fusion protein and Figure 4.1B shows the *in vitro* GC activity assays which were determined by measuring the cGMP levels using the EIA cyclic GMP kit (Sigma-Aldrich, Inc.). As is shown in Figure 4.1B and over a time period of 20 min, the recombinant protein produced >160 fmol cGMP/ μ g protein when assayed in the presence of Mn^{2+} ion as compared to the 60 fmol cGMP/ μ g protein produced

when the assay was carried out in the presence of Mg^{2+} ion as cofactors. *AtNOGCI* has an activity of >200 fmol/ μ g in the presence of Mn^{2+} and a reduced level when Mg^{2+} was used as a cofactor which also increases gradually with time (Figure 4.1B). This experiment therefore, demonstrated a time dependence enzymatic activity since an increase in the GC activity was observed over time before stabilising after 15 min.

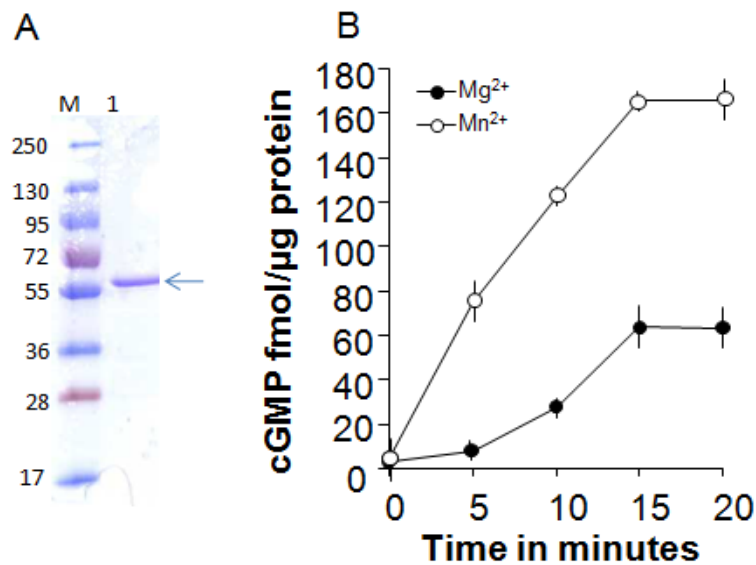


Figure 4.1: Expression of the *AtNOGCI* fusion protein and determination of its *in vitro* GC activity. (A) SDS PAGE gel showing the purified *AtNOGCI* fusion protein, Lane M represents the pre-stained molecular weight marker while lane 1 corresponds to the purified *AtNOGCI* fusion protein with a molecular weight of ~ 67.7 kDa. (B) cGMP levels generated in a reaction mixture containing 50 mM Tris-HCl, pH: 8.0; 1 mM GTP; either 5 mM Mn^{2+} or Mg^{2+} and 10 μ g recombinant protein. The reaction was carried out at time interval of 0, 5, 10, 15 and 20 min at room temperature and the generated cGMP levels were measured using the EIA cGMP kit (Sigma-Aldrich, Inc.) based on the acetylation protocol. Error bars represent the standard errors of the mean deviations (SEM) (n = 3).

The ATP affinity was also tested in a competitive type of an experiment by adding 1mM GTP and 1mM ATP into the reaction as substrates in the presence of the cofactor Mn^{2+} . Figure 4.2 below shows the cGMP levels produced when both GTP and ATP were used as sole

substrates of *AtNOGCI*. In the presence of ATP alone or in a combination with GTP, no change was observed on the GC activity of *AtNOGCI* and thus indicating that the presence of ATP does not interfere with the binding and substrate specificity of GTP to *AtNOGCI*.

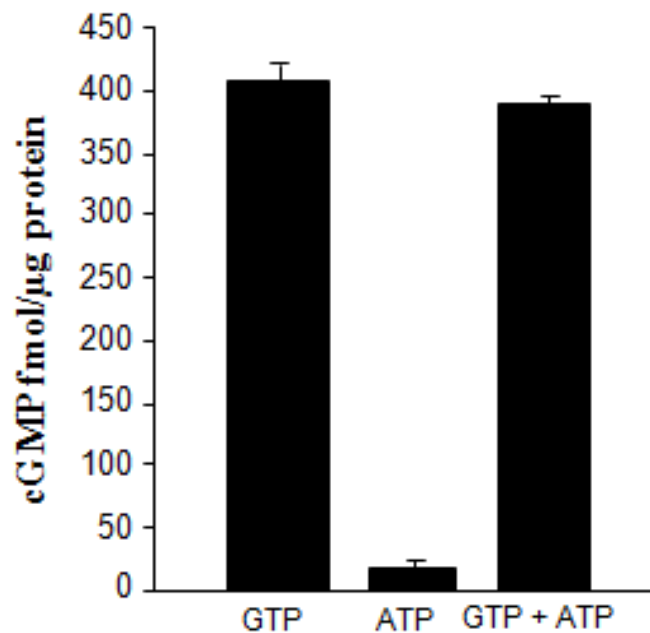


Figure 4.2: Competitive *in vitro* GC activity assays of *AtNOGCI* using both GTP and ATP as substrates. Cyclic GMP levels were measured in a reaction mixture containing 10 μg recombinant protein, either 1 mM GTP and/or 1mM ATP as substrates, 5 mM Mn²⁺ as the cofactor and the buffer 50 mM Tris-HCl at pH 8.0. The cGMP levels generated by the *AtNOGCI*'s enzymatic reaction were then measured using the EIA cGMP kit (Sigma-Aldrich, Inc.). Error bars represent the standard errors of the mean deviations (SEM) (n = 3).

4.3.2 Activation of the GC activity of the *AtNOGCI* by NO

Nitric oxide has been reported to be able to activate soluble GCs up to 100-200 fold, and resulting in the production of cGMP from GTP (Boon and Marletta, 2005b). Electrochemical studies on *AtNOGCI* demonstrated the ability of *AtNOGCI* to bind to NO with high affinity than it could to O₂ (Chapter 3). To further investigate if the binding of NO to *AtNOGCI* could activate *AtNOGCI*-catalysed synthesis of cGMP from GTP, some GC activity assays

were conducted *in vitro* in the presence of different DEA/NO donor concentrations (0, 5, 10, 20 and 50 μM). Figure 4.3 below shows the cGMP levels generated in the presence of different DEA/NO donor concentrations over a time period of 20 min. The results indicate that there was a significant increase in the cGMP levels from 0 μM to 5 μM NO concentrations, and however, there were no observable increases in the cGMP levels at the NO concentrations of 10 to 50 μM . An increase in the cGMP levels generated was observed from ~ 350 to 450 fmol cGMP/ μg protein in the presence of NO. For an easier comparison a negative control experiment in the absence of 10 μg protein was also conducted (figure 4.3, first bar).

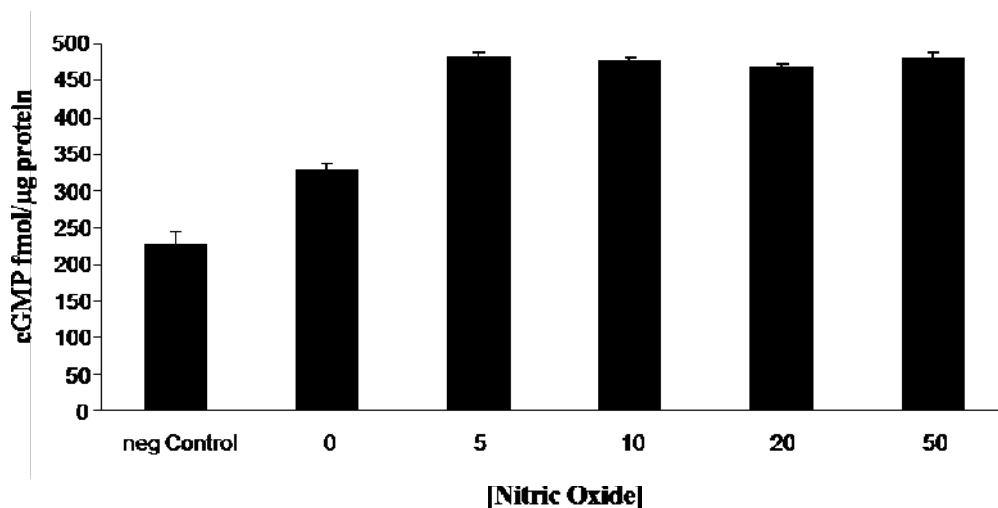


Figure 4.3: *in vitro* GC activity assays of *AtNOGCI* and its activation by NO. Cyclic GMP levels were measured in a reaction mixture containing 10 μg recombinant protein, 1 mM GTP as the substrate, 5 mM Mn^{2+} as a cofactor, and DEA/NO donor concentrations of 0-50 μM and the buffer was 50 mM Tris-HCl pH 8.0. The negative control reaction was also conducted in the absence of the recombinant protein. The cGMP levels generated by *AtNOGCI*'s enzymatic reaction were then measured using the EIA cGMP kit (Sigma-Aldrich, Inc.). Error bars represent the standard errors of the mean deviations (SEM) ($n = 3$).

4.3.3 Effect of calcium on GC activity assays of *AtNOGCI*

Calcium ion has been shown to have a regulatory effect on the activity of some GCs (Karmakar et al., 2006). A well characterised example of the regulatory effect of Ca^{2+} on GCs is that of the *AtPSKR1*, a GC from *Arabidopsis thaliana*, which showed a measurable increase in cGMP levels in the presence of Ca^{2+} (Dr Oziniel Ruzvidzo, personal communication). This study also investigated the regulatory effects of Ca^{2+} on the GC activity of *AtNOGCI*. Different concentrations of Ca^{2+} were indeed used to measure the amount of cGMP levels produced over a time period of 20 min. Figure 4.4 below shows the amount of cGMP generated by *AtNOGCI* in the presence of 0; 0.1; 1 and 10 μM Ca^{2+} concentrations. *AtNOGCI* exhibited an increase in the amount of cGMP levels in the presence of different Ca^{2+} concentrations with a maximum amount of ~ 450 fmol cGMP/ μg protein produced when Ca^{2+} was 0.1 μM as compared to ~ 300 fmol cGMP/ μg protein at 0 μM Ca^{2+} concentration. The results therefore, show the ability of Ca^{2+} to increase the GC activity of *AtNOGCI*.

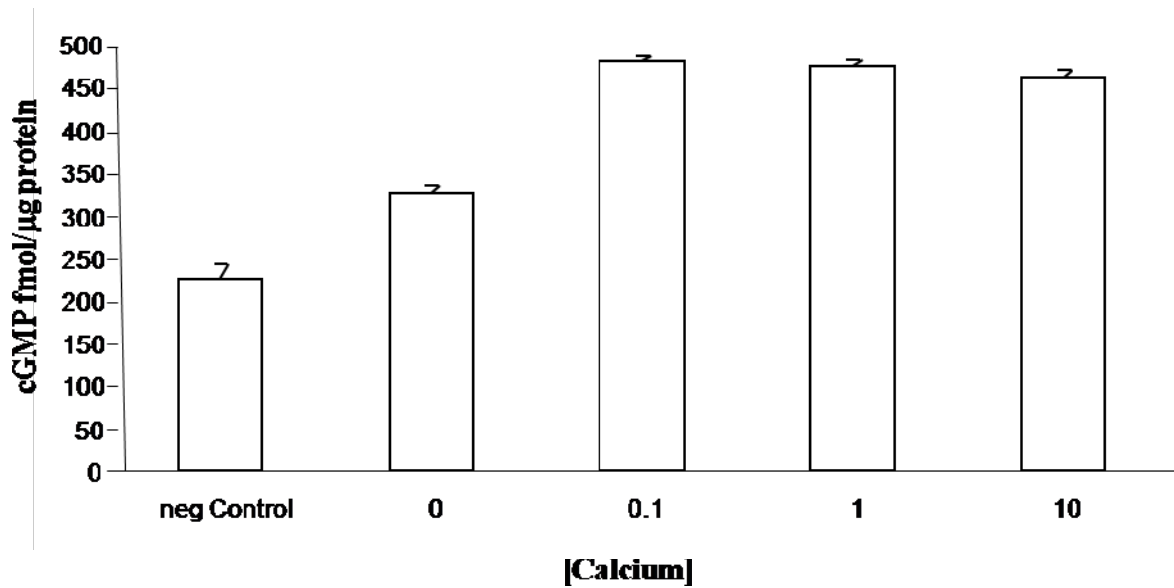


Figure 4.4: Effect of calcium on the GC activity of the purified recombinant *AtNOGCI*. Cyclic GMP levels were measured in a reaction mixture containing 10 μg recombinant protein, 1 mM GTP as the substrate, 5 mM Mn^{2+} as a cofactor, and CaCl_2 concentrations at 0, 0.1, 1 and 10 μM and the buffer was 50 mM Tris-HCl pH 8.0. A negative control was also conducted with the exclusion of the recombinant protein. The generated cGMP levels by *AtNOGCI*'s enzymatic reaction were then measured using the EIA cGMP kit (Sigma-Aldrich, Inc.). Error bars represent the standard errors of the mean deviations (SEM) ($n = 3$).

4.4 Discussion

Since there is evidence of endogenous levels of cGMP in plants in responses to pathogen challenge, peptides, NaCl and drought stress, ozone and other signals (Pharmawati et al., 2001; Donaldson et al., 2004; Pasqualini et al., 2008; Meier et al., 2009) and a number of physiological processes mediated by cGMP in plants, a number of plants GC's have since been identified (Ludidi and Gehring, 2003; Kwezi et al.; 2007; Meier et al., 2010; Kwezi et al., 2011 personal communication). Despite the physiological relevance of cGMP-mediated processes in plants, there has previously been a lack of well-characterised plant GCs that are NO-dependent, characterisation of these GC's showed that they catalyse the synthesis of cGMP from GTP *in vitro*, thus bringing insights into the understanding of cGMP-mediated processes. In addition to the cGMP signalling pathways, Denninger and co-workers reported that some of these physiological roles are NO-regulated (Denninger and Marletta, 1999). In this regard, the identification and characterisation of a plant GC that senses NO will be a break-through into the understanding of NO/cGMP-mediated processes. A search motif that was used specifically for the search of HNOX domains (Boon et al., 2005) has led to the identification of one of the four candidate genes containing both the heme motif and the GC motif in *Arabidopsis thaliana*, and the candidate gene was then named *AtNOGCI*. This study therefore explores the ability of *AtNOGCI* to function as a GC *in vitro* in an NO-dependent manner.

Soluble GC is a mammalian NO sensor, and contains the heme-binding motif required for sensing gases, sequence analysis showed that *AtNOGCI* contains a heme-binding motif (YxSxR) at the N-terminal that senses both NO and O₂ (Chapter 3). From sequence analysis,

it can be predicted that *AtNOGCI* is not similar to sGC although it bears a heme-binding motif.

The divalent cations, Mg^{2+} and Mn^{2+} ions up-regulate the activity of both ACs and GCs (Hurley, 1999; Seebeck et al., 2008). This study investigated the possibility of either Mg^{2+} and Mn^{2+} ions as possible cofactors of *AtNOGCI* activity. The results show that both ions increased the activity of *AtNOGCI* to catalyse the synthesis of cGMP from GTP (Figure 4.1B), with Mn^{2+} increasing the enzyme activity more than Mg^{2+} .

Similar binding affinities for ATP and GTP have been reported for mammalian sGC (Gille, 2004). Sequence analysis show that *AtNOGCI* contains the conserved residues, which participate in hydrogen bonding and the cysteine that confers substrate specificity for GTP than for ATP. These results show that only GTP binds to the active site with no comparable affinities between GTP and ATP (Figure 4.2). Furthermore, a cAMP assay should be conducted in the future to rule out the possibility of ATP as another substrate for *AtNOGCI*.

Binding of NO to sGC serves as a key step in the activation of the enzyme to catalyse the conversion of GTP to cGMP (Boon et al., 2005; Meier et al., 2007). Contrast to that, sequence analysis of *AtNOGCI* showed that it contains the heme-binding motif that senses NO. Based on that observation, it was therefore necessary to demonstrate that the binding of NO to *AtNOGCI* will activate the enzyme to synthesize cGMP from GTP. The results show that in the presence of an NO donor, approximately >2 fold excess in cGMP was produced as compared to the cGMP obtained in the absence of a NO donor (Figure 4.3). Although an increase in the GC activity of *AtNOGCI* cannot be compared to that of mammalian sGCs,

other factors such as the amount of NO produced by the donor and the differences in the sequence structure of the two proteins must be considered. Most importantly, the results showed an increase in cGMP synthesis, this might suggest that NO does play a role in the activation of *AtNOGCI*'s GC activity. Our findings that *AtNOGCI* contains a heme-binding motif that senses NO and the fact that it is a GC that is activated by NO, suggests that NO/cGMP signalling via GC's is not restricted to animals and prokaryotes only but also extends to the plant kingdom. *AtNOGCI* appears to have the GC activity *in vitro* that is NO-dependent, but the exact biological function still remains to be elucidated and this will be an interesting target for further understanding of the NO/cGMP signalling in plants.

Nitric oxide synthase (NOS), the enzyme that produces NO from amino acid L-arginine is activated by Ca^{2+} and once NO is produced, it activates the sGC to catalyse the synthesis of cGMP, which leads to downstream responses such as Ca^{2+} ion-gated channels. The role of Ca^{2+} in the synthesis of cGMP by the *Leishmaniado novani* GC has been reported and it has also been observed that intracellular Ca^{2+} somehow regulates the synthesis of cGMP levels (Karmakar et al., 2006). In this current study, when the GC activity of *AtNOGCI* was assayed, an increase in the cGMP levels was observed in the presence of different Ca^{2+} concentration *in vitro* (figure 4.4). However, the effect and regulation of GC by Ca^{2+} still need to be investigated further in order to shed more light on the Ca^{2+} -/cGMP and NO signalling pathways.

Finally, since the green alga *Clamydomonas reinhardtii* has been reported to contain over 90 annotated putative GC's (Schaap, 2005) and the fact that three GCs have been identified and characterised in *Arabidopsis thaliana*, (Ludidi and Gehring, 2003; Kwezi et al.; 2007; Meier

et al., 2010), it all suggests that a number of GCs are yet to be identified. This work has since identified and characterised a GC in *Arabidopsis thaliana* that not only catalyses the synthesis of cGMP from GTP, but also binds NO. Further characterisation of this new NO binding GC protein will open new ways to better understand NO/cGMP signalling processes in plants.

CHAPTER 5: Modelling *AtNOGCI*, a Flavin-containing Monooxygenase and *At5g57690*, a Diacylglycerol Kinase from *Arabidopsis thaliana*

Abstract

The understanding of structure-function relationships of proteins normally requires detailed information that can be extracted from their three-dimensional structures. Determination of protein structure by experimental means such as x-ray crystallography, NMR and electron microscopy tend to be difficult and time-consuming. Modelling of protein structures by computer based techniques has become an important option to produce 3D models of protein structures. Specifically, structures of bacterial HNOX domains, flavin-containing monooxygenases and diacylglycerol kinase have been determined however, these structures in plants have not yet been reported. This chapter participated in homology modelling and fold recognition of the *AtNOGCI* and *At5g57690*. Models for both proteins have been build and evaluated to be of good quality. Secondary structure prediction by PSI-PRED also indicated that both proteins contain a proper fold consisting of helices and beta sheets interconnected by loops. In addition, functional prediction was also conducted for both proteins and implicated to contain ion binding properties.

5.1 Introduction

Knowledge of the three-dimensional structure is a prerequisite for the rational design of site directed mutations in a protein. The information obtained from these structures enhances a great understanding of where protein atoms are located and how they interact during biochemical reactions, which bring insight on protein functions. Structural determination techniques such as X-ray crystallography, nuclear magnetic resonance (NMR) and electron microscopy (EM) provide detailed information of protein structures yet however, these techniques involve technical procedures, which are sometimes complicated and time consuming. Most proteins fail to crystallise and sometimes cannot be obtained in large quantities for structural determination by NMR. The size of the protein is also another limiting factor for structure determination by NMR (Branden and Tooze, 1991).

Computational structure determination tools such as model building based on the 3D structure of known homologs seem to be an alternative method to obtain structural information on proteins. The feasibility of homology model building has been indicated by the comparison between tertiary structures and primary structures. Since structure determination requires experimental information, both homology modelling and secondary structure prediction rely on proteins with known 3D structures. Comparative ("homology") modelling is a method that approximates the 3D structure of a target protein for which only the sequence is available. For the structure to be predicted, the 3D template structure should be provided with >30 % sequence identity. Sequences that are lower than 30 % will be fine if they have strong conserved features such as conserved cysteine residues. Comparative models are useful in getting a rough idea of where the alpha carbons of important residues are

found in the folded protein (Chothia and Lesk, 1986; Baker and Sali, 2001; Vitkup et al., 2001).

Unfortunately, any experimental procedure including model building will contain some errors associated with it, and these errors depend on the precision of the experimental measurements and are propagated into the precision of the final model. They result from errors in the interpretation of the experimental data and are related directly to the accuracy of the final structure. It is however crucial that every structural model undergo verification to obtain good results (Kleywegt, 2000). Several computational techniques are available for the verification of protein models and they include the Procheck program, which checks the stereochemical quality of a protein, by analysing its overall and residue-by-residues geometry (Laskowski et al., 1993; Laskowski et al., 1996).

In this chapter, the homology models of the two proteins ‘the *AtNOGCI*’ that is currently annotated as a flavin-containing monooxygenase and the ‘*At5g57690*’ currently annotated as a diacylglycerol kinase will be described and the topology of their structural conformations compared with the secondary structure fold predicted by the PSI-PRED. In addition, function prediction for the two proteins will also be described.

5.2 Materials and methods

5.2.1 Modelling of *AtNOGCI* and At5g57690

The sequences for both *AtNOGCI* and At5g57690 were analysed with BLAST in order to find similar sequences in the database. The sequences were therefore sent to Fugue server (Shi et al., 2001) to search for templates. The three-dimensional structure of *AtNOGCI* was solved according to the template based modelling strategy using the template of bacterial FMO from *Mythylophaga species* (pdb code: 2vq7), and the phenylacetone flavin-containing monooxygenase (pdb code: 1w4xa). The At5g57690 model was build based on the structures of the *Salmonella typhimurium* Yegs, a putative lipid kinase (pdb code: 2p1r) and the *E. coli* lipid kinase that is homologous to the mammalian diacylglycerol kinase (pdb code: 2bon. Protein sequences for *AtNOGCI* and At5g57690 were aligned using the mutialin program (Corpet, 1988).

Modeller 9v8 program was used to build 30 models (Sali and Blundell, 1993) and the best model was then selected based on the energy minimization (mol pdf) value and also based on the DOPE and the GAL scores. Procheck program was used to evaluate the model for stereochemical quality (Laskowski et al., 1993). Secondary structure prediction were performed with PSI-PRED sever (Bryson et al., 2005).

5.3 Results

5.3.1 *AtNOGCI* model

The 3D model of *AtNOGCI* (TAIR protein locus At1g62580, GenPept accession number, NP_176446) was performed according to the homology modelling strategy using template structures of bacterial FMOs from *Methylophaga sp.*, strain SK1 (PDB code: 2vq7a) and phenylacetone monoxygenase, a Baeyer-Villager monooxygenase (PDB code: 1w4xa) because the sequence identity of *AtNOGCI* and the two template proteins resulted in Z-scores of 59.47 and 19.13 respectively, which are both considered as a 99 % confidence prediction (Appendix III). The alignment of *AtNOGCI* with the two templates is shown in Figure 5.2. The residues which form part of the heme-binding motif are aligned to the other residues in the templates structures. Highly conserved residues and the three characteristic sequences in the FMO superfamily are: (1) the FAD binding domain (GAGAAG), (2) the FMO identifying sequence (FxGxxxHxxxF), and (3) the NADPH-binding domain (GSSVSG), where X can be any amino acid. Other crucially functional residues include the heme-binding motif (YxSxR) and the GC motif (SFSIGLGIDTWPG). Figure 5.1 show the alignment of *AtNOGCI* with mFMO and Baeyer-Villager monooxygenase.

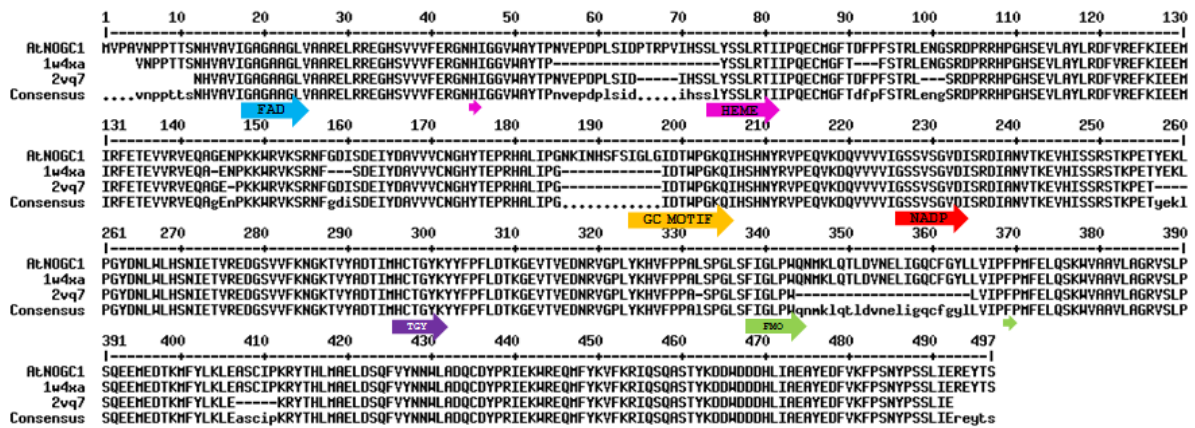


Figure 5.1: Alignment of *AtNOG1* with structures of the FMO from *Methylophaga Sp.* strain SK1 and a phenylacetone monoxygenase, a Baeyer-Villiger monoxygenase. Residues corresponding to the FAD binding domain, heme binding motif, GC motif, NADP binding motif, and the FMO signal sequence are highlighted in blue, magenta, orange, red, purple and green arrows respectively. The alignment was created by Multalin program.

Residues corresponding to the heme-binding motif are aligned with those from both template structures. Starting from this alignment, a set of 30 full-atom models was generated. Figure 5.2 shows the cartoon and surface representation of the *AtNOG1* best model, indicating the presence of the important and functional residues found in the protein structure. Figure 5.3 shows the ramachandran plot for the *phi* and *psi* angles of each residue in the model of *AtNOG1*, and indicates that *AtNOG1* model is stereochemically stable model. The best model had 87.8 % residues in the most favoured regions. This value when compared to those of the template structures of 89.2 % for 2vq7 and 89.9 % for 1u4xa indicated that a good model had been created. Although there is 1.2 % residues in the disallowed regions (E492, T176, I70, T298 and A473), these outliers when traced back in the structure, they were found to be located in the loop (Figure 5.3B).

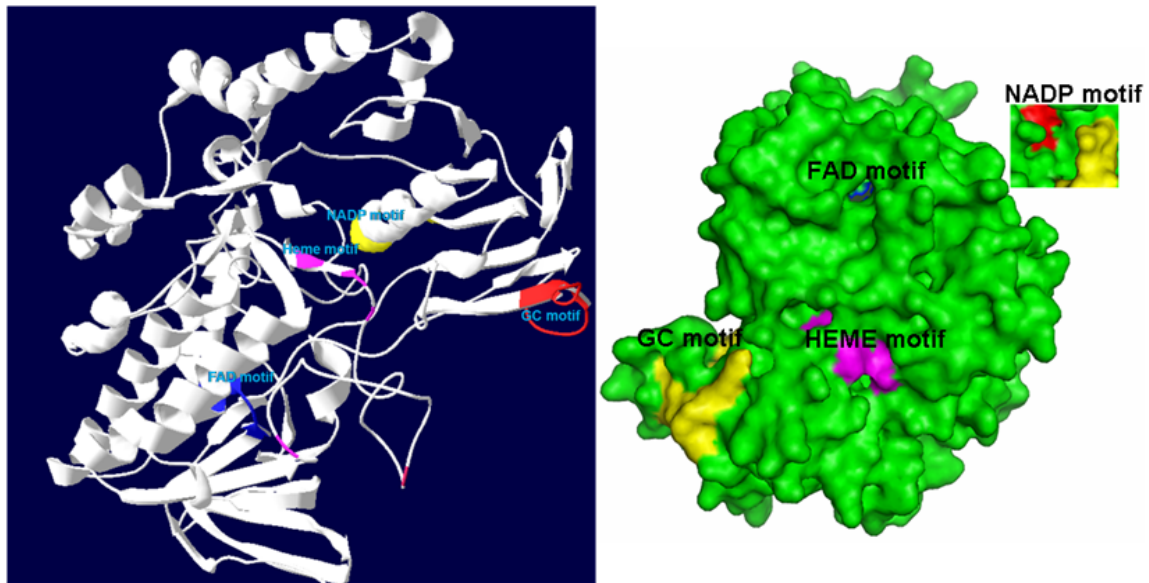


Figure 5.2: The three-dimensional model of *AtNOGCI*. Cartoon and surface representation of the *AtNOGCI* structure showing all the important residues, the FAD binding domain (blue), heme binding domain (magenta), GC domain (yellow) and the NADP binding domain (red).

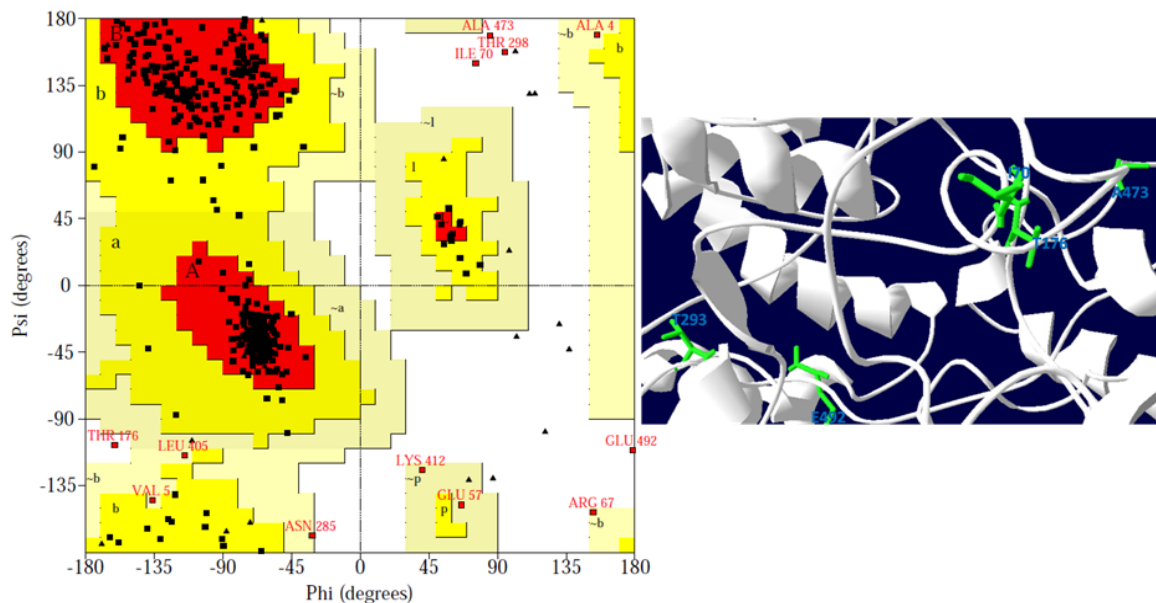


Figure 5.3: Evaluation of the *AtNOGCI* model by procheck. (A) Ramachandran plot showing the ϕ and ψ angles of the residues of the *AtNOGCI* model. There are 87.8 % residues in the most favoured region, 9.5 % in the additionally allowed region, 1.6 % in the generously allowed region and only 1.2 % in the disallowed region. (B) Cartoon representation of the residues in the outliers and as is found in the Ramachandran plot.

The structure of *AtNOGCI*, 2vq7 and 1w4xa were also compared by superimposition. Secondary structure predictions made by PSI-PRED programs agree with the obtained structure of *AtNOGCI* through template modelling. Comparison of the secondary structure evidenced that helices and β -strands are well conserved along the sequence and few changes are observed in length (Figure 5.4).

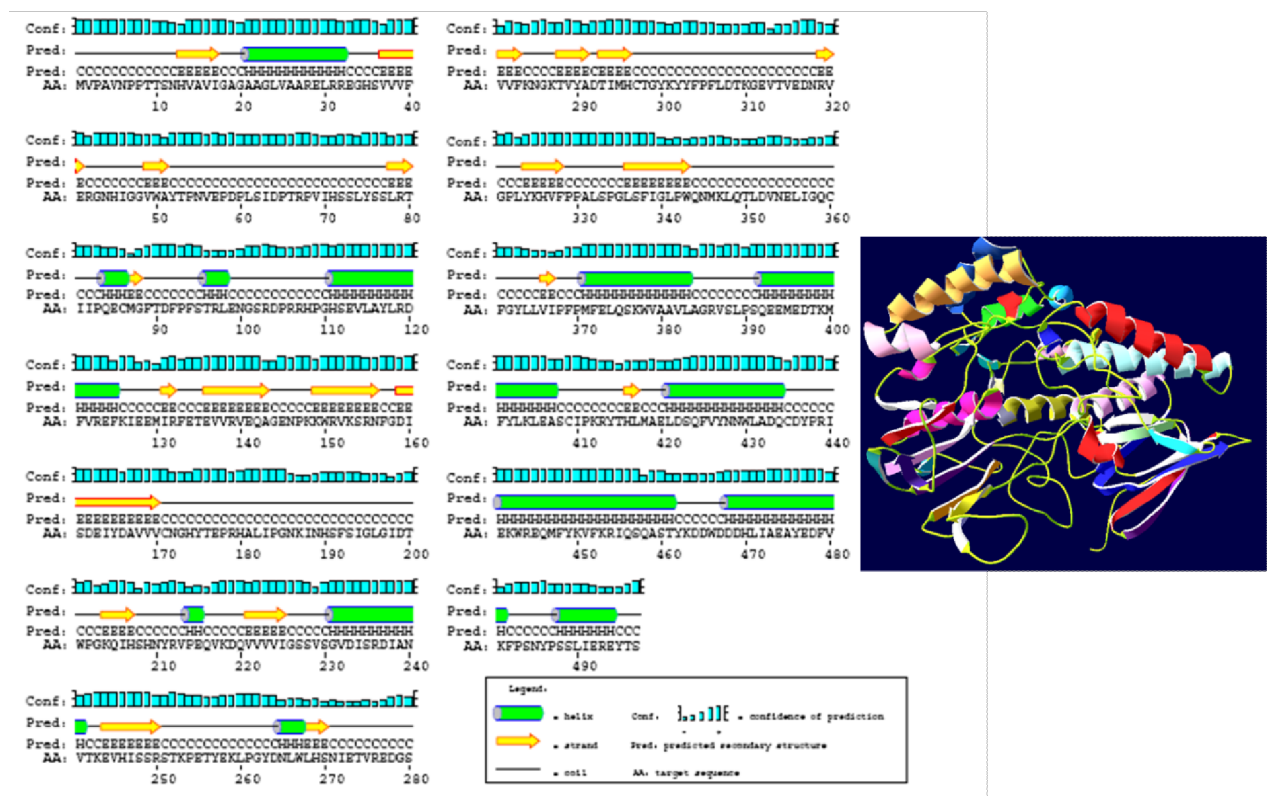


Figure 5.4: Fold recognition to determine the secondary structure of *AtNOGCI*. The secondary structure prediction shows that *AtNOGCI* consists of conserved helices and sheets, interlinked by loops. The 3D model created by modeller agrees with the secondary structure prediction.

5.3.1 At5g57690 model

The 3D model of At5g57690 (TAIR protein locus At1g62580, GenPept accession number, NP_176446) was performed according to the homology modelling strategy using template structures of the *Salmonella typhimurium* Yegs a putative lipid kinase (pdb code: 2p1r) and the *E. coli* lipid kinase that is homologous to the mammalian diacylglycerol kinase (pdb code:2bon). Figure 5.5 shows the alignment of At5g57690, *E. coli* lipid kinase and the *Salmonella typhimurium* lipid kinase. The two templates were selected because they had sequence identity of more than 30 %. The best model had 86.7 % of residues in the most favoured regions indicating a very quality model compared to 87.1 % and 87.5 % for 2p1r and 2bon templates respectively (see figure 5.6). The structure of At5g57690, 2p1r and 2bon were also compared by superimposition and secondary structure predictions made by PSI-PRED programs and agreed with the obtained structure of the At5g57690 by template modelling (Figure 5.7). Comparison of the secondary structure evidenced that α -helices and β -strands are well-conserved along the sequence and few changes are observed in length. The structure of the core is well-ordered, but the NH₂-terminal loop domain has conformational flexibility between regions 1-81. A refinement was done for the best model of the At5g57690 to obtain a more stabilized N-terminal. The model of At5g57690 was also checked for the presence of the GC motif 'RYGLGLCLEAFASR' and the HNOX motif 'Hx12Px14,16, YxSxR'.

```

1      10      20      30      40      50      60      70      80      90      100     110     120     130
|-----|-----|-----|-----|-----|-----|-----|-----|-----|-----|-----|-----|
At5g57690 MESPSIGDSL TARMIPRHSSLDSFGAMKVSLLVNLASIRVSKAELRQRVMLPQYLRIAIRDCILRKDDSFADSSSVAPPLENNALTPEVPLMYFVNPKSGGRQGPLIKERLQNLISEEQVYDLTEVKPNE
2BONa      MHHHHHAGSTSLYKKGSETLYIQGMREFPASLLI--LNGKSTDNLPLEAIMLLREEGMTI
2P1Ra      XANFPASLLI--LNGKSDNQPLREAITLLRDEGIQI
Consensus .....l..a.....a#fpaslli..Lngks.#NlpIrEa!.lLr#eg..i

131     140     150     160     170     180     190     200     210     220     230     240     250     260
|-----|-----|-----|-----|-----|-----|-----|-----|-----|-----|-----|-----|
At5g57690 FIRYGLGCLERAFASRGDECAKEIREKMRIVVAGGDDTVGVVLGCLGELNMQNRPVPPVSI MPLGTGNDLSRSFGGGSFPFAWKSAIKRTLHRASVAPISRLDSHWLITMPSGEIV--DPPYSLKAT-
2BONa      HVR--VTMEKGDARRYVEEARKFVAT-VIAGGGDGTINEVSTALIQCEGDD---IPALGILPLGTANDFATSVGIPEALDKALKLAIAGDAIADMAQVVKQTCFINMRTGGFGTRITTEPEKLKAL
2P1Ra      HVR--VTMEKGDARRYVEEARRLGVET-VIAGGGDGTINEVSTALIQIRDGV---APALGILPLGTANDFATSVGIPEALDKALKLAIAGNAXEIDAXVNDKTCFINXRTGGFGTRITTEPEKLKAL
Consensus h!R..vtwekgdA.Ryv#eAr..gv.t.!!agGGDGT!neVst.aLi#.....Palgi$PLGTaNDfatS.GipealdkAlKlAIag.a..id.A.in..tcf.in.aTggfGtr!tt#tPekLKAal

261     270     280     290     300     310     320     330     340     350     360     370     380     390
|-----|-----|-----|-----|-----|-----|-----|-----|-----|-----|-----|-----|
At5g57690 -QECYIDQNLIEIEGIEIPPSTNGYEGVFYNYFYSIGMDAQVAYGFHHLRNEK--PYLANGPIANKIISGYGCSQGMFLTHCINDPGLRGLKNIMTLHIKKLDSSEMEKVPVPKSVRAVVALNLHSYGSGR
2BONa      GSVSYIINGLMRMDLQPDRCCEIRGENFHMQGDALVIGIGNGRQAGGGQLCPNALINDGLLQLRIFTGDEILPALVSTLKSDEDN---PNIIEGASWFIDIQPHDITFNLGDEPLSGQNFHIEILPA
2P1Ra      GGVSYLIHGLXRXDTLTPDRCCEIRGENFHMQGDALVIGIGNGRQAGGGQLCPNALINDGLLQLRIFTGDEILPALVSTLQSDN---PNIIDGASWFIDIHAPHEITFNLGDEPLSGQEFHIEVLP
Consensus g.vsYiighL.r.d.t.l.PdrceirGen%hwqgda$vig!gnGrqaggg#qlcp.aLiNdglL#lrLzG.e.lpalfsTl...#dn.....pNIi.gas.ufDi.aph.!tfnldgeplsgq#FHie.lp

391     400     410     420     430     440     450     460     470     480     490     500     505
|-----|-----|-----|-----|-----|-----|-----|-----|-----|-----|-----|
At5g57690 NPMGNLKDQYLEKRGFVEAQADDGLLEIFGLKQGHASFVMVELISAKHIAQLMCKNLGFNEQRAAIRLEIRGGDKDAFMQMDGEPMKQPHTROYSTFYDIKRVPHQSLVYKGD
2BONa      ALRCRLPPDCPLLRSSTHHHHH
2P1Ra      ALRCRLPPDCPLLRS
Consensus aLrcrLppDcpLLR.....

```

Figure 5.5: Alignment of the At5g57690 with template structures *Salmonella typhimurium* Yegs (pdb code: 2p1r) and *E. coli* lipid kinase (pdb code: 2bon). The two templates lack the conserved heme-binding motif and the GC motif, highlighted in the At5g57690 sequence.

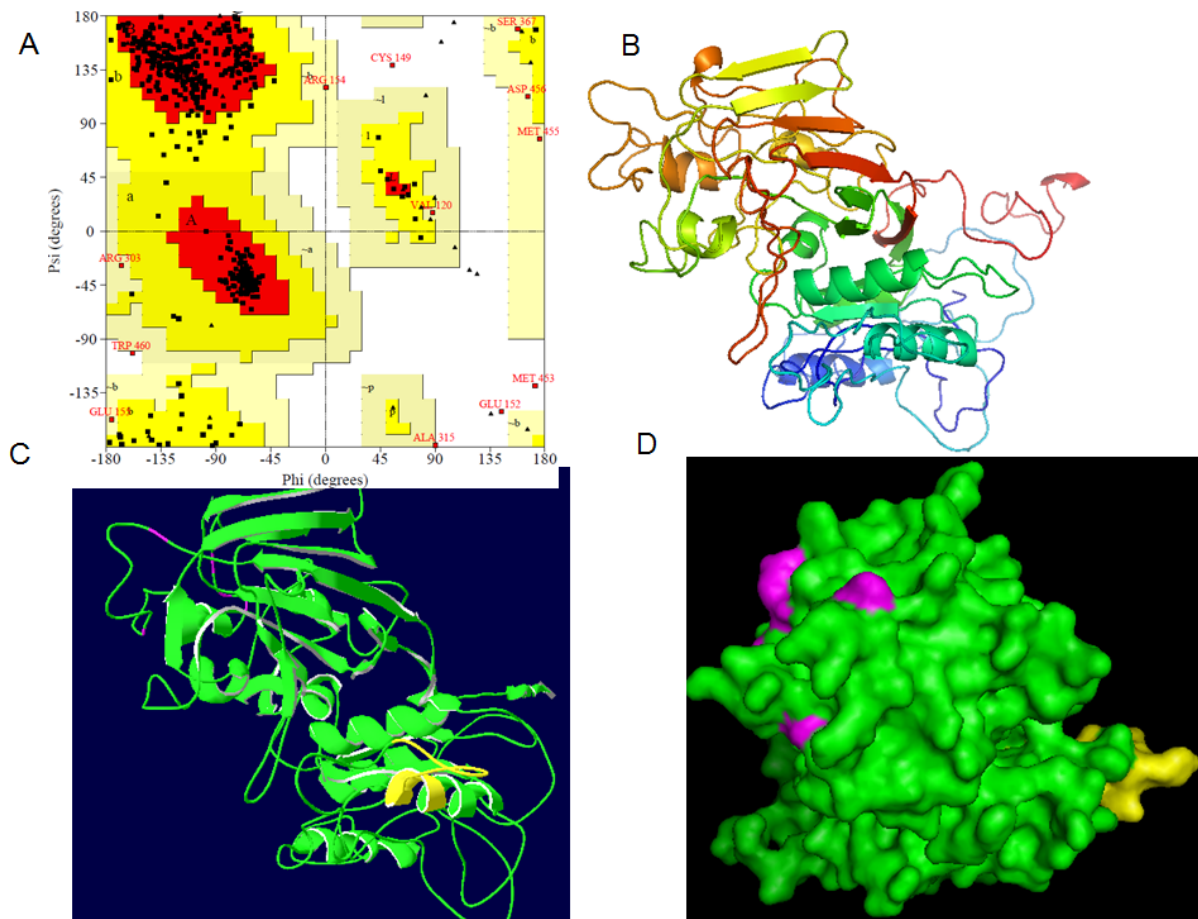


Figure 5.6: Evaluation of the model structure obtained for At5g57690. (A) Ramachandran plot showing the *phi* and *psi* angles of the residues of the At5g57690 model. There are 85.0 % residues in the most favoured region, 12.1 % in additional allowed region, 1.7 % in the generously allowed region and only 1.2 % in the disallowed region. With over 90 % residues in the allowed region, At5g57690 is therefore a stable model. (B) Cartoon representation of the 3D model of At5g57690 shown in different colours. At5g57690 consists of ~10 helices and ~9 sheets interconnected by loops. (C) Cartoon representation and (D) surface representation of At5g57690 showing the GC motif highlighted in yellow and the HNOX motif highlighted in magenta (Figure plotted using pymol).

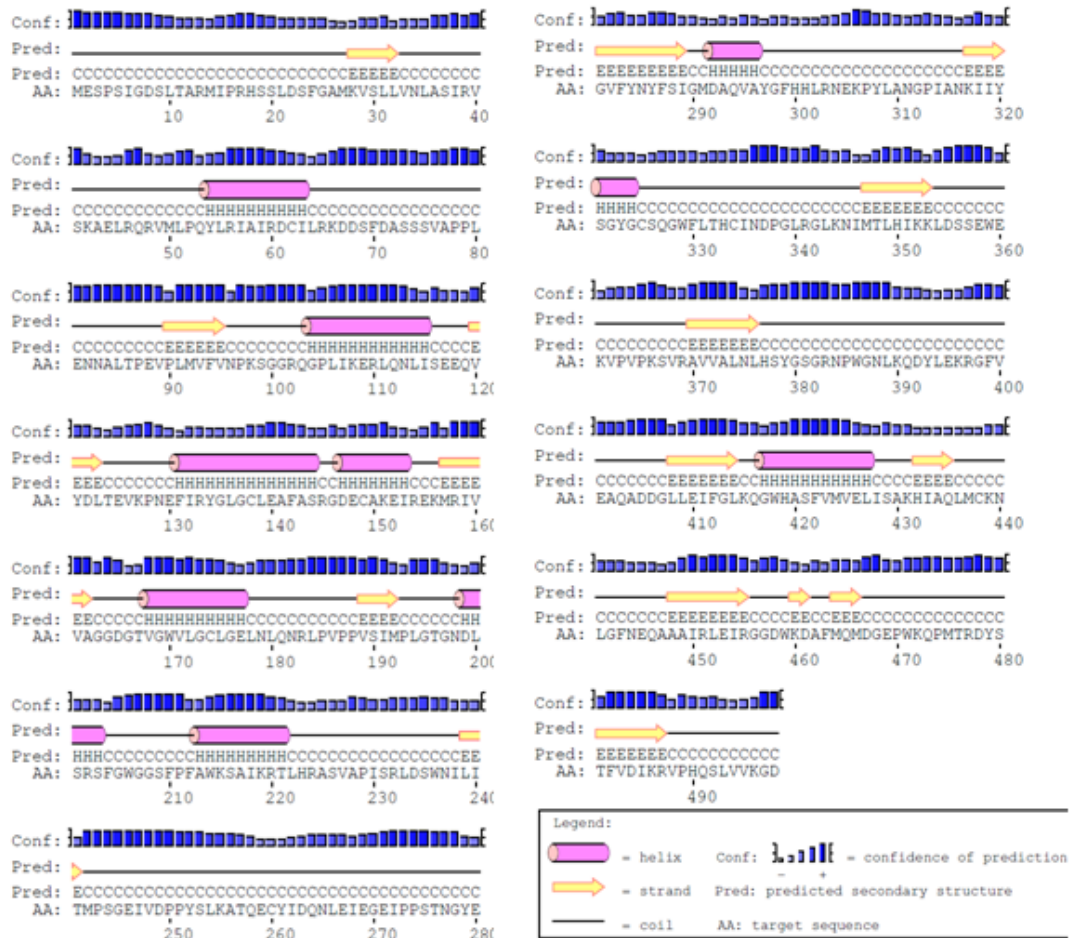


Figure 5.7: Fold recognition to determine the secondary structure of At5g57690. The secondary structure prediction shows that *AtNOGCI* consists of conserved helices and sheets interlinked by loops. The fold recognition was determined by the PSI-PRED server (Bryson et al., 2005).

4.4 Discussion

Several studies have demonstrated a physiological role of NO in regulation of intracellular Ca^{2+} concentrations and protein kinases, modulation of plant responses to pathogens, which are crucial for plant growth (Besson-Bard et al., 2008a; Hong et al., 2008; Qiao and Fan, 2008; Wilson et al., 2008). This study has identified a NO binding protein that also acts as a GC *in vitro*. *AtNOGCI* is a 409 amino acid protein, based on its size and the presence of most important functionally sequences might suggest it to be a multifunctional protein. Structural characterisations of the novel *AtNOGCI* will lighten up more functional roles that are related to this protein in plants. This chapter has explored the structural basis for the two HNOX domains identified from *Arabidopsis thaliana* and the residues involved in heme-binding are highlighted.

The *AtNOGCI* was modelled and analysed, and model evaluation showed that with over 90 % residues in the allowed regions, the model created was indeed of good quality. Secondary structure prediction by PSI-PRED indicated that *AtNOGCI* is made up of ~13 helices and ~20 sheets which are interconnected by loops, and this prediction correlated well with the prediction made by modeller with minor changes such as an extra helix.

AtNOGCI is an *Arabidopsis thaliana* protein that is currently annotated as a flavin containing monooxygenase. Sequences analysis highlighted some important motifs in the sequence of the *AtNOGCI*, which include the heme-binding motif and GC motif, and furthermore, using experimental methods, this study has also demonstrated a function of the *AtNOGCI* in NO/O₂ binding (Chapter 3) and in GC activity (Chapter 4). Plants contain a large number of

functionally characterized and annotated FMOs of which the Arabidopsis encode 29 annotated genes (Schlauch, 2007) compared to the animal and yeast kingdom and this suggesting that a wide range of functions are yet to be identified for FMOs in plants. Searching for the homologs to use as template structures for model building using FUGUE server (Shi et al., 2001), templates with high sequence identify to the *AtNOGCI* are also known to be from a family of FMOs. Based on the structural sequence alignment of *AtNOGCI* with the two templates (Figure 5.1), *AtNOGCI* binds the adenine moiety of the FAD via the FAD-binding motif 'GAGAAG' which is located at the N-terminus and NADPH-binding motif 'GSGVVG' located towards the centre of the protein. *AtNOGCI* is also characterized by an FMO identifying motif which on the alignment aligned with the 2vq7 template at the same position but not with the 1w4xa template, and this difference in position for the FMO identifying motif have also been previously reported (Fraaije et al., 2002; Eswaramoorthy et al., 2006). Like other FMO, *AtNOGCI* contains the HCTGYK motif indicating a role in oxidizing sulphur containing substrates.

Blast searches for sequences analysis also indicated that *AtNOGCI* is a multi-domain protein, which include a flavin-binding monooxygenase-like and a **TrkA domain, which is a predicted flavoprotein involved in K⁺ transport [inorganic ion transport and metablosim]**. The PHYRE server was also explored to gain more information on the function of *AtNOGCI*, and its Conserved Residue Function Prediction (confun) indicated *AtNOGCI* to be involved in processes such as monooxygenase activity, flavin-containing monooxygenase activity, oxidoreductase activity (acting on paired donors incorporating or reducing molecular oxygen), magnesium ion binding, metal ion binding and ion binding. These functions indicate that *AtNOGCI* might be a multifunctional domain protein with a wide range of functions yet

to be discovered. Therefore, the structural determination of the *AtNOGCI* will be a huge breakthrough in the understanding of many functions related to this protein.

At5g57690 is currently annotated as a diacylglycerol kinase and like *AtNOGCI*, it was also identified during the search for HNOX domains in *Arabidopsis thaliana*. Sequence alignment of At5g57690 with the two templates showed some conserved residues in the family of the lipid kinases however, none of the template contained the residues required for heme-binding and GC activity as found in At5g57690. The At5g57690 was modelled and analysed, and the model evaluation showed that with over 90 % residues in the allowed regions, the model created was of very good quality. Secondary structure prediction by PSI-PRED indicated that At5g57690 is made up of ~10 α -helices and ~9 β -sheets which are interconnected by loops.

Function prediction conducted by the PHYRE server, implicated At5g57690 in a number of functions including involvement in phosphotransferase activity, kinase activity, transferase activity (in transferring phosphorus containing groups), lipid binding, catalytic activity, molecular function and finally, in binding. Based on the model that was build for the At5g57690, its role in binding correlates very well with our prediction that it contains a heme-binding motif and a GC motif.

6. Final conclusion and future perspective

South Africa has an increasing population with high dependency on agriculture, however factors such as pathogens, drought, salinity, high and low temperatures, hinder plant growth which therefore lead to low crop yield and food availability (Denby and Gehring, 2005). To alleviate this problem, farmers use expensive equipment, chemicals and most importantly irrigation to maintain quality and high crop production. This in turn, affects food availability and prices drastically, both in South Africa and worldwide. Food shortage can also lead to malnutrition and associated diseases, a scenario has been commonly observed in several African countries. Food security is therefore dependent on the development and production of staple crop plants that have increased resistance to abiotic and biotic stresses such as drought and pathogen challenge respectively (Denby and Gehring, 2005).

The application of plant biotechnology and its recent advances in molecular research technologies will help to discover novel candidate molecules to help enhance crop production. Identification and analysis of genes encoding proteins that exhibit large expression responses to several different types of stress may provide insights into the functional basis of multiple stress tolerance and an understanding in the signalling cascades occurring in plants. This will aid as a promising target for maintaining plant growth and development.

Application of these rational approaches has led to the identification of guanylyl cyclases in higher plants (Ludidi and Gehring, 2003). These GCs have been demonstrated to synthesize cGMP, which in turn, plays a role as a second messenger and involved in important processes

such as drought and salinity tolerance in plants, (Donaldson et al., 2004), induction of pathogen resistance genes such as PAL (Durner et al., 1998) and mediation of homeostasis in plants (Ramirez et al., 2010). Several studies have shown a link between the second messenger cGMP and NO in mediating signalling cascades and stress signalling pathways in particular. Although a full understanding of how this NO/cGMP signalling cascade is conducted has not yet been reported. NO has been shown to be an important signalling molecule in many plant processes, such a response to pathogens (Delledonne et al., 1998), increased tolerance to drought in plants (Lamattina et al., 2003), and is also a major signal in the production of transient cGMP levels (Durner et al., 1998). Thus a heme protein containing soluble guanylyl cyclase member may provide the missing link between NO and cGMP signalling in plants.

Since major components of the NO/cGMP pathway including the NO-sensitive GC in higher plants are not yet reported, their identification was a great target for our understanding of the plant signalling pathways. An attempt has been made to search for candidates containing the heme-binding domains for sensing gases using the HNOX approach (Boon and Marletta, 2005a, b) and the GC motif (Ludidi and Gehring, 2003). A small number of new genes including the flavin-containing monooxygenase-like protein (At1g62580/*AtNOGCI*) and the diacylglycerol kinase (At5g57690) were identified in the *Arabidopsis thaliana* proteome. To elucidate the functional role of *AtNOGCI*, a recombinant protein was prepared (Chapter 2) and it's molecular and biochemical properties analysed (Chapters 3, 4 and 5).

Structural characterisation including homology modelling (Sali and Blundell, 1993), fold recognition (Bryson et al., 2005) and sequence analysis strongly indicated the presence of the conserved heme-binding motif as observed in other heme proteins (Pellicena et al., 2004;

Rothkegel et al., 2006) for both *AtNOGCI* and At5g57690. As heme proteins are known for their function in sensing gases, electrochemical studies were therefore undertaken and demonstrated that *AtNOGCI* senses NO with higher affinity than for O₂, (chapter 3) NO being an important signalling molecule in plants (Durner et al., 1998). The role of NO to modulate plant growth and development by mediating processes such as response to pathogens (Delledonne et al., 1998), increased drought resistance in wheat seedlings (Beligni and Lamattina, 2000; Neill et al., 2003) and roles in both apoptosis and anti-apoptotic (Beligni et al., 2002; Garcia-Mata and Lamattina, 2001), have been reported. In pathogen response, NO is suggested to induce the expression of disease resistance genes. Although most of these roles have been demonstrated to occur both *in vivo* and *in vitro*, an understanding of the signalling cascade is still missing. The involvement of *AtNOGCI* in sensing NO might suggest an important role of *AtNOGCI* in NO signalling pathways. Electrochemical-catalytic properties of *AtNOGCI* also suggested the reduction of NO at the *AtNOGCI* bioelectrode. The electrochemical oxidation and reduction of NO has been shown to result in the formation of metabolic compounds such as nitrite (NO₂⁻) and then to nitrate (NO₃⁻), nitrous oxide (N₂O), nitrogen gas (N₂), hydroxylamine (NH₃OH⁺) and ammonia (NH₃⁺) (Kosminsky et al., 2001; de Vooy et al., 2004). Inspection of the microarray data of the transcriptional activation of the *AtNOGCI* implied a significant elevation of transcript levels during NO₃ starvation (Appendix IV). Taken together with its role in NO sensing, the molecule might also have as yet unknown role in nitrogen metabolism. In addition, the microarray data also implies that increased expression levels of *AtNOGCI* may occur in stress processes including the defence against pathogens as well as in epidermal root tissue at several stages during root growth (Appendix IV).

It was also demonstrated that *AtNOGCI* has a GC activity *in vitro* that is NO-dependent (Chapter 4). Although GCs in higher plants have been identified and characterised including the AtGC1 (Ludidi and Gehring, 2003), the AtBRI1 (Kwezi et al., 2007), the AtWAKL10 (Meier et al., 2010), it should be noted that neither of them binds to NO and that their GC activities were not NO-dependent. Circumstantial evidence of the NO/cGMP signalling pathway in plants has been reported, although a clear understanding remains elusive (Wendehenne et al., 2004). The link between NO sensing and the GC activity which is NO-dependent by *AtNOGCI* suggests the presence of a soluble GC-like in higher plants, and this in turn may imply that *AtNOGCI* has an important role in cellular signalling.

Three-dimensional models for both *AtNOGCI* and At5g57690 were built and confirmed the presence of the heme-binding motifs and suggested that the structures of both proteins provide an additional basis of further understanding their functions. In assigning a biological role to *AtNOGCI* in plants, it will be necessary to elucidate the more biological aspects and stimuli activation of this protein molecule. One way of doing it would be to construct *AtNOGCI*-knockouts in the Arabidopsis and using transcriptomics, proteomics and biochemical methods to analyse the phenotypes under normal and stress conditions. Since the use of soluble GC inhibitors abolished NO related functions in plants (Durner et al., 1998), an Arabidopsis cell line lacking the *AtNOGCI* gene or selected mutants will further elucidate the biological roles of *AtNOGCI* in NO signalling.

7. References

- Arasimowicz, M., and Floryszak-Wieczorek, J. (2007). Nitric oxide as a bioactive signalling molecule in plant stress responses *Plant Science* **172**, 876–887.
- Baker, D., and Sali, A. (2001). Protein structure prediction and structural genomics. *Science* **294**, 93-96
- Bard, A.J., and Faulkner, L.R. (1980). *Electrochemical Methods, Fundamentals and Applications*. Wiley, New York, 181-164
- Bartsch, M., Gobbato, E., Bednarek, P., Debey, S., Schultze, J.L., Bautor, J., and Parkera, J.E. (2006). Salicylic acid-independent enhanced disease susceptibility 1 signaling in Arabidopsis immunity and cell death is regulated by the monooxygenase FMO1 and the nudix hydrolase NUDT7. *Plant Cell* **18**, 1038–1051.
- Beligni, M.V., Fath, A., Bethke, P.C., Lamattina, L., and Jones, R.L. (2002). Nitric Oxide Acts as an Antioxidant and Delays Programmed Cell Death in Barley Aleurone Layers. *Plant Physiol* **129**, 1642–1650.
- Beligni, M.V., and Lamattina, L. (1999). Nitric oxide counteracts cytotoxic processes mediated by reactive oxygen species in plant tissues. *Planta* **208**, 337–344.
- Beligni, M.V., and Lamattina, L. (2000). Nitric oxide stimulates seed germination and de-etiolation and inhibits hypocotyl elongation: three light-inducible responses in plants. *Planta* **210**, 215–221.
- Bertotti, M., Mori, V., Zanichelli, P., Toledo, J.C., and Wagner Franco, D. (2005). Electrochemical and spectrophotometric methods for evaluation of NO dissociation rate constants from nitrosyl metal complexes activated through reduction. *Methods Enzymol* **396**, 45-53.

- Besson-Bard, A., Courtois, C., Gauthier, A., Dahan, J., Dobrowolska, G., Jeandroz, S., Pugin, A., and Wendehenne, D. (2008a). Nitric oxide in plants: Production and cross-talk with Ca²⁺ signaling. *Mol Plant* **1**, 218-228.
- Besson-Bard, A., Pugin, A., and Wendehenne, D. (2008b). New Insights into Nitric Oxide Signaling in Plants. *Annu Rev Plant Biol* **59**, 21–39.
- Birnboim, H.C., and Doly, J. (1979). A rapid alkaline extraction procedure for screening recombinant plasmid DNA. *Nucleic Acids Res* **7**, 1513-1523.
- Boon, E.M., Huang, S.H., and Marletta, M.A. (2005). A molecular basis for NO selectivity in soluble guanylate cyclase. *Nat Chem Biol* **1**, 53-59.
- Boon, E.M., and Marletta, M.A. (2005a). Ligand discrimination in soluble guanylate cyclase and the H-NOX family of heme sensor proteins. *Curr Opin Chem Biol* **9**, 441-446.
- Boon, E.M., and Marletta, M.A. (2005b). Ligand specificity of H-NOX domains: from sGC to bacterial NO sensors. *J Inorg Biochem* **99**, 892-902.
- Branden, C., and Tooze, J. (1991). Introduction to Protein Structure. *Trends Endocrinol Metab:Garland Publishing* **3**, 380
- Bryson, K., McGuffin, L.J., Marsden, R.L., Ward, J.J., Sodhi, J.S., and Jones, D.T. (2005). Protein structure prediction servers at University College London. *Nucl Acids Res* **33**, (Web Server issue):W36-38.
- Capece, L., Estrin, D.A., and Marti, M.A. (2008). Dynamical characterization of the heme NO oxygen binding (HNOX) domain. Insight into soluble guanylate cyclase allosteric transition. *Biochemistry* **47**, 9416-9427.
- Casero, E., Darder, M., Pariente, F., and Lorenzo, E. (2000). Peroxidase enzyme electrodes as nitric oxide biosensors. *Anal Chim Acta* **403**, 1-9.
- Chan, M.K. (2001). Recent advances in heme-protein sensors. *Curr Opin Chem Biol* **5**, 216–222.

- Chothia, C., and Lesk, A.M. (1986). The relation between the divergence of sequence and structure in proteins. *EMBO J* **5**, 823-826.
- Ciszewski, A., and Milczarek, G. (2003). Electrochemical detection of nitric oxide using polymer modified electrodes. *Talanta* **61**, 11-26.
- Clarke, A., Desikan, R., Hurst, R.D., Hancock, J.T., and Neill, S.J. (2000). NO way back: nitric oxide and programmed cell death in *Arabidopsis thaliana* suspension cultures. *Plant J* **24**, 667 - 677.
- Corpet, F., (1988). Multiple sequence alignment with hierarchical clustering. *Nucl. Acids Res.* **16**, 10881-10890.
- Correa-Aragunde, N., Graziano, M., and Lamattina, L. (2004). Nitric oxide plays a central role in determining lateral root development in tomato. *Planta* **218**, 900–905
- De Stefano, M., Ferrarini, A., and Delledonne, M. (2005). Nitric oxide functions in the plant hypersensitive disease resistance response. *BMC Plant Biol* **5**, S10.
- de Vooy, A.C.A., Beltramo, G.L., van Riet, B., van Veen, J.A.R., and Koper, M.T.M. (2004). Mechanism of electrochemical reduction and oxidation of nitric oxide. *Electrochim Acta* **49**, 1307-1314.
- Delledonne, M. (2005). NO news is good news for plants. *Curr Opin Plant Biol* **8**, 390–339
- Delledonne, M., Xia, Y., Dixon, R.A., and Lamb, C. (1998). Nitric oxide functions as a signal in plant disease resistance. *Nature* **394**, 585-588.
- Delledonne, M., Zeier, J., Marocco, A., and Lamb, C. (2001). Signal interactions between nitric oxide and reactive oxygen intermediates in the plant hypersensitive disease resistance response. *Proc Natl Acad Sci USA* **98**, 13454-13459.
- Denby, K., and Gehring, C. (2005). Engineering drought and salinity tolerance in plants: lessons from genome-wide expression profiling in *Arabidopsis*. *Trends in Biotech* **23**, 547.

- Denninger, J.W., and Marletta, M.A. (1999). Guanylate cyclase and the NO/cGMP signaling pathway. *Biochim Biophys Acta* **1411**, 334-350.
- Desikan, R., Griffiths, R., Hancock, J., and Neill, S.J. (2002). A new role for an old enzyme: nitrate reductase-mediated nitric oxide generation is required for abscisic acid-induced stomatal closure in *Arabidopsis thaliana*. *Proc Natl Acad Sci USA* **99**, 16314–16318.
- Deutscher, M.P. (1990). Guide to protein purification. *Methods Enzymol* **182**, 309.
- Diaz-Gonzalez, M., Gonzalez-Garcia, M.B., Costa-Garcia, A. (2005). Recent advances in electrochemical enzyme immunoassay. *Electroanalysis* **17** (21), 1901-1918.
- Donaldson, L., Ludidi, N., Knight, M.R., Gehring, C., and Denby, K. (2004). Salt and osmotic stress cause rapid increases in *Arabidopsis thaliana* cGMP levels. *FEBS Lett* **569**, 317–320.
- Durner, J., Daniel, F., and Klessig, D.F. (1999). Nitric oxide as a signal in plants. *Curt Opin Plant Biol* **2**, 369–374.
- Durner, J., Wendehenne, D., and Klessig, D.F. (1998). Defense gene induction in tobacco by nitric oxide, cyclic GMP and cyclic ADP ribose. *Proc Natl Acad Sci USA* **95**, 10328-10333.
- Eswaramoorthy, S., B., J., Bonanno, J.B., Burley, S.K., and Swaminathan, S. (2006). Mechanism of action of a flavincontaining monooxygenase. *PNAS* **103**, 9832–9837
- Fan, C., Xinjian, L., Panga, J., Lia , G., and Scheerb, H. (2004). Highly sensitive voltammetric biosensor for nitric oxide based on its high affinity with hemoglobin. *Anal Chim Acta* **523**, 225–228.
- Fan, H.-F., Chang-Xia Du, C.-X., and Gu, S.-R. (2010). Nitric oxide enhances salt tolerance in cucumber seedlings by regulating free polyamine content *Environ Exp Bot*, doi:10.1016/j.envexpbot.2010.1009.1000.
- Fraaije, M.W., Kamerbeek, N.M., Van Berker, W.J.H., and Jansen, D.B. (2002). Identification of a Baeyer-Villiger monooxygenase sequence motif. *FEBS Lett* **518**, 43–47.

- Furchgott, R.F. (1995). Special topic: nitric oxide. *Ann Rev Physiol* **57**, 659-682.
- Garcia-Mata, C., and Lamattina, L. (2001). Nitric oxide induces stomatal closure and enhances the adaptive plant responses against drought stress. *Plant Physiol* **126**, 1196–1204.
- Gerzer, R., Bohme, E., Hofmann, F., and Schultz, G. (1981). Soluble guanylate cyclase purified from bovine lung contains heme and copper. . *FEBS Lett* **132**, 71-74.
- Gille, A. (2004). Differential inhibition of adenylyl cyclase isoforms and soluble guanylyl cyclase by purine and pyrimidine nucleotides. *J Biol Chem* **279**, 19955-19969.
- Gong, W., Hao, B., Mansy, S.S., Gonzalez, G., Gilles-Gonzalez, M.A., and Chan, M.K. (1998). Structure of a biological oxygen sensor: A new mechanism for heme-driven signal transduction. *Proc Natl Acad Sci USA* **95**, 15177–15182.
- Gouvêa, C.M.C.P., Souza, J.F., Magalhães, A.C.N., and Martins, I.S. (1997). NO–releasing substances that induce growth elongation in maize root segments. *Plant Growth Reg* **21**, 183-187.
- Guo, F.Q., Okamoto, M., and Crawford, N.M. (2003). Identification of a plant nitric oxide synthase gene involved in hormonal signaling *Science* **302**, 100–103.
- Guse, A.H. (1999). Cyclic ADP-ribose: A Novel Ca²⁺ Mobilising Second Messenger. *Cell Signal* **11**, 309–316.
- Hakim, T.S., Sugimori, K., Camporesi, E.M., and Anderson, G. (1996). Half-life of nitric oxide in aqueous solutions with and without haemoglobin. *Physiol Meas* **17**, 267-277.
- He, Y., Tang, R.H., Hao, Y., Stevens, R.D., Cook, C.W., and Ahn, S.M. (2004). Nitric oxide represses the Arabidopsis floral transition *Science* **305**, 1968–1971.
- Hong, J.K., Yun, B.W., Kang, J.G., Raja, M.U., Kwon, E., Sorhagen, K., Chu, C., Wang, Y., and Loake, G.J. (2008). Nitric oxide function and signalling in plant disease resistance. *J Exp Bot* **59**, 147-154.

- Hu, N. (2001). Direct electrochemistry of redox proteins or enzymes at various film electrodes and their possible applications in monitoring some pollutants. *Pure Appl Chem* **73**, 1979-1991.
- Huang, X., Stettmaier, K., Michel, C., Hutzler, P., Mueller, M.J., and Durner, J. (2004). Nitric oxide is induced by wounding and influences jasmonic acid signaling in *Arabidopsis thaliana*. *Planta* **218**, 938-946.
- Hurley, J.H. (1999). Structure, mechanism, and regulation of mammalian adenylyl cyclase. *J Biol Chem* **274**, 7599-7602.
- Iwuoha, E.I., Joseph, S., Zhang, Z., Smyth, M.R., Fuhr, U., and Ortiz de Montellano, P.R. (1998). Drug metabolism biosensors: electrochemical reactivities of cytochrome P450cam immobilised in synthetic vesicular systems. *J Pharm Biomed Anal* **17**, 1101-1110.
- Jih, P.J., Chen, Y.C., and Jeng, S.T. (2003). Involvement of hydrogen peroxide and nitric oxide in expression of the ipomoelin gene from sweet potato. *Plant Physiol* **132**, 381-389.
- Kaplan, B., Sherman, T., and Fromm, H. (2007). Cyclic nucleotide-gated channels in plants. *FEBS Lett* **581**, 2237-2246.
- Kapust, R.B., and Waugh, D.S. (1999). Escherichia coli maltose-binding protein is uncommonly effective at promoting the solubility of polypeptides to which it is fused. *Protein Sci* **8**, 1668-1674.
- Karmakar, S., Ukil, A., Mukherjee, S., and Das, P.K. (2006). Regulation of guanylyl cyclase by intracellular Ca^{2+} in relation to the infectivity of the protozoan parasite, *Leishmania donovani*. *J Biochem & Cell Biol* **38**, 1277-1289.
- Kleywegt, G.J. (2000). Validation of protein crystal structures. *Acta Crystallogr D* **56**, 249-265.

- Kopyra, M., and Gwozdz', E.A. (2003). Nitric oxide stimulates seed germination and counteracts the inhibitory effect of heavy metals and salinity on root growth of *Lupinus luteus*. *Plant Physiol Biochem* **41**, 1011–1017.
- Kosminsky, L., Mori, V., and Bertotti, M. (2001). Electrochemical studies on the oxidation of nitric oxide (NO) at glassy carbon electrodes modified by molybdenum oxides. *J Electroanal. Chem* **499**, 176-181.
- Kumar, D., and Klessig, D.F. (2000). Differentiation induction of tobacco MAP kinases by the defense signals nitric oxide, salicylic acid, ethylene, and jasmonic acid. *Mol Plant Microbe Interact* **3**, 347-351.
- Kurosaki, F., and Nishi, A. (1993). Stimulation of calcium influx and calcium cascade by cyclic AMP in cultured carrot cells. *Arch Biochem Biophys* **302**, 144-151.
- Kwezi, L., Meier, S., Mungur, L., Ruzvidzo, O., Irving, H., and Gehring, C. (2007). The *Arabidopsis thaliana* brassinosteroid receptor (AtBRI1) contains a domain that functions as a guanylyl cyclase *in vitro*. *PLoS One*, e449.
- Laemmli, U.K. (1970). Cleavage of structural proteins during the assembly of the head of bacteriophage T4. *Nature* **227**, 680-685.
- Lamattina, L., García-Mata, C., Graziano, C., and Pagnussat, G. (2003). Nitric oxide: The Versatility of an Extensive Signal Molecule. *Annu Rev Plant Biol* **54**, 109-136.
- Lanzilotta, W.N., Schuller, D.J., Thorsteinsson, M.V., Kerby, R.L., Roberts, G.P., and Poulos, T.L. (2000). Structure of the CO sensing transcription activator CooA. *Nat Struct Biol* **7**, 876–880.
- Laskowski, R.A., MacArthur, M.W., Moss, D.S., and Thornton, J.M. (1993). PROCHECK - a program to check the stereochemical quality of protein structures. *J App Cryst* **26**, 283-291.

- Laskowski, R.A., Rullmannn, J.A., MacArthur, M.W., Kaptein, R., and Thornton, J.M. (1996). AQUA and PROCHECK-NMR: programs for checking the quality of protein structures solved by NMR. *J Biomol NMR* **8**, 477-486.
- LaVallie, E.R., DiBlasio, E.A., Kovacic, S., Grant, K.L., Schendel, P.F., and McCoy, J.M. (1993). A thioredoxin gene fusion expression system that circumvents inclusion body formation in the *E. coli* cytoplasm. *Biotechnology (Nature Publishing Company)* **11**, 187-193.
- Leshem, Y.Y. (2000). Nitric oxide in plants: Occurance, Function and Use. *Kluwer; Dordrech, The Netherlands* **154**.
- Leshem, Y.Y., and Haramaty, E. (1996). Characterisation and contrasting effects of the nitric oxide free radical in vegetable stress and senescence of *Pisum sativum* Linn foliage. *J Plant Physiol* **148**, 258–263.
- Leshem, Y.Y., Wills, R.B.H., and Ku, V.V.V. (1998). Evidence for the function of the free radical gas nitric oxide (NO) as an endogenous maturation and senescence regulating factor in higher plants. *Plant Physiol Biochem* **36**, 825–833.
- Li, H., and Poulos, T.L. (2005). Structure-function studies on nitric oxide synthases. *J Inorg Biochem* **99**, 293-305.
- Lindwall, G., Chau, M., Gardner, S.R., and and Kohlstaedt, L.A. (2000). A sparse matrix approach to the solubilization of overexpressed proteins. *Protein Eng* **13**, 67-71.
- Liu, H.H., Tian, Z.Q., Lu, Z.X., Zhang, Z.L., Zhang, M., and Pang, D.W. (2004). Direct electrochemistry and electrocatalysis of heme-proteins entrapped in agarose hydrogel films. *Biosens Bioelectron* **20**, 294-304.
- Lombardo, M.C., Graziano, M., Polacco, J.C., and Lamattina, L. (2006). Nitric Oxide Functions as a Positive Regulator of Root Hair Development. *Plant Signal Behav* **1**, 28–33.

- Lucas, K.A., Pitari, G.M., Kazerounian, S., Ruiz-Stewart, I., Park, J., Schulz, S., Chepenik, K.P., and Waldman, S.A. (2000). Guanylyl cyclases and signaling by cyclic GMP. *Pharmacol Rev* **52**, 375-414.
- Ludidi, N., and Gehring, C. (2003). Identification of a Novel Protein with Guanylyl Cyclase Activity in *Arabidopsis thaliana*. *J Biol Chem* **278**, 6490–6494.
- Maathuis, F.J., and Sanders, D. (2001). Sodium uptake in *Arabidopsis* roots is regulated by cyclic nucleotides. *Plant Physiol* **127**, 1617-1625.
- Manjunatha, G., Lokesh, V., and Neelwarne, B. (2010). Nitric oxide in fruit ripening: Trends and opportunities. *Biotechnol Adv* **28**, 488-499.
- Manjunatha, G., Niranjana, R.S., Nandini, S., and Shetty, H.S. (2008). Nitric oxide donor seed priming enhances defense responses and induces resistance against pearl millet downy mildew disease. *Pestic Biochem Physiol* **91**, 1-11.
- Marblestone, J.G., Edavettal, S.C., Lim, Y., Lim, P., X. Zuo, X., and T.R. Butt., T.R. (2006). Comparison of SUMO fusion technology with traditional gene fusion systems: enhanced expression and solubility with SUMO. *Protein Sci* **15**, 182-189.
- Meier, S., Madeo, L., Ederli, L., Donaldson, L., Pasqualini, S., and Gehring, C. (2009). Deciphering cGMP signatures and cGMP-dependent pathways in plant defence. *Plant Sig Behav* **4**, 307-309.
- Meier, S., Ruzvidzo, O., Morse, M., Donaldson, L., Kwezi, L., and Gehring, C. (2010). The *Arabidopsis* Wall Associated Kinase-Like 10 Gene Encodes a Functional Guanylyl Cyclase and Is Co-Expressed with Pathogen Defense Related Genes. *PLoS ONE* **5**, e8904.
- Meier, S., Seoighe, C., Kwezi, L., Irving, H., and Gehring, C. (2007). Plant Nucleotide Cyclases: an increasingly complex and growing family. *Plant Sig Behav* **2**, 536-539.
- Misra, A.N., Misra, M., and Singh, R. (2010). Nitric oxide biochemistry, mode of action and signalling in plants *J Medicinal Plants Res* **4**, 2729-2739.

Miyatake, H. (2000). Sensory mechanism of oxygen sensor FixL from *Rhizobium meliloti*: crystallographic, mutagenesis and resonance Raman spectroscopic studies. *J Mol Biol* **301**, 415-431.

Moitinho, A., Hussey, P.J., Trewavas, A.J., and Malho, R. (2001). cAMP acts as a second messenger in pollen tube growth and reorientation. *Proc Natl Acad Sci USA* **98**, 10481-10486.

Mori, V., and Bertotti, M. (2000). Nitric oxide solutions: standardisation by chronoamperometry using a platinum disc microelectrode. *Royal Society of Chemistry, Cambridge, ROYAUME-UNI* **125**, 1629-1632

Murgia, I., de Pinto, M.C., Delledonne, M., Soave, C., and de Gara, L. (2004). Comparative effects of various nitric oxide donors on ferritin regulation, programmed cell death, and cell redox state in plant cells *J Plant Physiol* **161**, 777-783.

Namiki, S., Hirose, K., and Iino, M. (2001). Mapping of heme-binding domains in soluble guanylyl cyclase beta1 subunit. *Biochem Biophys Res Commun* **288**, 798-804.

Neill, S.J., Desikan, R., and Hancock, J.T. (2003). Nitric oxide signalling in plants. *New Phytol* **159**, 11-35

Newton, R.P., and Smith, C.J. (2004). Cyclic nucleotides. *Phytochemistry* **65**, 2423-2437.

Niiranen, L., Espelid, S., Karlsen, C.R., Mustonen, M., Paulsen, S.M., Heiknheimo, P., and Willassen, N.P. (2007). Comparative expression study to increase the solubility of cold adapted *Vibrio* proteins in *Escherichia coli*. *Prot Exp Purif* **52**, 210-218.

Ninnemann, H., and Maier, J. (1996). Indications for the occurrence of nitric oxide synthases in fungi and plants and the involvement in photooxidation of *Neurospora crassa*. *Photochem Photobiol* **64**, 393-398.

Orozco-Cardenas, M.L., and Ryan, C.A. (2002). Nitric oxide negatively modulates wound signalling in tomato plants. *Plant Physiol* **130**, 487-493.

- Otvos, K., Pasternak, T.P., Miskolczi, P.M., Domoki, M., Dorjgotov, D., and Szucs, A. (2005). Nitric oxide is required for, and promotes auxin-mediated activation of, cell division and embryogenic cell formation but does not influence cell cycle progression in alfalfa cell cultures. *Plant J* **43**, 849–860.
- Pagnussat, G.C., Lanteri, M.L., Lombardo, M.C., and Lamattina, L. (2004). Nitric oxide mediates the indole-acetic acid activation of a mitogen-activated protein kinase cascade involved in adventitious root formation. *Plant Physiol* **135**, 279-286.
- Pasqualini, S., Meier, S., Gehring, C., Madeo, L., and Fornaciari, M. (2008). Ozone and nitric oxide induce cGMP-dependent and -independent transcription of defense genes in tobacco. *New Phytol* **181**, 860–870.
- Pellicena, P., Karow, D.S., Boon, E.M., Marletta, M.A., and Kuriyan, J. (2004). Crystal structure of an oxygen-binding heme domain related to soluble guanylate cyclases. *Proc Natl Acad Sci U S A* **101**, 12854-12859.
- Penson, S.P., Schuurink, R.C., Fath, A., Gubler, F., Jacobsen, J.V., and Jones, R.L. (1996). cGMP is required for gibberellic acid-induced gene expression in barley aleurone. *Plant Cell* **8**, 2325-2333.
- Pharmawati, M., Maryani, M.M., Nikolakopoulos, T., Gehring, C.A., and Irving, H.R. (2001). Cyclic GMP modulates stomatal opening induced by natriuretic peptides and immunoreactive analogues. *Plant Physiol Biochem* **39**, 385–394.
- Polverari, A., Molesini, B., Pezzotti, M., Buonauro, R., Marte, M., and Delledonne, M. (2003). Nitric oxide-mediated transcriptional changes in *Arabidopsis thaliana*. *Mol Plant Microbe Interact* **16**, 1094-1105.
- Prado, A.M., Porterfield, D.M., and Feijo, J.A. (2004). Nitric oxide is involved in growth regulation and re-orientation of pollen tubes. *Development* **131**, 2707–2714.

- Procházková, D., and Wilhelmová, N. (2011). Nitric oxide, reactive nitrogen species and associated enzymes during plant senescence. *Nitric Oxide* **24**, 61-65.
- QIAexpressionist., T. (2003). A handbook for high-level expression and purification of 6xHis-tagged proteins. *QIAGEN Inc.*
- Qiao, W., and Fan, L.M. (2008). Nitric oxide signaling in plant responses to abiotic stresses. *J Integr Plant Biol* **50**, 1238-1246.
- Ramirez, L., Zabaleta, E.J., and Lamattina, L. (2010). Nitric oxide and flataxin: two players contributing to maintain cellular iron homeostasis. *Ann Bot* **105**, 801-810.
- Rodgers, K.R. (1999). Heme-based sensors in biological systems. *Curr Opin Chem Biol* **3**, 158–167.
- Rodgers, K.R., and Lukat-Rodgers, G.S. (2005). Insights into heme-based O₂ sensing from structure–function relationships in the FixL proteins. *J Inorg Biochem* **99**, 963–997.
- Romero-Puertas, M.C., and Delledonne, M. (2003). Nitric Oxide Signaling in Plant-Pathogen Interactions. *IUBMB Life* **55**, 579–583.
- Romero-Puertas, M.C., Perazzolli, M., Zago, E., and Delledonne, M. (2004). Nitric oxide signalling functions in plant pathogen interaction. *Cell Microbiol* **6**, 795-.
- Rothkegel, C., Schmidt, P.M., Atkins, D.J., Hoffmann, L.S., Schmidt, H.H., Schroder, H., and Stasch, J.P. (2007). Dimerization region of soluble guanylate cyclase characterized by bimolecular fluorescence complementation *in vivo*. *Mol Pharmacol* **72**, 1181-1190.
- Rothkegel, C., Schmidt, P.M., Stoll, F., Schroder, H., Schmidt, H.H., and Stasch, J.P. (2006). Identification of residues crucially involved in soluble guanylate cyclase activation. *FEBS Lett* **580**, 4205-4213.
- Sali, A., and Blundell, T.L. (1993). Comparative protein modelling by satisfaction of spacial restraints. *J Mol Biol* **234**, 779-815.

- Saviani, E.E., Orsi, C.H., Oliveira, J.F.P., Pinto-Maglio, C.A.F., and Salgado, I. (2002). Participation of the mitochondrial permeability transition pore in nitric oxide-induced plant cell death. *FEBS Lett* **510**, 136-140.
- Schaap, P. (2005). Guanylyl cyclase across the tree of life. *Front Biosci* **10**, 1485-1498.
- Schlaich, N.L. (2007). Flavin-containing monooxygenases in plants: looking beyond detox. *Trends Plant Sci* **12**, 412-418.
- Schmidt, H.H.H.W., and Walter, U. (1994). NO at work. *cell* **78**, 919-925.
- Schmidt, P.M., Schramm, M., Schroder, H., Wunder, F., and Stasch, J.P. (2004). Identification of residues crucially involved in the binding of the heme moiety of soluble guanylate cyclase. *J Biol Chem* **279**, 3025-3032.
- Seebeck, B., Reulecke, I., Kamper, A., and Rarey, M. (2008). Modelling of metal intercation geometries for protein-ligand docking. *Proteins* **71**, 1237-1254.
- Shelver, D., Kerby, R.L., He, Y., and Roberts, G.P. (1997). CooA, a CO-sensing transcription factor from *Rhodospirillum rubrum*, is a CO-binding heme protein. *Proc Natl Acad Sci USA* **94**, 11216–11220
- Shi, J., Blundell, T.L., and Mizuguchi, K. (2001). FUGUE:sequence-structure homology recognition using environment-specific substitution tables and structure-dependent gap penalties. *J Mol Biol* **310**, 243-257.
- Shi, Q., Ding, F., Wang, X., and Wei, M. (2007). Exogenous nitric oxide protect cucumber roots against oxidative stress induced by salt stress. *Plant Physiol Biochem* **45**, 542e550.
- Smith, D.B., and Johnson., K.S. (1988). Single-step purification of polypeptides expressed in *Escherichia coli* as fusions with glutathione S-transferase. *Gene* **67**, 31-40.
- Stehr, M., Diekmann, H., Smau, L., Seth, O., Ghisla, S., Singh, M., and Macheroux, P. (1998). A hydrophobic sequence motif common to Nhydroxylating enzymes. *Trends Biochem Sci* **23**, 56–57.

- Stempfer, G., Holl-Neugebauer, B., and Rudolph, R. (1996). Improved refolding of an immobilized fusion protein. *Nat Biotech* **14**, 329-334.
- Suh, J.K., Poulsen, L.L., Ziegler, D.M., and Roberts, G.P. (2000). Redox regulation of yeast flavin-containing monooxygenase. *Arch Biochem Biophys* **381**, 317–322.
- Suh, J.K., Poulsen, L.L., Ziegler, D.M., and Robertus, J.D. (1999). Yeast flavin-containing monooxygenase generates oxidizing equivalents that control protein folding in the endoplasmic reticulum. *Proc Natl Acad Sci USA* **96**, 2687-2691.
- Szmidt-Jaworska, A., Jaworski, K., and Kopcewicz, J. (2009). Cyclic GMP stimulates flower induction of *Pharbitis nil* via its influence on cGMP regulated protein kinase. *Plant Growth Regul* **57**, 115–126.
- Tatusova, T.A., and Madden, T.L. (1999). BLAST 2 sequences: a new tool for comparing protein and nucleotide sequences. *FEMS Microbiol Lett* **174**, 247-250.
- Teng, Y., Xu, W., and Ma, M. (2010). cGMP is required for seed germination in *Arabidopsis thaliana*. *J Plant Physiol* **167**, 885–889.
- Vitkup, D., Melamud, E., Moulton, J., and Sander, C. (2001). Completeness in structural genomics. *Nat Struct Biol* **8**, 482-484.
- Volotovskii, I.D., Sokolovsky, S.G., Molchan, O.V., and Knight, M.R. (1998). Second messengers mediate increases in cytosolic calcium in tobacco protoplasts. *Plant Physiol* **117**, 1023-1030.
- Wedel, B., Humbert, P., Harteneck, C., Foerster, J., Malkewitz, J., Bohme, E., Schultz, G., and Koesling, D. (1994). Mutation of His-105 in the beta 1 subunit yields a nitric oxide-insensitive form of soluble guanylyl cyclase. *Proc Natl Acad Sci USA* **91**, 2592–2596.
- Wendehenne, D., Durner, J., and Klessig, D.F. (2004). Nitric oxide: a new player in plant signalling and defence responses. *Curr Opin Plant Biol* **7**, 449–455.

- Wendehenne, D., Pugin, A., Klessig, D., and Durner, J. (2001). Nitric oxide: comparative synthesis and signaling in animal and plant cells. *Trends Plant Sci* **6**, 177–183.
- Wilhelmova, H., Fuksova, M., Srbova, D., Mikov, Z., Mytinova, D., and Prochazkova, R. (2006). The effect of plant cytokinin hormones on the production of ethylene, nitric oxide, and protein nitrotyrosine in ageing tobacco leaves. *Biofactors* **27**, 203–211.
- Wilson, I.D., Neill, S.J., and Hancock, J.T. (2008). *Plant Cell Environ* **31**, 622-631.
- Wink, D.A., and Mitchell, J.B. (1998). Chemical biology of nitric oxide: Insights into regulatory, cytotoxic, and cytoprotective mechanisms of nitric oxide. *Free Radic Biol Med* **25**.
- Yang, H., Fung, S.Y., Pritzker, M., and Chen, P. (2009). Ionic-complementary peptide matrix for enzyme immobilization and biomolecular sensing. *Langmuir* **25**, 7773-7777.
- Zhang, H., Lu, M., Zhang, Y., and Li, Z. (2008). Primary response of the sGC heme binding domain to the cleavage of the Fe-His bond. *Bioinformation* **2**, 296-300.
- Zhao, Y., Christian, S.K., Fankhauser, C., Cashman, J.R., Cohen, J.D., Weigel, D., and Chory, J. (2001). A role for flavin monooxygenase-like enzymes in auxin biosynthesis *Science* **291**, 306–309.
- Zhao, Y., Hoganson, C., Babcock, G.T., and Marletta, M.A. (1998). Structural changes in the heme proximal pocket induced by nitric oxide binding to soluble guanylate cyclase. *Biochemistry* **37**, 12458-12464.
- Zhao, Z., Zhang, F., Guo, J., Yang, Y., B. Li, B., and Zhang, L. (2004). Nitric oxide functions as a signal in salt resistance in the calluses from two ecotypes of reed *Plant Physiol* **134**, 849–857.

8. Appendix

Appendix I: Chemicals, stock solutions, buffers and bacterial strains

Bacterial media and solutions

0.1 M IPTG (Isopropyl-1-thio- (D-galactoside)): Stock solution prepared by dissolving 1.19 g in 5 ml distilled H₂O, filter sterilized, aliquots stored at -20 °C

2 X SDS sample buffer: 4 % SDS, 0.125 M Tris pH 6.8, 15 % glycerol, 1 mg/mL Bromophenol Blue, 2 M DTT stored at -20 °C.

50 % glutaraldehyde

Bacterial strains: MC1061 and BL21pLyS competent cells

Bovine Serum albumin (BSA)

Electrophoresis buffer: 10 % stock solution prepared by dissolving 30 g Tris-Cl, 144 g Glycine, 10 g SDS, made up to 1000 mL with distilled water.

Elution buffer: 50 mM NaH₂PO₄, 300 mM NaCl, 250 mM Imidazole, and pH adjusted to 8.0 with NaOH.

Didodecyldimethylammonium bromide (DAB)

IPTG (Isopropyl-1-thio- (D-galactoside)): 0.1 M stock solution prepared by dissolving 1.19 g IPTG dissolved in 50 mL water. Solution divided into 5 mL aliquots, sterilized by filtration and stored at -20 °C. Stable for 2 to 4 months.

Kanamycin stock solution: 50 mg/mL stock solution prepared in distilled H₂O, filter sterilized, aliquots stored at -20 °C. Stock diluted 1:1000 in LB medium or LB medium- agar.

Luria Broth (LB) medium: 10 g pancreatic digest, 5 g yeast extract, 5 g NaCl.

LB agar: LB medium containing 15 g/l Bacteriological Agar

Lysis buffer: 50 mM NaH₂PO₄, 300 mM NaCl, 10 mM Imidazole, pH adjusted to 8.0 with NaOH.

Primers: 100 μM stock solutions stored at -20 °C.

SDS: 10 % stock solution prepared by dissolving 100 g of SDS was dissolved in 900 mL water, heated to 68 °C to dissolve the crystals, and the volume made up to 1000 mL. Stored at room temperature

Separating buffer: 1.5 M Tris pH 8.8, stored at 4 °C.

Sodium azide: 10 % stock solution prepared by dissolving 10 g in 100 mL distilled water.

Stacking buffer: 0.5 M Tris pH 6.8, stored at 4 °C.

TBE: 10 X stock solution prepared by dissolving 108 g Tris, 55 g boric acid, and 9.3 g EDTA, made up to 1000 mL with distilled water.

Tris-Cl: 1 M stock solution prepared by dissolving 121.4 g in 500 mL of distilled water, pH adjusted with HCl and the volume made up to 100 mL.

Wash buffer: 50 mM NaH₂PO₄, 300 mM NaCl, 20 mM Imidazole, pH adjusted to 8.0 with NaOH.

Appendix II: Prediction of protein parameters for the *AtNOGCI* protein

ProtParam

User-provided sequence:

10 20 30 40 50 60
MVPVAVNPPTT SNHVAVIGAG AAGLVAAREL RREGHSVVVF ERGNHIGGVW AYTPNVEPDP

70 80 90 100 110 120
LSIDPTRPVI HSSLYSSLRT IIPQECMGFT DFPFSTRLEN GSRDPRRHPG HSEVLAYLRD

130 140 150 160 170 180
FVREFKIEEM IRFETEVVRV EQAGENPKKW RVKSRNFGDI SDEIYDAVVV CNGHYTEPRH

190 200 210 220 230 240
ALIPGNKINH SFSIGLGIDT WPGKQIHSHN YRVPEQVKDQ VVVVIGSSVS GVDISRDIAN

250 260 270 280 290 300
VTKEVHISSR STKPETYEKL PGYDNLWLHS NIETVREDGS VVFKNGKTVY ADTIMHCTGY

310 320 330 340 350 360
KYYFPFLDTK GEVTVEDNRV GPLYKHFVFP ALSPGLSFIG LPWQNMKLQT LDVNELIGQC

370 380 390 400 410 420
FGYLLVIPFP MFELQSKWVA AVLAGRVSLP SQEEMEDTKM FYLKLEASCI PKRYTHLMAE

430 440 450 460 470 480
LDSQFVYNNW LADQCDYPRI EKWREQMFYK VFKRIQSQAS TYKDDWDDDH LIAEAYEDFV

490
KFPSNYPSSL IEREYTS

Number of amino acids: 497

Molecular weight: 56739.2

Theoretical pI: 5.82

Amino acid composition:

Ala (A)	24	4.8%
Arg (R)	28	5.6%
Asn (N)	21	4.2%
Asp (D)	28	5.6%
Cys (C)	6	1.2%
Gln (Q)	15	3.0%
Glu (E)	37	7.4%
Gly (G)	30	6.0%

His (H)	17	3.4%
Ile (I)	29	5.8%
Leu (L)	33	6.6%
Lys (K)	25	5.0%
Met (M)	10	2.0%
Phe (F)	23	4.6%
Pro (P)	32	6.4%
Ser (S)	37	7.4%
Thr (T)	24	4.8%
Trp (W)	9	1.8%
Tyr (Y)	23	4.6%
Val (V)	46	9.3%
Pyl (O)	0	0.0%
Sec (U)	0	0.0%
(B)	0	0.0%
(Z)	0	0.0%
(X)	0	0.0%

Total number of negatively charged residues (Asp + Glu): 65
Total number of positively charged residues (Arg + Lys): 53

Atomic composition:

Carbon	C	2558
Hydrogen	H	3909
Nitrogen	N	685
Oxygen	O	748
Sulfur	S	16

Formula: C₂₅₅₈H₃₉₀₉N₆₈₅O₇₄₈S₁₆
Total number of atoms: 7916

Extinction coefficients:

Extinction coefficients are in units of M⁻¹ cm⁻¹, at 280 nm measured in water.

Ext. coefficient 84145
Abs 0.1% (=1 g/l) 1.483, assuming all pairs of Cys residues form cystines

Ext. coefficient 83770
Abs 0.1% (=1 g/l) 1.476, assuming all Cys residues are reduced

Estimated half-life:

The N-terminal of the sequence considered is M (Met).

The estimated half-life is: 30 hours (mammalian reticulocytes, in vitro).
>20 hours (yeast, in vivo).
>10 hours (Escherichia coli, in vivo).

Instability index:

The instability index (II) is computed to be 47.68
This classifies the protein as unstable.

Aliphatic index: 80.32

Grand average of hydropathicity (GRAVY): -0.379

Appendix III: DNA sequencing results: Sequence analysis of AtNOGG1 cloned into pET SUMO vector sequenced at INQABA Biotechnical industries (Pty) Ltd.

Area highlighted in yellow are from the vector sequence and the Red highlighted is the start of the AtNOGC1 clone. The heme-binding motif and the GC motif are highlighted in magenta and green respectively.

```

gatattattgagggtcacagagaacagattggtggtgatggatccatgggtaccagcagta
D I I E A H R E Q I G G D S S M V P A V
aatcctctaccacatccaaccacgtggcagtaatcggtgctggagcagccggactcgtg
N P P T T S N H V A V I G A G A A G L V
gctgctcgagagctccgctgaggccactctgtctgttttcgaacgtgggaaccac
A A R E L R R E G H S V V V F E R G N Y S S L R
atcggaggcgtggtgggttacacgcaaacgtgaaccgaccccttagcatcgaccg
I G G V W A Y T P N V E P D P L S I D P
accgacccgtaatccattcgagcctctacagttctctccgaaccatcattccacaagaa
T R P V I H S S L Y S S L R T I I P Q E
tgcattgggttccactgatttccggttttcgaccagactcgaaaacgggtctagagatccg
C M G F T D F P F S T R L E N G S R D P
agaagacatccaggtcatagtgaggttcttcttacctgagagactttgtgaggagttc
R R H P G H S E V L A Y L R D F V R E F
aagattgaggagatgattcgtttcgagacggaggttgtaggggtgagcaggcgggggaa
K I E E M I R F E T E V V R V E Q A G E
aatcccaaaaagtggagagtcagtctagaatttcgggtgatctccgacgagatttat
N P K K W R V K S R N F G D I S D E I Y
gacgctgtagttgttaacggtcactatacagagcctcgtcatgctctaataactggc
D A V V V C N G H Y T E P R H A L I P G

```

Forward AtNOGC1 strand: T7 forward primer

Alignment of AtNOGC1 sequence (Length 1494) with the sequenced AtNOGC1 (Length 963). Query-AtNOGC1 sequence, subject-Sequenced AtNOGC1, Score = 1065 bits (554), Expect = 0.0,Identities = 554/554 (100%), Gaps = 0/554 (0%). The sequence highlighted in red denotes the N-terminal of AtNOGC1

```

Query 1 ATGGTACCAGCAGTAAATCCTCTACCACATCCAACCACGTGGCAGTAATCGGTGCTGGA 60
|||||
Sbjct 406 ATGGTACCAGCAGTAAATCCTCTACCACATCCAACCACGTGGCAGTAATCGGTGCTGGA 465

Query 61 GCAGCCGGACTCGTGGCTGCTCGAGAGCTCCGCCGTGAGGGCCACTCTGTCGTTGTTTTTC 120
|||||
Sbjct 466 GCAGCCGGACTCGTGGCTGCTCGAGAGCTCCGCCGTGAGGGCCACTCTGTCGTTGTTTTTC 525

Query 121 GAACGTGGGAACCCACATCGGAGCGTGTGGGCTTACACGCCAAACGTTGAACCCGACCCC 180
|||||
Sbjct 526 GAACGTGGGAACCCACATCGGAGCGTGTGGGCTTACACGCCAAACGTTGAACCCGACCCC 585

Query 181 CTTAGCATCGACCCGACCCGACCCGTAATCCATTTCGAGCCTCTACAGTTCTCTCCGAACC 240
|||||
Sbjct 586 CTTAGCATCGACCCGACCCGACCCGTAATCCATTTCGAGCCTCTACAGTTCTCTCCGAACC 645

```



```

Query 241 ATCATCCCACAAGAATGCATGGGTTTCACTGATTTCCTCCGTTTTTCGACCAGACTCGAAAAAC 300
          ||||||||||||||||||||||||||||||||||||||||||||||||||||||||||||
Sbjct 646 ATCATCCCACAAGAATGCATGGGTTTCACTGATTTCCTCCGTTTTTCGACCAGACTCGAAAAAC 705

Query 301 GGGTCTAGAGATCCGAGAAGACATCCAGGTCATAGTGAGGTTCTTGCTTACCTGAGAGAC 360
          ||||||||||||||||||||||||||||||||||||||||||||||||||||||||||||
Sbjct 706 GGGTCTAGAGATCCGAGAAGACATCCAGGTCATAGTGAGGTTCTTGCTTACCTGAGAGAC 765

Query 361 TTTGTGAGGGAGTTCAAGATTGAGGAGATGATTCGTTTCGAGACGGAGGTTGTGAGGGTT 420
          ||||||||||||||||||||||||||||||||||||||||||||||||||||||||||||
Sbjct 766 TTTGTGAGGGAGTTCAAGATTGAGGAGATGATTCGTTTCGAGACGGAGGTTGTGAGGGTT 825

Query 421 GAGCAGCGGGGGAAAAATCCCAAAAAGTGGAGAGTCAAGTCTAGAAAATTCGGTGATATC 480
          ||||||||||||||||||||||||||||||||||||||||||||||||||||||||||||
Sbjct 826 GAGCAGCGGGGGAAAAATCCCAAAAAGTGGAGAGTCAAGTCTAGAAAATTCGGTGATATC 885

Query 481 TCCGACGAGATTTATGACGCCGTAGTTGTTTGTAAACGGTCACTATACAGAGCCTCGTCAT 540
          ||||||||||||||||||||||||||||||||||||||||||||||||||||||||||||
Sbjct 886 TCCGACGAGATTTATGACGCCGTAGTTGTTTGTAAACGGTCACTATACAGAGCCTCGTCAT 945

Query 541 GCTCTAATACCTGG 554
          ||||||||||||
Sbjct 946 GCTCTAATACCTGG 959

```

Reverse AtNOGC1 strand: T7 reverse primer

Alignment of AtNOGC1 sequence (Length 1494) with the sequenced AtNOGC1 (Length 690). Query-AtNOGC1 sequence, subject-Sequenced AtNOGC1, Score = 667 bits (347), Expect = 0.0, Identities = 347/347 (100%), Gaps = 0/347 (0%). The sequence highlighted in red denotes the N-terminal of AtNOGC1

```

Query 1148 TGGCAGGTAGGTTTCACTCCCCTCACAAGAAGAGATGGAAGATACTAAGATGTTTATT 1207
          ||||||||||||||||||||||||||||||||||||||||||||||||||||||||||||
Sbjct 433 TGGCAGGTAGGTTTCACTCCCCTCACAAGAAGAGATGGAAGATACTAAGATGTTTATT 374

Query 1208 TGAAGCTCGAAGCCTCATGTATTCCCAAAAGATACACACATCTTATGGCAGAATTAGATT 1267
          ||||||||||||||||||||||||||||||||||||||||||||||||||||||||||||
Sbjct 373 TGAAGCTCGAAGCCTCATGTATTCCCAAAAGATACACACATCTTATGGCAGAATTAGATT 314

```

Query 1268 CTCAGTTGTATACAATAACTGGCTTGCTGATCAATGTGACTATCCTCGGATCGAGAAAT 1327
 ||||||||||||||||||||||||||||||||||||||||||||||||||||||||||||
 Sbjct 313 CTCAGTTGTATACAATAACTGGCTTGCTGATCAATGTGACTATCCTCGGATCGAGAAAT 254

Query 1328 GGAGAGAGCAAATGTTTTACAAGGTGTTCAAGAGAATACAATCCCAAGCCAGTACATATA 1387
 ||||||||||||||||||||||||||||||||||||||||||||||||||||||||||||
 Sbjct 253 GGAGAGAGCAAATGTTTTACAAGGTGTTCAAGAGAATACAATCCCAAGCCAGTACATATA 194

Query 1388 AGGACGATTGGGACGATGATCACCTCATCGCAGAAGCATATGAAGATTTCGTCAAATTCC 1447
 ||||||||||||||||||||||||||||||||||||||||||||||||||||||||||||
 Sbjct 193 AGGACGATTGGGACGATGATCACCTCATCGCAGAAGCATATGAAGATTTCGTCAAATTCC 134

Query 1448 CATCTAACTATCCCAGTTCTTTAATCGAAAGAGAATATACA **AGCTGA** 1494
 ||||||||||||||||||||||||||||||||||||||||||||||||||||||||||||
 Sbjct 133 CATCTAACTATCCCAGTTCTTTAATCGAAAGAGAATATACA **AGCTGA** 87

Appendix IV: Data for the determination of protein concentration using Bradford assay

Table 2.2: The concentration and absorbance of the standard BSA and the dilution factors of *AtNOGCI*.

Concentration of standard protein ($\mu\text{g/ml}$)	Absorbance of standard protein (595 nm)
125	0.885
100	0.836
75	0.673
50	0.547
25	0.27
20	0.236
0	0
Dilution factor for <i>AtNOGCI</i>	Absorbance values of <i>AtNOGCI</i>
1:10	0.046

Equations for the calculation of *AtNOGCI* protein concentration

1

$$Y = 0.008 X$$

$$0.046 = 0.008 X$$

$$X = 0.046 \div 0.008$$

$$=5.75 \mu\text{g/mL} \times 10 \text{ (dilution factor)}$$

$$=57.5 \mu\text{g/mL}$$

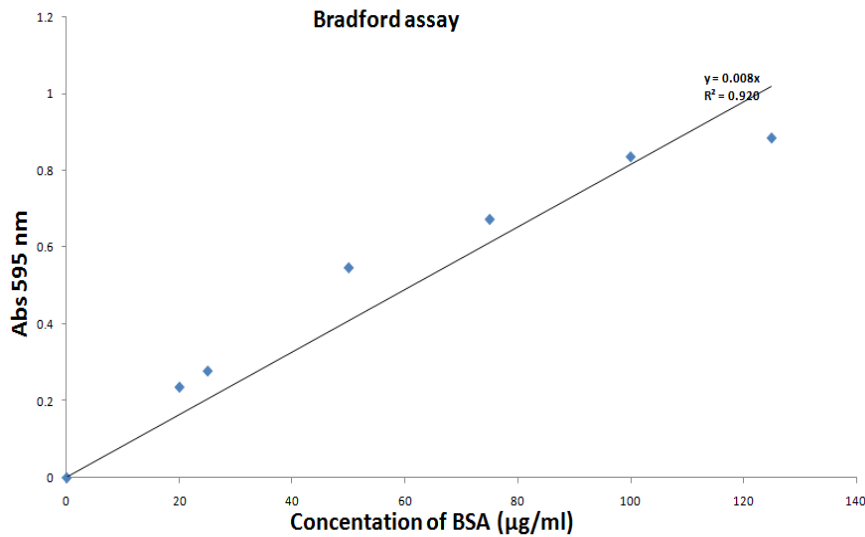


Figure 2.9: Standard curve of the BSA for the Bradford assay to determine the concentration of recombinant *AtNOGCI*. A_{595} values corresponding to different standard (BSA) concentrations are plotted against concentration ($\mu\text{g/mL}$). The unknown concentration of *AtNOGCI* fusion protein was determined using the measured absorbance values at 1:50 and 1:100 dilution factors. The values corresponding to the concentration are calculated using the formula corresponding to the straight line fitted to the data.

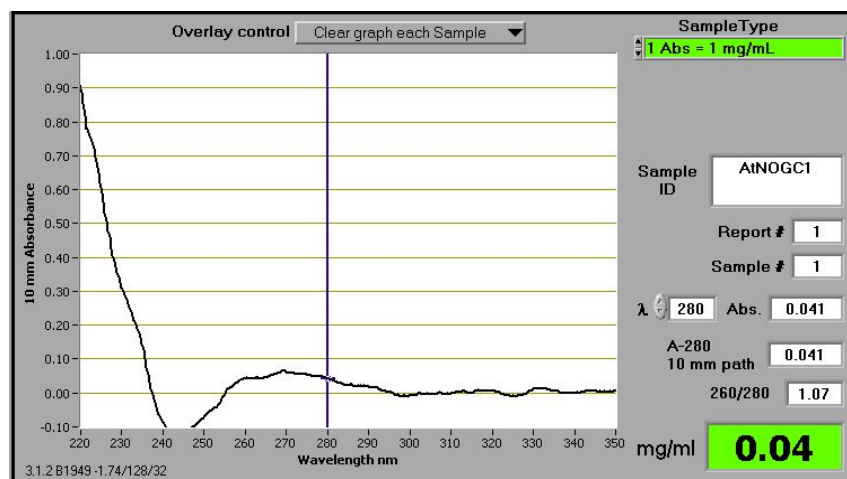


Figure 2.10: UV absorption spectrum of the *AtNOGCI* as determined by the NanoDrop. The recombinant *AtNOGCI* protein was measured at 280 nm and its concentration found to be $\sim 40 \mu\text{g/mL}$.

Appendix V: Results for *AtNOGCI* and *At5g57690* obtained from the Fugue server

FUGUE v2.s.07 (01 Apr 2003)

Results for *AtNOGCI*

Search sequence(s) against fold library using environment-specific substitution tables and structure-dependent gap penalties.

Fold library and substitution tables are based on the HOMSTRAD database.
<http://tardis.nibio.go.jp/homstrad/>

FUGUE server is available at:
<http://tardis.nibio.go.jp/fugue/>
<http://tardis.nibio.go.jp/fugue/prfsearch.html>

Citation:

J. Shi, T. L. Blundell and K. Mizuguchi (2001), *J Mol Biol*, 310(1), 243-57

Size of fold library: 12258
Probe sequence ID : *AtNOGCI*
Probe sequence len : 497
Probe divergence : 0.632
Recommended cutoff : ZSCORE >= 6.0 (CERTAIN 99% confidence)
Other cutoff : ZSCORE >= 4.0 (LIKELY 95% confidence)
Other cutoff : ZSCORE >= 3.5 (MARGINAL 90% confidence)
Other cutoff : ZSCORE >= 2.0 (GUESS 50% confidence)
Other cutoff : ZSCORE < 2.0 (UNCERTAIN)

PLEN : Profile length
RAWS : Raw alignment score
RVN : (Raw score)-(Raw score for NULL model)
ZSCORE : Z-score normalized by sequence divergence
ZORI : Original Z-score (before normalization)
AL : Alignment algorithm used for Zscore/Alignment calculation
0 -- Global, 2 -- GloLocSeq (No sequence termini gap penalty)
3 -- GloLocPrf (No profile termini gap penalty)

Profile Hit	PLEN	RAWS	RVN	ZSCORE	ZORI		ALIGNMENT
hs2vq7a	443	783	1382	59.47	61.86	00	CERTAIN Alignment
hs3dlca	350	106	413	21.24	23.77	00	CERTAIN Alignment
hslw4xa	533	269	458	19.13	21.69	00	CERTAIN Alignment
hslgtea	1005	186	176	12.12	14.40	33	CERTAIN Alignment
hsgrs	558	465	225	9.83	12.27	00	CERTAIN Alignment

hslid7ya	401	301	219	9.45	11.97	00	CERTAIN	Alignment
hs2ba9a	423	436	209	8.96	11.56	00	CERTAIN	Alignment
hstdlan9ai	247	-148	94	8.79	11.44	22	CERTAIN	Alignment
hslyvva	320	-369	157	8.67	11.33	02	CERTAIN	Alignment
hslm6ia	459	-357	233	8.52	11.00	00	CERTAIN	Alignment

Hint: check 'ma' first if your query is a single sequence, otherwise start with 'aa'.

Profile Hit	HTML	POSTSCRIPT	TEXT(PIR FORMAT)	Confidence	View Model	Z-score
hs2vq7a	aa ma mh hh	aa ma mh hh	aa ma mh hh	CERTAIN	PDBChime	59.47
hs3dlca	aa ma mh hh	aa ma mh hh	aa ma mh hh	CERTAIN	PDBChime	21.24
hslw4xa	aa ma mh hh	aa ma mh hh	aa ma mh hh	CERTAIN	PDBChime	19.13
hslgtea	aa ma mh hh	aa ma mh hh	aa ma mh hh	CERTAIN	PDBChime	12.12
hsgrsa	aa ma mh hh	aa ma mh hh	aa ma mh hh	CERTAIN	PDBChime	9.83
hslid7ya	aa ma mh hh	aa ma mh hh	aa ma mh hh	CERTAIN	PDBChime	9.45
hs2ba9a	aa ma mh hh	aa ma mh hh	aa ma mh hh	CERTAIN	PDBChime	8.96
hstdlan9ai	aa ma mh hh	aa ma mh hh	aa ma mh hh	CERTAIN	PDBChime	8.79
hslyvva	aa ma mh hh	aa ma mh hh	aa ma mh hh	CERTAIN	PDBChime	8.67
hslm6ia	aa ma mh hh	aa ma mh hh	aa ma mh hh	CERTAIN	PDBChime	8.52

Keys

aa: query sequences (including PSI-BLAST homologues) aligned against all the representative structures from a HOMSTRAD family
ma: master sequence aligned against all the representative structures from a HOMSTRAD family
mh: master sequence aligned against a single structure of highest sequence identity from a HOMSTRAD family
hh: single sequence/structure pair with highest sequence identity in 'aa'

Note: If your query is a single sequence, master sequence is equivalent to your query and all the other

sequences (if any) are collected by PSI-BLAST.

If your query is a sequence alignment, master sequence is set to the first sequence in the alignment.

Results for At5g57690

Search sequence(s) against fold library using environment-specific substitution tables and structure-dependent gap penalties.

Fold library and substitution tables are based on the HOMSTRAD database.
<http://tardis.nibio.go.jp/homstrad/>

FUGUE server is available at:

<http://tardis.nibio.go.jp/fugue/>

<http://tardis.nibio.go.jp/fugue/prfsearch.html>

Citation:

J. Shi, T. L. Blundell and K. Mizuguchi (2001), J Mol Biol, 310(1), 243-57

Size of fold library: 12445

Probe sequence ID : Diacylglycerolkinase

Probe sequence len : 487

Probe divergence : 0.542

Recommended cutoff : ZSCORE >= 6.0 (CERTAIN 99% confidence)

Other cutoff : ZSCORE >= 4.0 (LIKELY 95% confidence)

Other cutoff : ZSCORE >= 3.5 (MARGINAL 90% confidence)

Other cutoff : ZSCORE >= 2.0 (GUESS 50% confidence)

Other cutoff : ZSCORE < 2.0 (UNCERTAIN)

PLEN : Profile length

RAWS : Raw alignment score

RVN : (Raw score)-(Raw score for NULL model)

ZSCORE : Z-score normalized by sequence divergence

ZORI : Original Z-score (before normalization)

AL : Alignment algorithm used for Zscore/Alignment calculation

0 -- Global, 2 -- GloLocSeq (No sequence termini gap penalty)

3 -- GloLocPrf (No profile termini gap penalty)

The sequence(s) you submitted is [HERE](#) (in original format).

The sequence(s) actually used by FUGUE is [HERE](#) (in PIR format).

Download all the results in compressed format [HERE](#). **new!**

View Ranking (Click on a profile hit will bring you to the corresponding HOMSTRAD family)

Profile Hit	PLEN	RAWS	RVN	ZSCORE	ZORI	AL		
hs2jgra	255	-182	257	17.35	19.69	02	CERTAIN	Alignment
hs2bona	287	-191	25	14.53	16.89	02	CERTAIN	Alignment
hs3s40a	270	-196	189	12.74	14.59	02	CERTAIN	Alignment
hsd1ndoal	154	-345	46	3.76	5.93	02	MARGINAL	Alignment
hs3bjea	327	-393	57	3.30	5.27	00	GUESS	Alignment
hs2b78a	376	-406	43	3.29	5.53	00	GUESS	Alignment

hs3ilaa	328	-386	55	3.23	5.07	00	GUESS	Alignment
hs3mlra	310	-378	80	3.22	5.15	02	GUESS	Alignment
hslolxa	142	-382	12	3.09	5.12	02	GUESS	Alignment
hsly7pa	212	-109	81	3.00	4.80	22	GUESS	Alignment

[View Alignments](#) (What do they mean -- aa, ma, mh, hh? See note at the bottom of the page.)

Hint: check 'ma' first if your query is a single sequence, otherwise start with 'aa'.

Profile Hit	HTML	POSTSCRIPT	TEXT(PIR FORMAT)	Confidence	View Model	Z-score										
hs2jgra	aa	ma	mh	hh	aa	ma	mh	hh	aa	ma	mh	hh	CERTAIN	PDB	Chime	17.35
hs2bona	aa	ma	mh	hh	aa	ma	mh	hh	aa	ma	mh	hh	CERTAIN	PDB	Chime	14.53
hs3s40a	aa	ma	mh	hh	aa	ma	mh	hh	aa	ma	mh	hh	CERTAIN	PDB	Chime	12.74
hslndoal	aa	ma	mh	hh	aa	ma	mh	hh	aa	ma	mh	hh	MARGINAL	PDB	Chime	3.76
hs3bjea	aa	ma	mh	hh	aa	ma	mh	hh	aa	ma	mh	hh	GUESS	PDB	Chime	3.30
hs2b78a	aa	ma	mh	hh	aa	ma	mh	hh	aa	ma	mh	hh	GUESS	PDB	Chime	3.29
hs3ilaa	aa	ma	mh	hh	aa	ma	mh	hh	aa	ma	mh	hh	GUESS	PDB	Chime	3.23
hs3mlra	aa	ma	mh	hh	aa	ma	mh	hh	aa	ma	mh	hh	GUESS	PDB	Chime	3.22
hslolxa	aa	ma	mh	hh	aa	ma	mh	hh	aa	ma	mh	hh	GUESS	PDB	Chime	3.09
hsly7pa	aa	ma	mh	hh	aa	ma	mh	hh	aa	ma	mh	hh	GUESS	PDB	Chime	3.00

Keys

aa: query sequences (including PSI-BLAST homologues) aligned against all the representative structures from a HOMSTRAD family

ma: master sequence aligned against all the representative structures from a HOMSTRAD family

mh: master sequence aligned against a single structure of highest sequence identity from a HOMSTRAD family


hh: single sequence/structure pair with highest sequence identity in 'aa'

Note: If your query is a single sequence, master sequence is equivalent to your query and all the other

sequences (if any) are collected by PSI-BLAST.

If your query is a sequence alignment, master sequence is set to the first sequence in the alignment.

Appendix VI: Microarray data showing the expression profiles for *AtNOGCI* obtained from Genevestigator



[Home](#) | [Guided Tour](#) | [FAQ](#) | [Profile](#) | [News](#)

Digital Northern

Introduction

The *Digital Northern* queries the database to answer the following questions:

1. How is my gene of interest (or a set of genes) expressed throughout selected experiments?
2. In which arrays is my gene of interest most strongly expressed?

The output is given either as a graph or as a table of signal intensity values.

Submission form

Selected arrays

2507

Selected ID's (max 10)

265105_s_at|AT1G63340

Scale Type (Graph only)

Linear Log₂(n)

Scale base

minimum signal 0 (zero)

Remarks

Proceed as follows:

1. Select the chips you want to view using the Chip selection tool.
2. Enter up to 10 gene identifiers (as either probeset or AGI code).
3. Choose scale type (linear or log)
4. Choose output form (either graph or data)

Open symbols indicate absent or marginal calls ($p > 0.05$; "signals not significantly higher than background"), closed symbols indicate present calls ($p \leq 0.05$; "signals significantly higher than background").

The background level is based on signals from the mismatch probes.

Please also read the section about possible pitfalls and precautions to take to avoid them ([Documentation](#), chapter 6)

23.2 Mycorrhiza_with_rep2	■	64.89
23.3 Mycorrhiza_without_rep1	■	65.12
23.4 Mycorrhiza_without_rep2	□	65.87
24.1 Nematode_with	■	55.15
24.2 Nematode_without	□	55.81
25.1 Ozone_with_rep1	□	61.56
25.2 Ozone_with_rep2	□	64.21
25.3 Ozone_with_rep3	□	61.85
25.4 Ozone_without_rep1	■	59.05
25.5 Ozone_without_rep2	■	60.45
25.6 Ozone_without_rep3	□	61.80
26.1 Pod_control_rep1	■	57.22
26.2 Pod_control_rep2	■	61.04
26.3 Pod_heat_rep1	■	58.40
26.4 Pod_heat_rep2	□	58.29
26.5 Pod_senescence_rep1	■	55.06
26.6 Pod_senescence_rep2	■	53.28
27.1 Pho3_wt_rep1	■	60.14
27.2 Pho3_wt_rep2	■	55.05
27.3 Pho3_wt_rep3	■	56.58
27.4 Pho3_mut_rep1	■	62.32
27.5 Pho3_mut_rep2	■	61.45
27.6 Pho3_mut_rep3	■	59.35
28.1 Glyox_icl_rep1	■	50.46
28.2 Glyox_icl_rep2	■	51.82
28.3 Glyox_icl_rep3	■	53.46
28.4 Glyox_irv_rep1	□	53.99
28.5 Glyox_irv_rep2	□	52.13
28.6 Glyox_irv_rep3	□	52.83
28.7 Glyox_nsx_rep1	□	49.06
28.8 Glyox_nsx_rep2	□	53.81
28.9 Glyox_nsx_rep3	□	53.48
28.10 Glyox_wsx_rep1	■	53.92
28.11 Glyox_wsx_rep2	□	53.37
28.12 Glyox_wsx_rep3	□	52.88
29.1 Root_col0_rep1	■	56.28
29.2 Root_col0_rep2	□	57.09
29.3 Root_rh2d-1_rep1	□	53.76
29.4 Root_rh2d-1_rep2	■	60.86
30.1 Apical_meristem_axr1-12	□	59.54
30.2 Apical_meristem_axr3-1	■	56.54
31.1 Defence_ces2cir1_ein2	■	37.86
31.2 Defence_cir1	□	48.52
31.3 Defence_ein2	■	49.83
31.4 Defence_PRR1-luc	■	49.19
46.1 H202_nontreated_wt	■	56.19
46.2 H202_nontreated_OX1	□	53.42
46.3 H202_treated_OX1	□	56.76
46.4 H202_treated_wt	■	53.02
48.1 bountiful_mutant	□	59.23
48.2 bountiful_wt	■	58.33
50.1 ng_a_01	□	60.01
50.2 ng_a_02	□	62.62
50.3 ng_a_81	■	62.41
50.4 ng_a_82	■	63.29
50.5 ng_a_301	■	61.09
50.6 ng_a_302	□	60.03
50.7 ng_a_481	■	61.80
50.8 ng_a_482	■	62.30
50.9 ng_b_01	■	61.96
50.10 ng_b_02	■	65.23
52.1 ROS_PTHW_HL_0h_rep1	□	54.82
52.2 ROS_PTHW_HL_0h_rep2	□	51.23
52.3 ROS_PTHW_HL_3h_rep1	□	61.92

154.2 senesc_sugar_lowN_rep2	<input type="checkbox"/>	63.26
154.3 senesc_sugar_lowN_rep3	<input type="checkbox"/>	63.54
154.4 senesc_sugar_lowN_glu_rep1	<input type="checkbox"/>	66.67
154.5 senesc_sugar_lowN_glu_rep2	<input type="checkbox"/>	66.10
154.6 senesc_sugar_lowN_glu_rep3	<input type="checkbox"/>	66.47
154.7 senesc_sugar_highN_glu_rep1	<input type="checkbox"/>	66.79
154.8 senesc_sugar_highN_glu_rep2	<input type="checkbox"/>	65.84
154.9 senesc_sugar_highN_glu_rep3	<input type="checkbox"/>	67.58
155.1 ATGE_nitrate_con_rep1	<input type="checkbox"/>	70.98
155.2 ATGE_nitrate_con_rep2	<input type="checkbox"/>	66.26
155.3 ATGE_nitrate_con_rep3	<input type="checkbox"/>	66.64
155.4 ATGE_nitrate_starv_2d	<input type="checkbox"/>	72.87
155.5 ATGE_nitrate_starv_2d+30min	<input checked="" type="checkbox"/>	75.35
155.6 ATGE_nitrate_starv_2d+3h	<input checked="" type="checkbox"/>	74.84
155.7 ATGE_nitrate_starv_2d+30minKNO3resup_rep1	<input checked="" type="checkbox"/>	71.83
155.8 ATGE_nitrate_starv_2d+30minKNO3resup_rep2	<input checked="" type="checkbox"/>	72.66
155.9 ATGE_nitrate_starv_2d+3hKNO3resup_rep1	<input checked="" type="checkbox"/>	73.24
155.10 ATGE_nitrate_starv_2d+3hKNO3resup_rep2	<input checked="" type="checkbox"/>	73.51
155.11 ATGE_nitrate_starv_2d+30minHClresup	<input checked="" type="checkbox"/>	72.59
155.12 ATGE_nitrate_starv_2d+3hKClresup	<input checked="" type="checkbox"/>	73.78
156.1 BA_Co10_mock_2h_rep1	<input type="checkbox"/>	66.27
156.2 BA_Co10_mock_2h_rep2	<input type="checkbox"/>	67.76
156.3 BA_Co10_BA_15min_rep1	<input checked="" type="checkbox"/>	70.23
156.4 BA_Co10_BA_15min_rep2	<input type="checkbox"/>	53.72
156.5 BA_Co10_BA_2h_rep1	<input checked="" type="checkbox"/>	53.45
156.6 BA_Co10_BA_2h_rep2	<input type="checkbox"/>	51.53
156.7 BA_CKX1_mock_2h_rep1	<input type="checkbox"/>	54.07
156.8 BA_CKX1_mock_2h_rep2	<input type="checkbox"/>	54.18
156.9 BA_CKX1_mock_2h_rep3	<input type="checkbox"/>	51.19
156.10 BA_CKX1_BA_15min_rep1	<input checked="" type="checkbox"/>	55.59
156.11 BA_CKX1_BA_15min_rep2	<input type="checkbox"/>	54.18
156.12 BA_CKX1_BA_15min_rep3	<input type="checkbox"/>	46.65
157.1 miRNA_A_emptyvector_rep1	<input type="checkbox"/>	73.13
157.2 miRNA_A_emptyvector_rep2	<input type="checkbox"/>	69.67
157.3 miRNA_A_emptyvector_rep3	<input type="checkbox"/>	66.48
157.4 miRNA_A_miR159a_rep1	<input type="checkbox"/>	71.70
157.5 miRNA_A_miR159a_rep2	<input type="checkbox"/>	69.01
157.6 miRNA_A_miR159a_rep3	<input type="checkbox"/>	66.95
157.7 miRNA_B_emptyvector_rep1	<input type="checkbox"/>	68.30
157.8 miRNA_B_emptyvector_rep2	<input checked="" type="checkbox"/>	67.98
157.9 miRNA_B_miR156b_rep1	<input checked="" type="checkbox"/>	67.76
157.10 miRNA_B_miR156b_rep2	<input checked="" type="checkbox"/>	66.13
157.11 miRNA_B_miR164b_rep1	<input type="checkbox"/>	68.28
157.12 miRNA_B_miR164b_rep2	<input type="checkbox"/>	67.80
157.13 miRNA_C_emptyvector_rep1	<input checked="" type="checkbox"/>	68.69
157.14 miRNA_C_emptyvector_rep2	<input checked="" type="checkbox"/>	70.37
157.15 miRNA_C_miR164b_rep1	<input checked="" type="checkbox"/>	70.51
157.16 miRNA_C_miR164b_rep2	<input type="checkbox"/>	69.92
157.17 miRNA_C_miR172a_rep1	<input type="checkbox"/>	70.01
157.18 miRNA_C_miR172a_rep2	<input checked="" type="checkbox"/>	69.67
158.1 Seedling_aero_rep1	<input type="checkbox"/>	67.81
158.2 Seedling_aero_rep2	<input type="checkbox"/>	62.10
158.3 Seedling_anoxia_rep1	<input type="checkbox"/>	65.74
158.4 Seedling_anoxia_rep2	<input type="checkbox"/>	60.11
158.5 Seedling_anoxia_suc_rep1	<input checked="" type="checkbox"/>	63.30
158.6 Seedling_anoxia_suc_rep2	<input type="checkbox"/>	62.73
159.1 BR_brz1-1D_rep1	<input checked="" type="checkbox"/>	63.66
159.2 BR_brz1-1D_rep2	<input checked="" type="checkbox"/>	64.04
159.3 BR_brz1-1D_rep3	<input type="checkbox"/>	66.36
159.4 BR_det2_rep1	<input checked="" type="checkbox"/>	65.25
159.6 BR_det2_rep3	<input type="checkbox"/>	63.26
160.1 Auxin_wt_flowers1-14_con	<input type="checkbox"/>	70.15
160.2 Auxin_wt_flowers1-14_IAA	<input checked="" type="checkbox"/>	70.86
160.3 Auxin_wt_flowers1-14_mock	<input type="checkbox"/>	55.08

189.27	Flowering_fri_flg_0d_rep3		<input type="checkbox"/>			65.78
189.28	Flowering_fri_flg_3d_rep1		<input type="checkbox"/>			65.54
189.29	Flowering_fri_flg_3d_rep2		<input type="checkbox"/>			66.82
189.30	Flowering_fri_flg_3d_rep3		<input type="checkbox"/>			66.98
189.31	Flowering_fri_flg_5d_rep1		<input type="checkbox"/>			68.21
189.32	Flowering_fri_flg_5d_rep2		<input type="checkbox"/>			68.70
189.33	Flowering_fri_flg_5d_rep3		<input checked="" type="checkbox"/>			68.32
189.34	Flowering_fri_flg_7d_rep1		<input checked="" type="checkbox"/>			67.42
189.35	Flowering_fri_flg_7d_rep2		<input checked="" type="checkbox"/>			68.12
189.36	Flowering_fri_flg_7d_rep3		<input type="checkbox"/>			68.76
190.1	Eco-SA_Co10_siluet_4h_rep1		<input type="checkbox"/>			64.63
190.2	Eco-SA_Co10_siluet_4h_rep2		<input type="checkbox"/>			68.18
190.3	Eco-SA_Co10_siluet_4h_rep3		<input type="checkbox"/>			60.84
190.4	Eco-SA_Co10_siluet_28h_rep1		<input type="checkbox"/>			67.38
190.5	Eco-SA_Co10_siluet_28h_rep2		<input checked="" type="checkbox"/>			64.52
190.6	Eco-SA_Co10_siluet_28h_rep3		<input type="checkbox"/>			63.72
190.7	Eco-SA_Co10_siluet_52h_rep1		<input checked="" type="checkbox"/>			67.11
190.8	Eco-SA_Co10_siluet_52h_rep2		<input checked="" type="checkbox"/>			66.85
190.9	Eco-SA_Co10_siluet_52h_rep3		<input checked="" type="checkbox"/>			64.78
190.10	Eco-SA_Co10_SA_4h_rep1		<input type="checkbox"/>			66.82
190.11	Eco-SA_Co10_SA_4h_rep2		<input type="checkbox"/>			67.08
190.12	Eco-SA_Co10_SA_4h_rep3		<input type="checkbox"/>			66.03
190.13	Eco-SA_Co10_SA_28h_rep1		<input type="checkbox"/>			66.67
190.14	Eco-SA_Co10_SA_28h_rep2		<input checked="" type="checkbox"/>			65.69
190.15	Eco-SA_Co10_SA_28h_rep3		<input type="checkbox"/>			62.90
190.16	Eco-SA_Co10_SA_52h_rep1		<input type="checkbox"/>			68.77
190.17	Eco-SA_Co10_SA_52h_rep2		<input type="checkbox"/>			62.03
190.18	Eco-SA_Co10_SA_52h_rep3		<input type="checkbox"/>			60.85
190.19	Eco-SA_Cvi-1_siluet_4h_rep1		<input type="checkbox"/>			64.84
190.20	Eco-SA_Cvi-1_siluet_4h_rep2		<input checked="" type="checkbox"/>			65.52
190.21	Eco-SA_Cvi-1_siluet_4h_rep3		<input type="checkbox"/>			66.06
190.22	Eco-SA_Cvi-1_siluet_28h_rep1		<input type="checkbox"/>			66.95
190.23	Eco-SA_Cvi-1_siluet_28h_rep2		<input type="checkbox"/>			65.11
190.24	Eco-SA_Cvi-1_siluet_28h_rep3		<input type="checkbox"/>			64.78
190.25	Eco-SA_Cvi-1_siluet_52h_rep1		<input type="checkbox"/>			67.47
190.26	Eco-SA_Cvi-1_siluet_52h_rep2		<input checked="" type="checkbox"/>			66.87
190.27	Eco-SA_Cvi-1_siluet_52h_rep3		<input type="checkbox"/>			63.88
190.28	Eco-SA_Cvi-1_SA_4h_rep1		<input checked="" type="checkbox"/>			67.19
190.29	Eco-SA_Cvi-1_SA_4h_rep2		<input type="checkbox"/>			65.12
190.30	Eco-SA_Cvi-1_SA_4h_rep3		<input type="checkbox"/>			65.58
190.31	Eco-SA_Cvi-1_SA_28h_rep1		<input type="checkbox"/>			60.00
190.32	Eco-SA_Cvi-1_SA_28h_rep2		<input type="checkbox"/>			64.70
190.33	Eco-SA_Cvi-1_SA_28h_rep3		<input type="checkbox"/>			64.29
190.34	Eco-SA_Cvi-1_SA_52h_rep1		<input type="checkbox"/>			66.52
190.35	Eco-SA_Cvi-1_SA_52h_rep2		<input checked="" type="checkbox"/>			64.38
190.454	Eco-SA_Cvi-1_SA_52h_rep3		<input checked="" type="checkbox"/>			65.18
191.1	Root_endodermis_rep1			<input checked="" type="checkbox"/>		40.88
191.2	Root_endodermis_rep2			<input checked="" type="checkbox"/>		55.37
191.3	Root_endodermis_rep3			<input checked="" type="checkbox"/>		60.98
191.4	Root_endodermis+cortex_rep1		<input type="checkbox"/>			58.72
191.5	Root_endodermis+cortex_rep2			<input checked="" type="checkbox"/>		57.38
191.6	Root_endodermis+cortex_rep3		<input type="checkbox"/>			54.45
191.7	Root_epid_atrichoblasts_rep1		<input type="checkbox"/>			56.33
191.8	Root_epid_atrichoblasts_rep2		<input type="checkbox"/>			53.88
191.9	Root_epid_atrichoblasts_rep3		<input type="checkbox"/>			53.18
191.10	Root_lateral_cap_rep1		<input type="checkbox"/>			52.94
191.11	Root_lateral_cap_rep2		<input type="checkbox"/>			55.91
191.12	Root_lateral_cap_rep3		<input type="checkbox"/>			54.18
191.13	Root_stageI_root_tip_rep1		<input type="checkbox"/>			50.42
191.14	Root_stageI_root_tip_rep2		<input type="checkbox"/>			59.22
191.15	Root_stageI_root_tip_rep3		<input type="checkbox"/>			56.51
191.16	Root_stageI_root_tip_rep4		<input type="checkbox"/>			50.43
191.17	Root_stageII_elong_zone_rep1			<input checked="" type="checkbox"/>		57.47
191.18	Root_stageII_elong_zone_rep2			<input checked="" type="checkbox"/>		58.09

191.19	Root_stageII_elong_zone_read			53.37
191.20	Root_stageII_elong_zone_read			52.11
191.21	Root_stageIII_hair_zone_read			60.62
191.22	Root_stageIII_hair_zone_read			58.70
191.23	Root_stageIII_hair_zone_read			52.50
191.24	Root_stageIII_hair_zone_read			51.37

This document was created with Win2PDF available at <http://www.win2pdf.com>.
The unregistered version of Win2PDF is for evaluation or non-commercial use only.
This page will not be added after purchasing Win2PDF.